

**Multi-component Platinum Group Metals for the methanol
electro-oxidation process**

Bulelwa Patricia Javu

Postgraduate diploma IWRM (University of the Western Cape)

B-Tech Chemistry (Tshwane University of Technology)

B-Tech Chemistry (Cape Peninsula University of Technology)

A thesis submitted in fulfilment of the requirements for the degree of

Magister Scientiae in Chemistry

**UNIVERSITY of the
WESTERN CAPE**

Department of Chemistry

University of the Western Cape

November 2017

Supervisor: Prof. Leslie F. Petrik

**Multi-component Platinum Group Metals for the methanol electro-oxidation
process**

Bulelwa Patricia Javu

Key words

Platinum Group Metals

Carbon nanotubes

Nanoparticles

Electro-catalyst

Metal alloys

Methanol electro-oxidation

Plurimetallic



Abstract

The purpose of this study was to develop a high performance-lower cost catalyst to be applied in Direct Methanol Fuel Cells (DMFC). The study also aimed to prepare plurimetallic supported platinum (Pt), platinum-ruthenium (PtRu), platinum-ruthenium-vanadium (PtRuV) and platinum ruthenium-vanadium-iron (PtRuVFe) upon multi-walled carbon nanotube (MWCNT) as well as upon multi-walled carbon nanotube-titanium oxide (MWCNT/TiO₂) supports. Platinum is very active but prone to poisoning by carbon monoxide (CO), which may be present in the fuel used in fuel cells. The focus on the use of methanol was because of its better reaction kinetics, and better performance in direct methanol fuel cells (DMFC) better than proton exchange membrane fuel cell (PEMFC). When Pt is alloyed with another platinum group metals (PGM) the alloying decreases the over-potential for reactions critical in the fuel cells. Proton exchange membrane fuel cell (PEMFC) performance may be improved at low metal loading, when supported pluri-metallic catalysts are applied since the trimetallic catalysts may promote high catalyst utilisation. In practice, DMFC require electrodes with a Pt loading to achieve acceptance fuel cell (FC) power performance. The aim of this study was therefore the reduction of the catalyst loading through further improvement of mass activity of Pt based catalysts by partial substitution of the noble metal/metals, and the use of a carbon support that will provide high surface area, good electrical conductivity and high stability. MWCNT supported pluri-metallic (PtRuVFe,) and bimetallic (PtRu) nanoparticles possessed characteristic of increased surface area, improved electron transfer rate, enhance electro-catalytic activity and promoted stability.

Chemical vapour deposition (CVD) that was used in this study showed advantages such as being a simple, fast synthesis method and not using reducing agents or acids. The different supports that were characterised initially in this study were activated carbon and MWCNT. The commercial platinum/carbon catalyst from Johnson Matthey [(JM) Pt/C] was used as the reference. These supports and commercial platinum carbon (Pt/C) were all characterised using HRTEM, HRSEM and XRD initially. Various loadings of platinum group metals (PGM) /noble metals deposited on MWCNT and MWCNT/TiO₂ supports were synthesised via the chemical vapour deposition (CVD) method. The variations of Pt/MWCNT and Pt/MWCNT/TiO₂ ratio with different loading percentages were investigated. This was done to improve catalytic performance. Furthermore, pluri-metallic materials were prepared in a single step by CVD, which allowed a very fast and economic combination of PtRu/MWCNT, platinum-ruthenium-vanadium/multi-walled carbonnanotube (PtRuV/MWCNT), Platinum-Ruthenium-Vanadium-Iron/multi-walled carbonnanotube (PtRuVFe/MWCNT), platinum-ruthenium-/multi-walled-carbonnanotube/titanium(PtRu/MWCNT/TiO₂) and platinum-rutheniumvanadium/multi-walled-carbonnanotube/titanium (PtRuV/MWCNT/TiO₂). The prepared catalysts were characterised by techniques such as high resolution transmission electron microscopy (HRTEM), high resolution scanning electron microscopy (HRSEM), X-ray diffraction (XRD) and fourier transforms infrared (FTIR). The electro-catalytic activity was investigated to find their activity for methanol oxidation. This was investigated by using cyclic voltammetry (CV). The platinum dispersion was determined by HRTEM, HRSEM, XRD and FTIR, which confirmed that electrostatically stabilised face

centered cubic (fcc) platinum nano-spheres were present, as well as some agglomeration that was observed. Crystallinity increased in XRD spectra with an increasing metal load when titanium oxide was loaded on MWCNT with the noble metals. HRSEM results demonstrated the distribution of nanoparticles upon the MWCNTs. The commercial catalyst Pt/C used as a reference, showed agglomeration when compared with Pt/MWCNT on HRTEM and HRSEM images. Optimising the activity of platinum based electro-catalysts has been achieved in this study through the formation of pluri-metallic alloys such as PtRuFeV and bi-metallic alloy such as PtRu for anodic methanol oxygen reaction (MOR). Metal oxide (TiO_2) that was used on this study as a support has also improved the catalytic activity of platinum based catalysts for MOR. 30%PtRuV-MWCNT/ TiO_2 gave the highest activity and was the best catalyst. This was due to its suitable surface properties as a promoter of the methanol electro-oxidation reaction when combined with Pt/MWCNT.

Declaration

I declare that “Multicomponent Platinum Group Metals for the methanol electro-oxidation process” is my own work and it has not been submitted for any degree or examination in any university, and all the resources I have used or quoted have been indicated and acknowledged by complete references.

Bulelwa Patricia Javu



November 2017

Signed.....

Acknowledgments

My appreciation goes to God Almighty for his grace and seeing me through this journey.

It is a pleasure to show gratitude to my supervisor Prof L. F. Petrik for the support and guidance in this research.

I would like to thank Dr. Lindiwe Khotsong, Dr. Bulelwa Ntsendwana, senior lecture at University of South Africa for their assistance in CV, Dr. Chionyedia Theresa Onwordi, Andisiwe Bangisa and Emmanuel Ameh for their suggestions and contributions to my research.

Special thanks to A. Abbott, V. Kellerman, Ilse Wells and the members of the Environmental Nanoscience Group (ENS) and my friends for their advice, assistance, understanding and encouragement throughout my work.

I would also like to thank Dr S Botha, Mr A Josephs in the Physics Department of UWC and Dr R. Bucher at Ithembalabs for their assistance in HRSEM, EDS, HRTEM, and XRD which was highly appreciated.

Finally, I wish to thank my husband Mr Cebo Macanda, my dearest kids Buthe, Lukho, Zingce and Akho for their patience, encouragements, understanding, prayers and appreciating my effort.

Abbreviations

Abs	Absorbance
EDS	Energy dispersive spectroscopy
FTIR	Fourier transforms infrared
HRFEGSEM	High resolution field emission gun scanning electron microscopy
HRTEM	High resolution transmission electron microscopy
SEM	Scanning electron microscopy
XRD	X – ray diffraction
MWCNT	Multi-walled carbon nanotube
JM Pt/C	Johnson Matthey Platinum carbon
CV	Cyclic Voltammetry
CVD	Chemical vapour deposition
ATR	Attenuated total reflectance
SAED	Selected Area Electron Diffraction
PGM	Platinum group metals
CNT	Carbon nano tubes
DMFEC	Direct Methanol Fuel Cells
PEMFC	Proton exchange membrane fuel cell
MOR	Methanol Oxidation reaction
WC	Wet Chemistry

Table of Contents

Key words i

Abstract ii

Declaration v

Acknowledgments vi

Abbreviations viii

Table of Contents ix

List of Tables xi

List of Figures xii

CHAPTER ONE 1

1 INTRODUCTION 1

1.1 Background 1

1.2 Rationale and motivation 2

1.3 Problem statement 3

1.4 Aim of the research 4

1.5 Research objectives 4

1.6 Research questions 4

1.7 Research Hypothesis 5

1.8 Research approach 5

1.9 Scope of the research 6



1.10	Limitations.....	7
1.11	Outline of the research	7
CHAPTER TWO		8
2	LITERATURE REVIEW	8
2.1	Introduction	8
2.2	Nanotechnology.....	8
2.3	Catalysis	9
2.3.1	Impregnation method	10
2.3.2	Micro-emulsion method.....	10
2.3.3	Colloidal method.....	11
2.3.4	Chemical vapour deposition.....	11
2.3.5	Carbon materials as support for electro-catalyst.....	12
2.3.6	Activated Carbons.....	12
2.3.7	Carbon nanotubes.....	13
2.4	Titanium dioxide (TiO ₂).....	19
2.5	Platinum Group Metals (PGMs).....	20
2.5.1	Properties of platinum.....	20
2.5.2	Metal alloys.....	21
2.6	Characterisation technique	24
2.6.1	Scanning electron microscopy (SEM/EDS).....	24

2.6.2	Energy-dispersive spectroscopy (EDS)	25
2.6.3	Fourier- Transform Infra-Red (FTIR).....	25
2.6.4	X-ray diffraction (XRD)	26
2.6.5	High-resolution transmission electron microscopy (HRTEM).....	27
2.6.6	Electrochemical characterization	28
CHAPTER THREE.....		32
3	METHODOLOGY.....	32
3.1	Introduction	32
3.2	Materials and Methods.....	33
3.3	Experimental overview.....	34
3.4	Pre-treatment of Multi-walled carbon nanotubes.....	34
3.5	CVD method.....	35
3.5.1	Chemical vapour deposition procedure.....	36
3.6	Analytical methods.....	38
3.6.1	Scanning electron microscopy/ Energy dispersive spectroscopy ...	38
3.6.2	Fourier-Transform infrared.....	39
3.6.3	X-ray diffraction	40
3.6.4	High Resolution Transmission Electron Microscopy	42
3.6.5	Cyclic voltammetry.....	43
3.7	The synthesis method	47

3.7.1	Synthesis of 10% Pt supported on MWCNT with wet-chemical method (A1)	47
3.7.2	Synthesis of 10% Pt supported on MWCNT with CVD method (A2)	47
3.7.3	Synthesis of 10%, 20%, and 30% Pt catalysts supported on multi-wall carbon nanotubes (A2-A4)	48
3.7.4	Synthesis of 20:20 (w/w) PtRu supported on MCNTs (A5-A7)	48
3.7.5	Synthesis of TiO ₂ - MWCNTs support	49
3.7.6	Synthesis of 10%, 20%, and 30% Pt catalysts supported on TiO ₂ / multi-wall carbon nanotubes (A8 - A10)	50
3.7.7	Synthesis of (w/w) 30%PtRu supported on TiO ₂ /MCNTs (A11)	50
3.7.8	Synthesis of (w/w) 30%PtRuVFe supported on TiO ₂ /MCNTs (A15)	50
3.7.9	Synthesis of (w/w) 30% PtRuV supported on TiO ₂ /MCNTs (A12)	51
CHAPTER FOUR		52
4	Results and discussion	52
4.1	Introduction	52
4.2	Results and discussion	53
4.2.1	FT-IR of metal loaded MWCNT samples	73
4.3	Morphology of electrocatalyst, activated carbon and MWCNT	74
4.3.1	Support morphology compared to JM Pt/C catalyst	74
4.3.2	Commercial electro-catalyst morphology	75

TABLE OF CONTENTS

4.4	Structural characterisation using HRTEM	78
4.4.1	Structural images of commercial JM Pt/C electro-catalyst.....	79
4.4.2	Structural images of MWCNT as received.....	80
4.4.3	Structural images of acid treated MWCNT	82
4.6	Electro-catalysts morphology.....	83
4.7	Cyclic voltammetry results and discussion	89
4.8	Electrocatalytic activity discussion of results.....	94
4.9	Summary	95
Chapter five.....		97
5	Conclusions.....	97
References.....		100
Appendices.....		115



List of Tables

Table 3.1: Materials and chemicals used	33
Table 3.2: HRFESEM operational parameters.....	39
Table 3.3: Operational parameters for FTIR.....	40
Table 3.4: Operational parameters for (XRD)	42
Table 3.5: Tecnai G2 transmission electron microscope operational parameters.	43
Table 3.6: Standard Operating Parameters for CV	45
Table 3.7: The % loadings of platinum group metals on MWCNT support.....	46
Table 4.1: Experimental comparison of the degree value (2θ)	54
Table 4.2: Lattice parameter and crystalline size in nano-meter	69
Table 4.3: EDS composition for element in a MWCNT.....	78
Table 4.4: ECSA values of electro-catalysts supported in MWCNT/TiO ₂	94

List of Figures

Figure 2.1: Multi-walled carbon-nanotubes diagram.....	16
Figure 2.2: Multi carbon nanotube without a cap.	18
Figure 2.3: Geometries of nanotubes a) armchair (n,n), b) zig zag (n,0) ,c) chiral (n,m).....	18
Figure 2.4: Synthesis of carbon supported Pt-Ru nanoparticles	23
Figure 2.5: A XRD pattern of the Pt/CNTs samples synthesised using WC (acid treated CNT) and OMCVD (Heat treatment) methods.....	27
Figure 2.6: Cyclic voltammograms of a commercial screen-printed electrode at three different scan rates.	29
Figure 2.7: Cyclic voltammograms on the Pt/CNT samples in a nitrogen degassed solution of 0.5 M sulphuric acid, using a scan rate of 50 mV/s , and an Ag/AgCl reference electrode.	30
Figure 3.1: Research approach schematically outlined.....	34
Figure 3.2: Furnace.	36
Figure 3.3: Schematic demonstration of horizontal furnace.....	36
Figure 4.1: (a) XRD pattern for Pt/C JM catalyst.....	53
Figure 4.2: XRD pattern for (a) Activated carbon, (b) MWCNT and (c) Acid treated MWCNT.	57
Figure 4.3: XRD spectra comparing various loadings of Pt on a MWCNT support.	59
Figure 4.4: Various Pt/Ru compositions on the support of untreated MWCNT. .	61

Figure 4.5: 10-30% Pt- MWCNT/TiO ₂ (untreated) catalyst prepared by the CVD method.....	63
Figure 4.6: Xray diffractograms of trimetallic catalysts on TiO ₂ / MWCNT PtRuV/MWCNT/TiO ₂ , trimetallic catalyst.....	65
Figure 4.7: X-ray diffractograms of multi-metallic catalysts on TiO ₂ / MWCNT PtRuVFe/MWCNT/TiO ₂ , multi-metallic catalyst.....	67
Figure 4.8: Comparison of a FTIR for Activated carbon and JM Pt/C.....	70
Figure 4.9: FTIR spectra of MWCNT.	71
Figure 4.10: FTIR spectra of MWCNT and 4.2c spectra of MWCNT/TiO ₂ and MWCNT/TiO ₂ (CVD).....	72
Figure 4.11: PtRuV/MWCNT & PtRuV/MWCNT/TiO ₂ on the same axis	73
Figure 4.12: HRSEM for activated carbon.....	74
Figure 4.13: HRSEM images of JM Platinum/C electro-catalyst.....	75
Figure 4.14: SEM images of Untreated MWCNTs.....	120
Figure 4.15: SEM image of Untreated MWCNTs.....	76
Figure 4.16: HRSEM images of acid treated MWCNT.....	77
Figure 4.17: HRTEM images of a commercial JM platinum/ carbon.	79
Figure 4.18: Selected Area Electron Diffraction (SAED) for commercial Pt/C...	80
Figure 4.19: HRTEM image for MWCNT.	81
Figure 4.20: HRTEM bright-field micrographs without purification, for a commercial MWCNT (Multi-walled carbon nanotube).	81

Figure 4.21: HRTEM are bright-field micrographs that are purified with H ₂ SO ₄ - HNO ₃ for acid treated MWCNT.	83
Figure 4.22: 30% PtRu-MWCNT	84
Figure 4.23: 30%PtRuV-MWCNT/TiO ₂	84
Figure 4.24: 30%PtRuVFe-MWCNT/TiO ₂	85
Figure 0.1: 30% PtRu/MWCNT (10 mVs ⁻¹) catalyst with H ₂ SO ₄	Error!
Bookmark not defined.	
Figure 4.26: 30% PtRu/MWCNT (10 mVs ⁻¹) catalyst with H ₂ SO ₄ and CH ₃ OH.	Error! Bookmark not defined.
Figure 0.3: 30% PtRu/MWCNT (20 mVs ⁻¹) catalyst with H ₂ SO ₄	116
Figure 4.24: 30% PtRu/MWCNT (20 mVs ⁻¹) catalyst with H ₂ SO ₄ + CH ₃ OH.	90
Figure 0.4: 30% PtRu/MWCNT (50 mVs ⁻¹) catalyst with H ₂ SO ₄	117
Bookmark not defined.	
Figure 0.5: 30% PtRu/MWCNT (50 mVs ⁻¹) catalyst with H ₂ SO ₄ + CH ₃ OH.	117
Figure 0.6: 30% PtRuVFe/MWCNT-TiO ₂ (10 mVs ⁻¹) catalyst with H ₂ SO ₄	118
Figure 0.7: 30% PtRuVFe/MWCNT-TiO ₂ (20 mVs ⁻¹) catalyst with H ₂ SO ₄	118
Figure 4.25: 30% PtRuVFe/MWCNT-TiO ₂ (20 mVs ⁻¹) catalyst with H ₂ SO ₄ + CH ₃ OH.	91
Figure 0.8: 30% PtRuVFe/MWCNT-TiO ₂ (50 mVs ⁻¹) catalyst with H ₂ SO ₄ + CH ₃ OH.	119
Figure 4.26: 30% PtRuV/MWCNT-TiO ₂ (20 mVs ⁻¹) catalyst with H ₂ SO ₄ + CH ₃ OH.	91

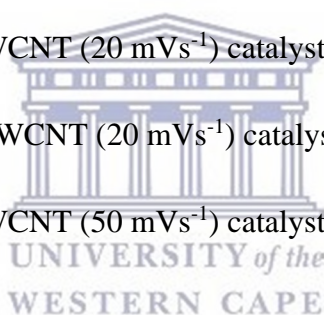


Figure 4.36: 30% PtRuV/MWCNT-TiO₂ (50 mVs⁻¹) catalyst with H₂SO₄ + CH₃OH..... 119



CHAPTER ONE

1 INTRODUCTION

1.1 Background

Platinum group metals (PGM) were discovered in June 1919 in South Africa, in the East Rand. The discovery of platinum quartz bodies in Naboomspruit led to the opening of the first platinum mine in 1924. Platinum group metals (PGM) refer to six metallic elements known as ruthenium, rhodium, palladium, osmium, iridium and platinum. Their physical properties are similar and these metals tend to occur in the same mineral deposits. The platinum metals have outstanding catalytic properties, high temperature characteristics and stable electrical properties (Nogxina et al., 2003). Platinum based electro-catalysts are used for catalysing the oxygen reduction and methanol oxidation reaction in Direct Methanol Fuel Cells (DMFC). The high cost, low availability of platinum and irreversible inactivation of the catalysts by CO-like poisoning species, hinders the commercialisation of DMFCs (Wang et al., 2012).

Platinum plays an important role in different forms. Due to the increase of the price of platinum, the ways to reduce the amount of platinum used in a specific application has to be investigated. This can be done by increasing its catalytic activity in order to lower the overall cost (Chen et al., 2008). These authors also mentioned that the demand of platinum has grown whilst its price increased four times, compare to the decline demand of ruthenium (Ru) due to lower net purchase of Ru (David Jollie, 2008). The literature shows that platinum catalysts

have been extensively studied for the electro-oxidation of fuels such as methanol and ethanol.

1.2 Rationale and motivation

Against the background of environmental needs for cleaner air, it has become necessary to overcome an increase in environmental problems, by development of clean fuel technology for power generation. Human health is compromised daily due to air pollution. In addition, polluted air affects both biotic and abiotic factors in the environment for instance animals, plants and water creating a variety of complications. The coal industry and vehicle emissions play a huge role in polluting the atmosphere by generating toxic gases that later end up in the environment. The core of the problem is the change from a society that derives energy from fossil fuel by means of the internal combustion technology such as fuel cells, and fuels preferably from renewable source and/or fuels that have low carbon and hydrogen ratio to minimize the carbon fast print energy, drastic reduction of carbon dioxide emission per kWh generated. In order to reduce the amount of air pollution, industries have been attempting to use methods that are more economically friendly.

Particle size plays an important role in catalysis for renewable energy systems. Heterogeneous catalysis refers to the form of catalysis where the phase of the catalyst differs from that of the reactants. The great majority of practical heterogeneous catalysts are solids and the great majority reactants are gases or liquids. Heterogeneous catalysis is of paramount importance in many areas of the chemical and energy industries.

A heterogeneous catalyst is a composite material, characterised by, the relative amounts of different model supported catalysts and their properties for studies in fundamental catalysis. (Campanati, et al., 2003).

Thus, the smaller the size of the material, the more effective it becomes for catalytic activity. If the particle size could decrease, it would result in a higher surface area and thus more effective catalytic processes in renewable energy systems, better production and a decrease in cost. The alloying of PGM metals with less costly metals would be a great advantage (Naidoo et al., 2012). Since platinum is costly, when alloyed with another metal it could reduce the amount of platinum used without compromising the quality of the product. It is therefore important to investigate nanostructured pluri-metallic PGM catalysts for activity and resistance to poisoning. Fabricated materials that are on the nano-scale can achieve properties that could not be found in their macroscopic counterparts (Sample and Charles, 2012). Titanium oxide (TiO_2) is a potential promoter of electro-catalytic activity as was reported by Naidoo et al., (2012).

1.3 Problem statement

Nakashima et al., (2006) and Academia Romana (2004), reported that Pt-Ru alloy was the best electro-catalyst for use in solid polymer electrolyte fuel cells and direct methanol fuel cells. Both metals are so expensive that their use has to be limited which is a current problem. For a fuel cell to become more cost effective, the cost of an adequately active catalyst should come down. The current problem is that the surface utilization of the catalyst materials with the appropriate activity is too low.

1.4 Aim of the research

The aim of this research was to prepare a supported, high surface area, pluri-metallic carbon or TiO₂ supported nano-composite electro-catalyst with high activity for methanol oxidation. Alloying platinum with less expensive transitional metals is useful for cost reduction of electro-catalysts. Nakashima et al., (2006) and Sharma et al., (2010) reported that platinum based alloys showed high catalytic activity for methanol oxidation and high CO tolerance. The research objectives are highlighted in Section 1.5.

1.5 Research objectives

The investigations of this study are therefore to:

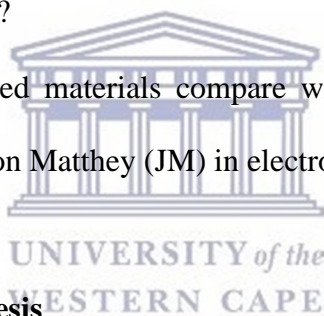
- Develop pluri-metallic electro-catalysts composed of platinum (Pt), ruthenium (Ru), iron (Fe), and vanadium (V) supported on carbon nanotubes (CNT).
- Develop pluri-metallic electro-catalysts supported on MWCNTs/TiO₂.
- Find the metal alloy that will be most effective to decrease the amount of Platinum to achieve economically feasible electro-catalysts for fuel cell application.

1.6 Research questions

The research questions of the study are as follows:

- Will TiO₂ coated carbon nanotube show improved characteristics as a catalyst support?
- Which pluri-metallic catalyst can be prepared without agglomeration?

- What type of nonprecious metal can be used to substitute a part of platinum component without compromising the quality of the electro-catalyst?
- Can the electrochemical activity be improved by adding another metal(s) ie pluri-metallic system?
- Will the substitution of platinum with other metals reduce the activity of platinum catalysts?
- What composition could be considered as the optimum?
- Will pluri-metallic platinum alloy be stable upon a TiO₂ coated carbon nanotube substrate?
- Will the synthesised materials compare with or outperform a reference commercial Johnson Matthey (JM) in electro-catalytic activity?



1.7 Research Hypothesis

An optimum composition of pluri-metallic nano-size alloy containing platinum supported on TiO₂/CNT will result in a highly active, stable electro-catalyst.

1.8 Research approach

The chemical vapour deposition procedure was used for the synthesis of nano-materials. The use of Pt(acac)₂ and depositing of platinum nano-particles onto CNT were done under high temperature and a CVD method. Various masses of multi-walled carbon nanotube as a support and titanium oxide as promoter were calculated and weighed separately. Individual metal-acetylacetonate with different masses was quantified. Each catalyst precursor was mixed with multi-walled

carbon nanotubes and ground with pestle and mortar for the composition to be homogeneous. The heat treatment of the mixture was done at 400 °C at different time frames before being allowed to cool.

The catalysts were characterised by high-resolution transmission electron microscopy (HRTEM), High resolution scanning microscopy (HRSEM), X-ray diffraction (XRD), cyclic voltammetry (CV) and Fourier transform infrared (FTIR).

1.9 Scope of the research

In this research the nano-structured catalyst was prepared and characterised by physical, chemical and electrochemical techniques. The JM catalysts were used as a standard or baseline in order to compare the methanol oxidation activities of the electro-catalysts. The main focus in this research was to reduce the use of PGM for the electro-catalyst, to try and improve functionality of the catalyst by platinum alloying, and by applying the nano-phase catalyst for methanol oxidation in order to achieve high electrochemical activity at a low metal loading. Only one method namely chemical vapour deposition (CVD) was used for the preparation of nanoparticles. TiO₂ was deposited upon MWCNT as a support. The following metals were used as catalysts; platinum, ruthenium, vanadium, iron. Various catalyst loadings of 10%, 20%, and 30%, of metal loading were explored.

The dispersion of platinum nano-particles on the carbon nanotubes (CNT) was investigated. The nanostructure catalysts were characterised by physical chemical and electrochemical techniques. The methanol oxidation activities of the electro-catalysts were compared with JM standards. The electro-catalytic activity of selected catalysts was characterised by cyclic voltammetry.

1.10 Limitations

This study was limited to specified metals, loadings and supports that were used.

1.11 Outline of the research

This study is divided into five chapters and brief overviews of these chapters are presented below:

Chapter 2: presents an overview of the relevant literature including synthesis approaches and characterisation techniques. Theoretical overview and background information relevant to the research is presented.

Chapter 3: specifies the materials and the methods that were used with suppliers, and details of each experiment that was performed. Analytical techniques that were used to characterise when testing catalysts are described; such as XRD, HRSEM, EDS, HRTEM, FTIR and CV.

Chapter 4: presents the results obtained during synthesis of platinum group metal catalyst with different compositions and discusses the results that were obtained from characterisation and testing of the prepared nano-particulate electro-catalysts compared to the baseline commercial catalyst.

Chapter 5: presents the final conclusion of the study and recommendations, as well as answering the research questions.

Chapter 6: covers the list of all the journals, books, websites that were consulted to conduct the literature review.

CHAPTER TWO

2 LITERATURE REVIEW

2.1 Introduction

This chapter presents the review of studies previously carried out on nanotechnology, catalysts, and supports for electro-catalysts, carbon-nanotubes properties and instrumentation that is used for characterisation.

2.2 Nanotechnology

Chellaram et al., (2014) defines nanotechnology as the manipulation of matter at an atomic and molecular scale. It is also explained as the control of matter at an atomic and molecular scale with at least one characteristic dimension measured in nano-meters, ranging from 1 to 100 nm in scale. Nanotechnology is defined as those materials with constituent dimensions less than 100 nm (Zhang et al., 2008). The role that nanotechnology can play in society is being investigated by the scientific community. This was due to the first proposed seminal idea for the development of molecular machines, in 1959 by a Nobel award winner Richard Feynman (Zhang et al., 2008). Nano-meter-sized metal particles continue to attract interest because of their unique physical and chemical properties and the importance of these materials as catalysts (Nashner et al., 1997).

The application of nanotechnology has been spreading to various sectors such as, agricultural, environmental and industrial sectors. Applications of nanomaterials are ranging from fabrication of molecular assemblers to microbial array chips. Nano-technology has touched many spheres of utility services; including consumer products, health care, transportation, energy and agriculture (Brar et al., 2010). Nano-materials exhibit superior mechanical, electrical, optical, catalytic and

magnetic properties when compared to conventional (or micron structured) materials (Zhang et al., 2008). The unique characteristics of nanoparticles are considered to be dependent on their sizes and shapes.

2.3 Catalysis

Catalysis is the change in rate of a chemical reaction due to the participation of a substance called a catalyst. Catalytic activity is defined as the property of a catalytic component measured by its catalysed rate of conversion of a specified chemical reaction in a specified measurement (Dybkaer, 2002). Lamy et al., (2002) reported that platinum-ruthenium based catalysts have been used for many decades as active electrode materials in the electro-oxidation of methanol. The different methods that are used to prepare these catalysts are the colloidal method, the co-impregnation method, calcination, and reduction method. These methods could be used for preparation of pluri-metallic platinum based catalysts, in terms of particle size distribution, control of atomic composition and interaction with supporting materials.

Different methods of synthesis for carbon-supported platinum catalysts have been studied by Schlange et al., (2011). In their study it was also mentioned that the catalyst preparation method influences the noble metal cluster size and its dispersion on the carbon and the electro-catalytic activity. Schlange et al., (2011) stated that three methods used in their report were impregnation, micro emulsion, and colloidal method. Moreover, CVD has been used by Naidoo et al., (2012) in their study of the influence of carbon based supports and the role of synthesis procedures on the formation of platinum and platinum-ruthenium clusters and nanoparticles for the development of highly active fuel cells. CVD was used to prepare various catalysts and synthesizing highly

dispersed Pt and PtRu nanoparticles and nano-clusters supported on carbon nanomaterials (Naidoo et al., 2012).

2.3.1 Impregnation method

The impregnation method is based on the impregnation of the platinum precursor salt on carbon material followed by reduction with a suitable reducing agent sodium borohydride, hydrazine (NaBH_4 , N_2H_4) or under a gaseous reducing environment hydrogen (H_2). The main advantage of this method is its simplicity in execution (Sign et al., 2014). Yaldagard et al., (2013) reported the use of the impregnation method in their research on carbonaceous nanostructured support materials for low temperature fuel cell electro-catalysts. They mentioned that the drawbacks of this technique are related to using liquid media that cause a higher degree of agglomeration of particles in solution. Sign et al., (2014) also mentioned that the impregnation method usually produces nanoparticles (NPs) with large average particle sizes and broad size distributions. Matsumoto et al., (2004) synthesised platinum nanoparticles supported on CNTs using two Pt precursors. The two precursors that were used were H_2PtCl_6 and K_2PtCl_4 . In their research a commercial carbon black supported Pt(Pt-CB) electro-catalyst was used as a control to compare the electrode's performance. They observed some agglomeration on KPt-CNT and Pt was well dispersed on the HPt-CNT.

2.3.2 Micro-emulsion method

The micro-emulsion method is based on water oil systems where surfactant molecules are used for stabilisation of nanoparticles (Malik et al., 2012). The advantage is that it allows for better control of the nanoparticle size and distribution compared to the impregnation method. The disadvantage is high cost of the used surfactants and the time consuming removal at the completion of the process,

thus hindering its use in large scale production. Tojo et al., (2011) reported surfactant effects on micro emulsion based nanoparticle synthesis and Malik et al., (2012) studied a route to synthesise organic and inorganic nanomaterials.

2.3.3 Colloidal method

The colloidal method is based on adsorption of platinum colloids on the surface of the carbon support material followed by the chemical reduction step. The colloidal method consists of three steps, namely; preparation of Pt-metal colloids, deposition of the colloids onto the carbon support and chemical reduction of the suspension (Liu et al., 2006). Sign et al., (2014) used this method as preparation route for Pt-based catalysts. Sign et al., (2014) also mentioned that the colloidal route produces well-homogenised ultrafine Pt electro-catalysts; however, the complexity of the latter hinders its utilisation. Li et al., (2004) used the surfactant 3-(*N,N*-dimethyldodecylammonio) propanesulfonate (SB12) as a stabiliser to prepare Pt nanoparticles supported on the functionalised CNTs by methanol reduction of chloroplatinic acid (H_2PtCl_6). Uniform Pt nanoparticles of an average size of 2.2 nm that were well dispersed on the external walls of the CNTs were observed. Though the colloidal method can provide a narrow size distribution of metal nanoparticles, the problem is the presence of a protecting agent, which can be difficult to remove once the particles are adsorbed onto the support and may impede the catalytic performance of the nanoparticles.

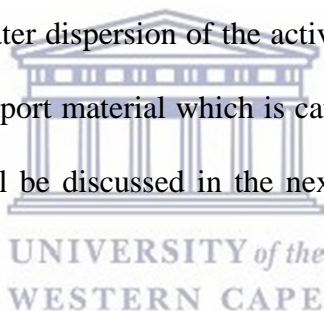
2.3.4 Chemical vapour deposition

Chemical vapour deposition (CVD) is known as the deposition of a solid from a gas or a mixture of gases through a heterogeneous chemical reaction. This reaction takes place at the interface of a gas-solid substrate and, depending on the deposition conditions; the growth process can be controlled

either by diffusion or surface kinetics. CVD is the best known technique for high yield and low impurity production of carbon nanotubes at a moderate temperature. CVD processes seem to offer the best chance to obtain a controllable process for the selective production of nanotubes with predefined properties (Smalley et al., 1996). Naidoo et al., (2012) reported that CVD is a simple but effective solvent free method for the synthesis of platinum group metal nanoparticles on carbon nanotubes.

2.3.5 Carbon materials as support for electro-catalyst

Carbon materials are usually used for electro-catalyst supports with an aim of maximising the specific surface area to achieve a greater dispersion of the active phase. In heterogeneous catalysts, the active phase is deposited on a support material which is catalytically inert (Bailon-Garcia et al. 2013). Various types of supports will be discussed in the next section namely; activated carbon, carbon nanotubes and titanium oxide.



2.3.6 Activated Carbons

Activated carbon is made of an organic material that contains high carbon content like coal, wood, peat or coconut shells. The carbon based material is converted to activated carbon by thermal decomposition in a furnace using a controlled atmosphere and heat. The product consists of a large surface area per unit volume, and a network of sub-microscopic pores where adsorption takes place. Beside physical adsorption, chemical reactions can also occur on a carbon surface (Eltom et al., 2012).

Activated carbon can be characterised by its physical and activity properties. Important physical properties are surface area, product density, mesh size, abrasion resistance and ash content. The pore size distribution is measured through adsorption of gases and liquids under pressure. The availability of pore volume of a carbon over three pore size regions is then defined. The micropore region, which is less than 20 Angstroms in size, secondly the mesopore region between 20-50 Angstroms, and thirdly the macroporous region up to 1000 Angstroms. These materials do not present any electronic effect (Bailon-Garcia et al., 2013). Activated carbon has also been used by Eltom et al., (2012) in their study of production and characterisation of activated carbon membranes. Their study showed that the specific surface area and apparent porosity are reasonable considering that the volumetric fraction of the pores which is needed for adequate permeability is between 40-75%.

2.3.7 Carbon nanotubes

Carbon nanotubes were discovered in 1991 by Sumio Ijima in his study of arc-discharge products. Nanotubes are defined as giant fullerene molecules made of sheets of carbon atoms, arranged in a cylindrical shape. They are divided into two different types, namely a single sheet of carbon atoms which is equal to the single walled nanotube and multiple sheets of carbon atoms that are multi-walled nanotubes (Ahmad et al., 2012). He et al, (2013) classified carbon nanotubes as either a single walled or multi-walled layer of graphite in the form of tubes. Multi-walled carbon nanotubes (MWCNTs) can be considered as a collection of concentric SWCNTs which consist of multiple layers of graphite rolled in on them to form a tube shape with different diameters (Ahmad et al., 2012). Carbon nanotubes have aroused interest because of their unique physiochemical properties (Xu et al., 2010).

Jang and Ma (2012) made a comparison of carbon-nanotubes (CNT) with activated carbon as a support. These authors stated that meso-porosity must be between (2-50 nm) in order to improve mass transfer. These substances should have high purity in order to avoid self-poisoning, and be a consistent material to achieve its high mechanical and thermal stability. Challenges were as follows: controlling surface chemistry of CNTs, functionalisation of CNTs; increasing mechanical strength of CNT when aggregated, preparation of rigid porous CNT granules; maintaining the unique properties of CNTs, especially the mesoporosity.

2.3.7.1 Properties of carbon nanotubes

Mechanical properties: Carbon nanotubes are the strongest and the stiffest material with tensile strength and a good elastic modulus. The elastic modulus is from the covalent sp^2 bond formed between the individual carbon atoms. Therefore, CNTs are expected to be extremely strong along their axes because of their C-C bond. The high value of elastic modulus makes it suitable for application as probe tips for scanning microscopy (Varshney, 2014). When it comes to MWCNTs the outer graphitic cell can support stress when the tubes are dispersed in epoxy matrix and for single wall nanotube bundles (also known as ropes), it has been demonstrated that shearing effects due to the weak inter tube cohesion gives significantly reduced moduli compared to individual tubes (Harris, 1999).

Electrical Properties: A single graphite sheet has properties intermediate between semiconductor and metals. When a graphite sheet has been rolled into nanotubes, not only do the carbon atoms have to line up around the circumference of the tube, but the quantum mechanical wave functions of the electrode must match up. (Varshney, 2014). Metallic nanotubes can carry an electrical current density of 4×10^9 A/cm² which is more than 1,000 times greater than metals such as copper (Dai et

al., 2006). Electrical transport inside the CNTs is affected by scattering by defects and by lattice vibrations that lead to resistance, similar to that in bulk materials (Bandaru, 2007)

Thermal properties: Varshney, (2014) has mentioned that the thermal expansion of CNTs will be largely isotropic, which is different from the conventional graphite fibres, which are strongly anisotropic. This may be beneficial for carbon-carbon composites. It is expected that low-defect CNTs will have very low coefficients of thermal expansion. All nanotubes are expected to be very good thermal conductors along the tube, exhibiting a property known as "ballistic conduction," but good insulators laterally to the tube axis. The temperature stability of carbon nanotubes is estimated to be up to 2800 °C in vacuum and about 750 °C in air (Pop et al., 2006).

Chemical properties: Chemical reactivity of CNT is enhanced, compared with a graphene sheet, as a direct result of the curvature of the CNT surface. This curvature causes the mixing of the π and σ orbital which leads to the hybridisation of the orbitals (Varshney, 2014). The degree of hybridisation becomes larger as the diameter of a SWNT gets smaller. Hence, carbon nanotube reactivity is directly related to the π -orbital mismatch caused by an increased curvature. A distinction must be made between the sidewall and the end caps of a nanotube. For the same reason, a smaller nanotube diameter results in increased reactivity (Stahl et al., 2000).

2.3.7.2 Types of carbon nanotubes:

Since the discovery of CNT they have attracted a great interest from both a fundamental as well as an applied point of view. A single walled carbon nanotube (SWCNT) consists of a single graphene cylinder whereas a multi walled carbon nanotube (MWCNT) comprises of several concentric graphene cylinders. Carbon nanotubes with long aspect ratio are ideal one dimensional nanomaterial, suitable for being used as a carrier to load functional nanoparticles (Xu et al., 2010). CNT are also considered as rolled graphene sheets with a co-axis and with fewer dangling bonds

and defects than carbon black. Carbon nanotubes are formed due to the bonding characteristic of the carbon atoms. CNT is an allotrope of carbon.

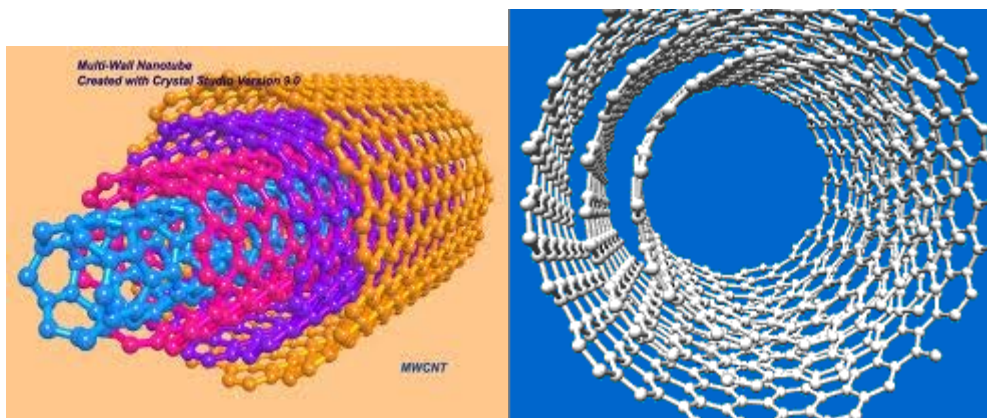


Figure 2.1: Multi-walled carbon-nanotubes diagram (Ganesh, 2013).

Kim et al., (2010) mentioned that nanoparticles deposited on carbon nanotubes are important due to their potential applications as the electrode system of solar cell devices. In order to prepare carbon nanotubes composites where nanoparticles are well distributed, the carbon nanotubes should be prepared prior to the composite preparation (Kim et al., 2010). Su et al., (2000) investigated a scalable CVD method for the synthesis of single-walled carbon nanotubes with high catalyst productivity characteristics of high agglomeration caused by strong attractive Van der Waals interaction among CNT which is a crucial obstacle for many industrial and academic applications. To overcome this problem, the CNT bundles in their native state should be treated either with strong acids or some surfactants to improve their solubility and processibility (Kim et al., 2010). Nanotubes have different forms of structure, namely straight, cork screw, and bamboo (Sinnot et al., 2001).

CNT have high mechanical strength and unique electrical properties. These materials are also considered to be potential supports for heterogeneous catalysts especially in a liquid phase reaction (Li et al., 2002). Nano composites have been prepared for application in areas of catalysis, lithium ion batteries, and gas detection. CNT/TiO₂ nano composites have attracted much attention because they combine the favourable properties of both CNT and TiO₂ nano crystals (Xu et al., 2010). These authors also highlighted that the key problem for CNT/nanoparticle composites as functional materials is the ability to controllably anchor nanoparticles on the surface of CNT.

Carbon nanotubes are used in many active research fields for preparing advanced materials because of their outstanding mechanical, chemical and electrical properties (Hongbing et al., 2005). Interest is on-going in the development of CNTs based composites for the purpose of practical use in the field of material science (Hongbing et al., 2005). These authors also mentioned that a wide range of possible composites have been made using single walled carbon nanotubes (SWNTs) or multi-walled carbon nanotubes (MWNTs) in combination with polymers, metals and ceramics. Carbon nanotubes are the most researched materials in terms of innovation and application (Petrik et al., 2009).

CNT materials are considered to be useful as a support in heterogeneous catalysis (Li et al., 2003). Kim et al., (2010) studied the structural and electrochemical properties of gold deposited on carbon nanotube composites whereas Li et al., (2003) reported that methanol electro-oxidation was performed using Pt-Ru alloy nanoparticles supported on carbon nanotubes. According to Petrik et al., (2009) CNTs have excellent structural properties and extremely interesting physical-chemical properties, but they remain difficult to exploit. Bucky paper however offers a possible method to take advantage of CNT's unique properties and allows ease of manipulation. Wang et al., (2009)

mentioned that some studies showed that carbon nanotubes were more resistant to electrochemical oxidation than carbon black.

The physical appearance of a carbon nanotube which is shaped like a tube (Figure 2.2).

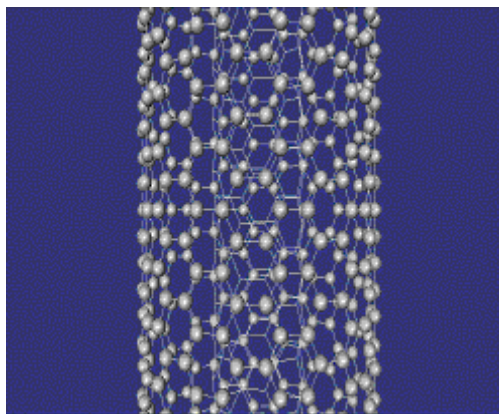


Figure 2.2: Multi carbon nanotube without a cap (Ganesh, 2013).

The various nanotube geometries are shown in Figure 2.3. These geometries are named according to the arrangements of their carbons.

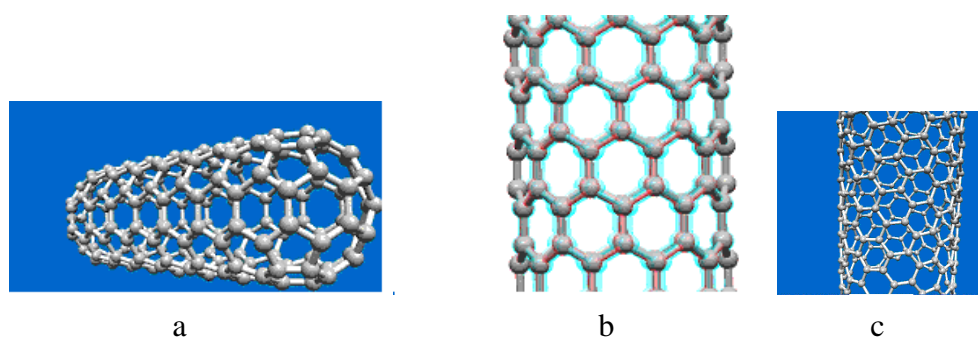
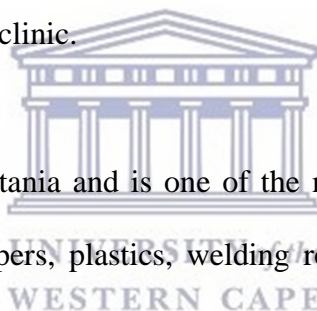


Figure 2.3: Geometries of nanotubes a) armchair (n,n), b) zig zag (n,0) ,c) chiral (n,m) (Ganesh, 2013).

The above three unique geometries of nano-tubes are also referred to as flavours. They are classified according to how the carbon sheet is wrapped into the tube (Ganesh 2013).

2.4 Titanium dioxide (TiO₂)

TiO₂ has been widely studied as a catalyst or catalytic support for photo-electrochemical and electrochemical oxidation reactions. It is widely used because of its exceptional physicochemical stability. The morphology and particle size distribution of TiO₂ catalysts could be controlled using simple preparation methods, (Kulesza et al., 2013). According to Gazquez et al., (2014), the production of pure titanium white which was an anatase form was initially reported in 1923 in France. The production of white pigments began in early in the early 1930s. Park et al., (2011), and Chandrasekar et al., (2009) reported that the crystal structure can occur in different polymorphs, that is; rutile, anatase, brookite and titanium dioxide (B). Anatase and rutile are tetragonal, brookite is orthorhombic and TiO₂ (B) is monoclinic.



Titanium dioxide is also known as titania and is one of the metal oxide semiconductors. TiO₂ is used in the production of paints, papers, plastics, welding rods, coating material etc, due to its unique physicochemical properties. TiO₂ is used as a semiconductor photo-catalyst and, it is the most studied photo-catalyst for a number of reasons. Among them is the stability of its chemical structure with the following properties; biocompatibility, physical, optical and electrical, (Macwan et al., 2011). Titanium dioxide has some of the following applications; photo-catalysis, sensors, photo-electrochromic and photovoltaics. Yu et al., (2010) and Chen et al., (2006) reported that TiO₂ exhibits superior photo-catalytic activity compares to conventional bulk material because of its high surface area.

TiO₂ which possessed optical and catalytically properties, has attracted a great attention as one of the most important environmental nanomaterials due to its application in catalysis and photovoltaics. It has been demonstrated that unique properties of TiO₂ were tied in with size,

crystalline, structure, and morphology (Lei et al., 2008). Hintso et al., (2014) also reported that silver titania CNT nano-composites were the most effective photo-catalyst for the degradation of methylene blue. These authors also mentioned that the combination of both Pt and Ru metals suppressed the photo-catalytic activity of the titania CNT nano-composite. Naidoo et al., (2012) reported that TiO₂ is a good surface promoter for the catalysts as the added additional TiO₂ resulted in a smaller PGM particle size and higher particle size dispersion of the PGM catalysts when compared with the catalysts supported only on CNTs.

2.5 Platinum Group Metals (PGMs)

Platinum group metals (PGMs) is a term used to collectively refer to six metallic elements clustered together in the periodic table. These elements are found as d-block elements (group 8, 9, and 10, in periods 5 and 6 and also called transition metals. Pre-Columbian Americans were the first to encounter naturally occurring platinum and platinum rich alloys long before it was first referenced by Europeans in 1557 in the writing of humanist Julius Caesar Scaliger (1484-1558) as a description of a mysterious metal found in American mines. Platina is the name given by Spaniards which means little silver. Platinum was regarded as an unwanted impurity in the silver that was being mined in Columbia, (McDonald. and Hunt, 1982).

2.5.1 Properties of platinum

Platinum is well suited for fine jewelry. PGM metals have outstanding catalytic properties. Moreover, it is resistant to chemical attack, has excellent high temperature characteristics and stable electrical properties. Platinum group metals are of special interest due to their economic importance and chemical ability as catalysts (International atomic energy agency, 2005).

The first true melting point of platinum using oxygen was established by Lavoisier in 1782. The refining of platinum was developed by Wollaston and Tennant in 1802. By 1804 other transitional elements were discovered, but ruthenium was discovered only later in 1844. Techniques of separation and refining of PGMs, the melting and casting of pure and homogeneous ingots were founded and perfected by Johnson and Matthey in 1851 (Donald McDonald et al., 1982).

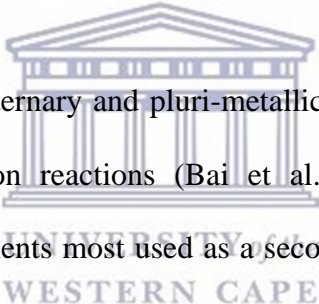
The crystal structure of Pt is face-centered cubic (fcc) and this crystal structure allows it to have good mechanical and electrical properties. The commonly observed Pt nanocrystals are all single crystals. Chen et al., (2008) reported that the hexagonal (111) surface of platinum was found to be five times more active than the square (100) surface for dehydrocyclisation of n-heptane, and also that the (100) surface was more active than the (111) surface for isomerisation of isobutene.

Chen et al., (2006) argues that platinum is the best single metal catalyst for methanol oxidation; however, it is easily poisoned by problematic intermediates such as CO. They also mentioned that modification of platinum by secondary metals such as Ru₂, Sn₃ or Co₄ has been widely studied in recent years. Methanol oxidation is performed using a 50:50 ratio of Pt:Ru binary metallic catalyst as the electro-catalyst (Chen et al., 2006). Neto et al., (2002) described that the introduction of Ru into Pt-based catalysts enriched the reactivity towards oxidation and moderated the poisoning effect through formation of meta-stable intermediates.

2.5.2 Metal alloys

Alloys are defined as metals that are composed of more than one element. A metal alloy is defined as a mixed material that has metallic properties and is made by melting at least one pure metal along with another pure chemical or metal. Metal alloyed nanoparticles with a core-shell are nanoparticles

with the shell enriched by one of the metals. Thus it is important to control which metal goes into the core and which goes into the shell, so that the core-shell particle should be designed with its desired properties, (Wang et al., 2009). Metal alloys have a wide range of applications as catalysts for example in fuel cells, batteries, petrochemical transformations, pharmaceutical applications, and other chemical conversion systems (Wu et al., 2011). These authors used the (gas reducing agent in liquid solution) GRAILS method which allows for the production of Pt alloy nanocrystals at a broad composition range without losing control of the shape. Negro et al., (2015) reported that the sintering of platinum alloys at higher operating temperatures plays an important role in the decrease of fuel cell performance due to the loss of active surface area.



Electro-catalysts that include binary, ternary and pluri-metallic compounds have been investigated in order to promote electro-oxidation reactions (Bai et al., 2007 and Naidoo et al., 2012). Ruthenium (Ru) is one of the components most used as a second metal of Pt-based binary electro-catalysts. It can mitigate CO or CO type intermediate accumulation on the catalyst surface and could lower the potential of oxidation to CO₂. The literature also states that the best results for the oxidation of CO at bimetallic Pt-Ru electro-catalyst have been obtained where the ratio is 1:1 (Lamy et al., 2002; Barczuk et al., 2011). Kulesza et al., (2013) stated in their study that because of the lower stability of the Ru component, a proper determination of the surface concentrations of the alloy constituents is very important. Vanadium (V) and iron have been studied as base metal catalysts for electrochemical oxidation, (Naidoo et al., 2012). Ruthenium as reported in literature has good mechanical properties (Naidoo et al., 2012; Kulesza et al., 2013; Yaldagard et al., 2013; Iwasita 2002, Sign et al., 2014). Nashner et al. (1997) investigated platinum-ruthenium bimetallic

nanoparticles and their experiments showed the formation of bimetallic nanoparticles have a Pt:Ru composition of 1:5 ratio and an average diameter of *ca* 1.5 nm that adopted face centred cubic (fcc). Figure 2.4 shows that the neutral complex $\text{PtRu}_5\text{C}(\text{CO})_{16}$ was used in the synthesis of carbon support Pt-Ru nanoparticles.

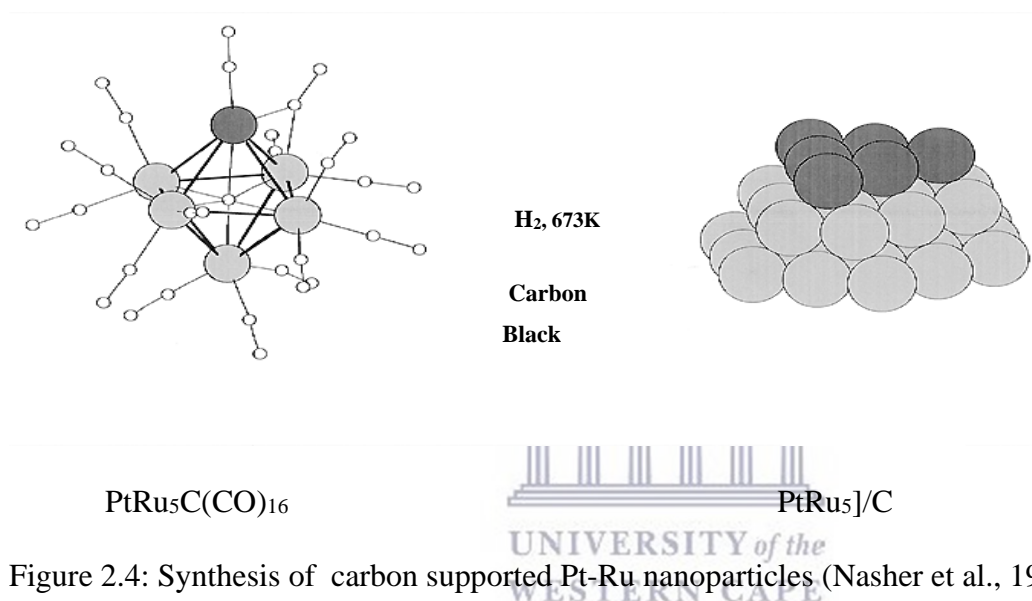


Figure 2.4: Synthesis of carbon supported Pt-Ru nanoparticles (Nasher et al., 1997).

The shape of a metal alloy particle plays an important role in catalytic performance. Wang et al, (2012) mentioned that, at that moment, PtRu alloy catalysts were still considered as the best binary catalyst for the methanol oxidation reaction. Nakashima et al. (2006) reported that the Pt-Ru alloy was the best electro-catalyst for use in solid polymer electrolyte fuel cells and direct methanol fuel cells. Alloying platinum with less expensive transitional metals is useful for cost reduction of electro-catalysts. Nakashima et al., (2005) mentioned that it has been reported that platinum based alloys Pt-Ru, Pt-Fe showed high catalytic activity for methanol oxidation and high CO tolerance.

2.6 Characterisation technique

The literature review discussion is followed by this section that provides a detailed description of the techniques that were employed in the characterisation of the electro-catalysts used in this study. These techniques were used in the investigation of physical-chemical properties of the supported electro-catalysts. Physical characterisation of the supported catalyst was done using XRD, HRTEM, HRSEM and EDS for elemental analysis. For electrochemical characterisation CV was employed.

2.6.1 Scanning electron microscopy (SEM/EDS)

Scanning electron microscopy uses an electron probe to scan the image of the sample point by point. The diameter of the electron probe contributes to the resolution of that image. A smaller electron beam diameter will create an image with higher resolution (Schulz et al., 2005). The morphology of electro-catalysts, their dimensions, and orientation can be easily revealed using SEM with high resolution. SEM imaging bombards a material with an electron beam. The SEM uses a focused beam and data are collected over a selected area of the surface of the sample, and a two dimensional image is generated that displays spatial variations in these properties. Areas ranging from approximately 1 cm to 5 microns in width can be imaged in a scanning mode using conventional SEM techniques (magnification ranging from '20 X' to approximately 30 000 X, spatial resolution of 50 to 100 nm). The SEM is also capable of performing compositional analyses of selected point locations on the sample; this approach is especially useful in qualitatively or semi-quantitatively determination of chemical compositions using energy-dispersive spectroscopy (EDS), crystalline structure and crystal orientations using electron backscatter diffraction (EBSD) (Wright et. al, 2011 and Britton et al, 2016).

The surface of the sample will accumulate charge if the electrons are not allowed to escape from the surface via a conductive path. If there is no escape path, the image that will form will be very poor. Charging can also lead to excessive heating of the sample, causing material degradation. Some

samples should be coated with a conductive material to prevent surface charging. The specimens are usually coated with either a metal or carbon. The first step when analysing a sample on a SEM is an assembly of the sample holder, secondly mounting the sample and then fastening the sample. Finally, the measurement of the z-height must be done correctly.

2.6.2 Energy-dispersive spectroscopy (EDS)

Energy-dispersive spectroscopy (EDS) is an analytical technique used for the elemental analysis or chemical characterisation of a sample. Its characterisation capabilities are due in large part to the fundamental principle that each element has a unique atomic structure allowing a unique set of peaks on its X-ray spectrum. It is also used to stimulate the emission of characteristic X-rays from a specimen, using a high-energy beam of charged particles such as electrons or protons. The number and energy of the X-rays emitted from a specimen can be measured by an energy-dispersive spectrometer. As the energy of the X-rays is characteristic of the difference in energy between the two shells, and of the atomic structure of the element from which they were emitted, this allows the elemental composition of the specimen to be measured (Zhang Fan, 2015).

2.6.3 Fourier- Transform Infra-Red (FTIR)

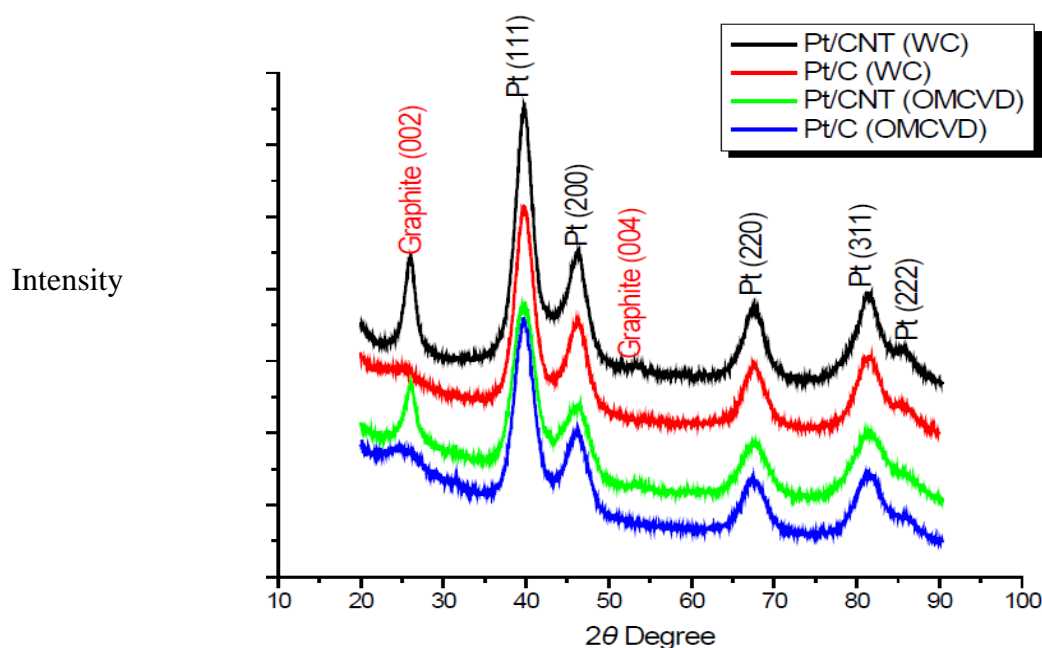
Infrared spectrophotometry (IR) is one of the most powerful tools for detection of impurities, in organic compounds, the quantitative amount of such impurities, identification of compounds and determination of their chemical structure. Fourier-transform spectrometers are used for obtaining complete spectra for qualitative identification. FTIR is non-dispersive in the sense that it neither employs a grating or prism to disperse radiation into its component wavelengths. Fourier-transform spectrometers offer the advantage of unusually high sensitivity, resolution, and speed of data acquisition, therefore data of a spectrum can be obtained in one second or less. All wavelengths are detected and measured simultaneously. They modulate the source of signal in order to separate

wavelengths in such a way that it can be decoded by a transformation (Thackray Arnold, 2000). The bands observed on an Infrared Spectra for both Pt(III)Ru and PtRu (85:15) alloy by Iwasita (2002) corresponded to CO₂ (2341 cm⁻¹) and CO₂ (2050 cm⁻¹). In the case of Pt(III) a band at approximately 1820 cm⁻¹ was due to adsorbed (CO₂) (Iwasita, 2002).

2.6.4 X-ray diffraction (XRD)

X-ray diffraction (XRD) is a versatile, non-destructive technique that reveals detailed information about the chemical composition and crystallographic detail and the mineralogical composition of natural and manufactured materials. Crystal structure is regarded as being formed by layers or planes, X-rays with a wavelength similar to the distances between the planes can be reflected such that the angle of reflection is equal to the angle of incidence. This behaviour is called diffraction, and it is described by Bragg's Law: $2d\sin\theta = n\lambda$. When Bragg's Law is satisfied, constructive interference of diffracted X-ray beams occur and a Bragg reflection will be picked up by a detector scanning at this angle. The positions of these reflections give information about the inter-layer spacing of atoms in the crystal structure. Peak intensities give information about how much X-ray scattering is contributing to that reflection. Analysis of the diffraction pattern allows the identification of mineral phases within a given sample. With that achieved, it may be possible to quantify each phase present, the crystallinity of a sample, the crystal structures and their lattice parameters, crystallite size and strain; all information that can be vital in material characterisation and quality control (Kniess et al.,2005)

In Figure 2.7: Pt peaks which were identified that corresponded to crystal faces which are characteristic of fcc platinum (Naidoo et al., 2012).



WESTERN CAPE

Figure 2.7: A XRD pattern of the Pt/CNTs samples synthesised using WC (acid treated CNT) and OMCVD (Heat treatment) methods (Naidoo et al., 2012).

The XRD pattern shows the difference in structure of the various loadings of Pt catalysts on carbon materials. Pt catalysts show fcc structure on the MWCNT support. Two characteristic diffraction peaks appear at 25 theta and 55 theta degrees for graphite. According to Naidoo et al. (2012) these peaks were attributed to the graphite structures.

2.6.5 High-resolution transmission electron microscopy (HRTEM)

High-resolution transmission electron microscopy (HRTEM) is an imaging mode of the transmission electron microscope (TEM) that allows the imaging of the crystallographic structure of a sample at an atomic scale. Due to its high resolution, it is a valuable tool to study nanoscale

properties of crystalline material such as semiconductors and metals. HRTEM can provide structural information at better than 0.2 nm spatial resolution. In most crystalline inorganic materials, including ceramics, semiconductors, and metals, the positions of individual atomic columns can be resolved, at least in low-index zones (Dumbrava et al., 2005).

Selected area electron diffraction (SAED) is a crystallographic experimental technique that can be performed inside a transmission electron microscope TEM. A thin crystalline specimen is subjected to a parallel beam of high-energy electrons. TEM specimens are approximately 100 nm thick and the electrons typically have energy of 100-400 keV, the electron pass through the sample easily. In this case electrons are treated as wave-like, rather than particle-like, because the wavelength of high-energy electrons is a few thousand of a nanometer, and the spacing between atoms in a solid is about a hundred times larger, the atoms act as a diffraction grating to the electrons which are diffracted.

2.6.6 Electrochemical characterization

Cyclic voltammetry (CV) is the most widely used technique for acquiring qualitative information about electrochemical reactions; it offers a rapid location of redox potentials of the electroactive species. Voltammetry is one of the techniques which electrochemists employ to investigate electrolysis mechanisms. There are numerous forms of voltammetry namely; potential step; linear sweep (LSV); cyclic voltammetry (CV) (Andrienko, 2008)

Cyclic voltammetry (CV) is very similar to LSV. In this case the voltage is swept between two values at a fixed rate, however when the voltage reaches potential (V₂) the scan is reversed and the voltage is swept back to potential (V₁). A typical cyclic voltammogram is recorded for a reversible single electrode transfer reaction. Again the solution contains only a single electrochemical reactant. The forward sweep produces an identical response to that of the LSV experiment. When the scan is

reversed the reaction simply moves back through the equilibrium positions gradually converting electrolysis product for example (Fe^{2+} back to reactant (Fe^{3+}). The current flow is now from the solution species back to the electrode and so occurs in the opposite sense to the forward sweep but otherwise the behaviour can be explained in an identical manner. For a reversible electrochemical reaction the CV recorded has certain well defined characteristics (Andrienko 2008).

In Figure 2.8 Cyclic voltammograms of a commercial screen-printed electrode that showed different scan rates is presented (Fragkou et al., 2013).

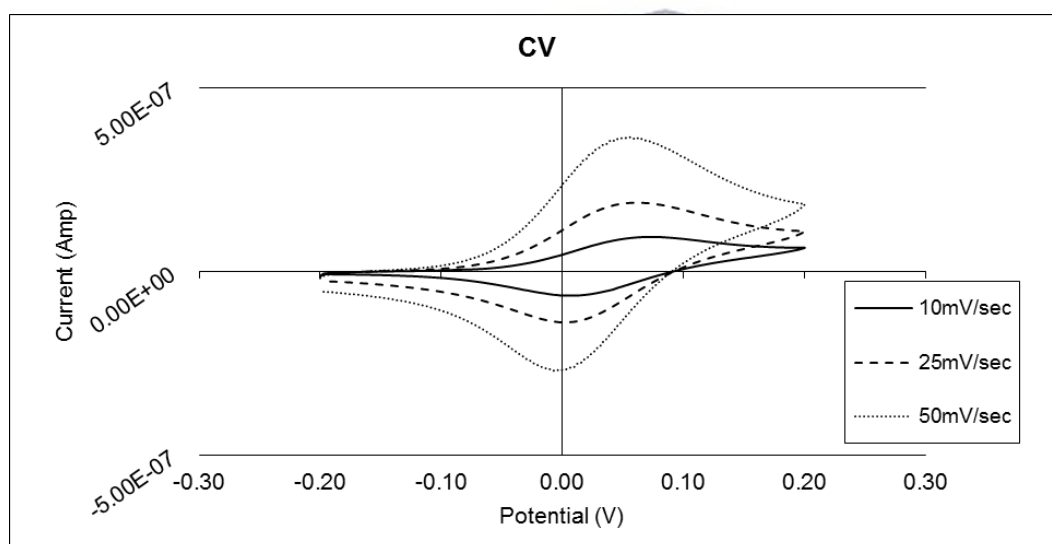


Figure 2.8: Cyclic voltammograms of a commercial screen-printed electrode at three different scan rates (Fragkou et al., 2013).

Typical cyclic voltammograms (CV) on various Pt based electro-catalyst samples are presented in Figure 2.9. The hydrogen desorption peak was observed within the potential range of -0.21 to 0.10 V and the oxygen reduction peak between 0.30 and 0.80 V.

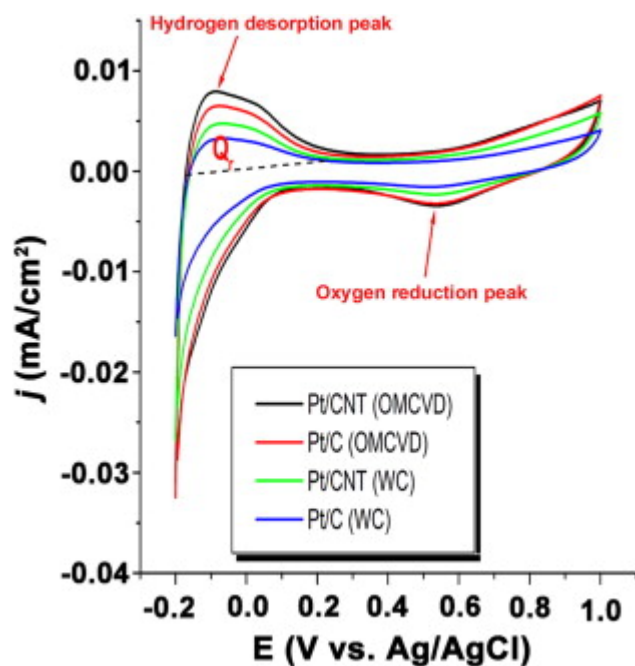
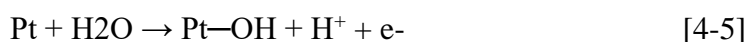
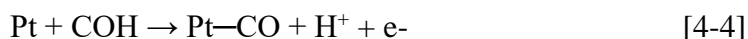
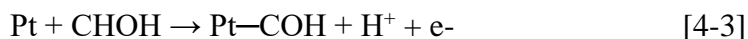
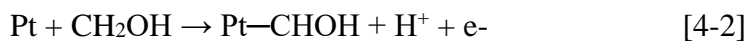
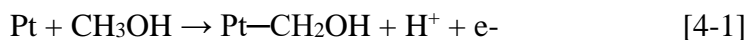


Figure 2.9: Cyclic voltammograms on the Pt/CNT samples in a nitrogen degassed solution of 0.5 M sulphuric acid, using a scan rate of 50 mV/s, and an Ag/AgCl reference electrode (Naidoo et al., 2012).

The experiments in Figure 2.9 were conducted in a three electrode cell, connected to a Metrohm Autolab. The three electrodes are the glassy rotating disk (GCRD) electrode tip as the working electrode, Pt wire as the counter electrode and silver/silver chloride (Ag/AgCl) as the reference electrode.

Methanol oxidation

According to (Hamnett, 1997) methanol oxidation is a slow reaction that requires multiple active sites for methanol adsorption and oxidation. It could be summarised in terms of two basic functionalities; electro-sorption of the methanol on to the substrate and also, addition of oxygen to adsorbed carbon-containing intermediates to generate CO₂. The mechanism of methanol oxidation of the platinum catalyst is written as: (Hogarth et al., 2002)



The reactions (4-1) to (4-4) represents the methanol electro sorption processes and (4-5) to (4-6) are the representation of the oxygen removal or oxidation of intermediates.

Summary:

Based on the literature search, the CVD method was selected to synthesise the different catalysts with MWCNTs and TiO₂ as a support, because some other methods that are used for synthesis are lengthy and use wet chemistry. The impregnation, colloidal and micro-emulsion methods are available to use and are expensive as well. Methods such as the impregnation method uses a liquid media which has the drawback that it can cause agglomeration. The colloidal method is more complex hinders its utilisation and protection agent which is difficulty to remove once the particles are absorbed on to the support. The micro-emulsion method is high in cost. CVD that is used in this study is simple but effective and a solvent free method to deposit metals. MWCNTs and TiO₂ will be use as both catalysts support in this study. It is expected that TiO₂ will enhance the catalytic activity.

CHAPTER THREE

3 METHODOLOGY

3.1 Introduction

This chapter comprises of experimental methodology, sample preparation and physical and chemical characterisation techniques, and electrochemical techniques that will be used in this study. Furthermore, it focusses on the procedures used. Schematics give steps of the experimental overview of the study (Figure 3.1). A special consideration is given to sample preparation. Analytical methods used are detailed. The material and chemical list that was used during the research is also included.

MWCNTs were used in different forms; that is, un-treated MWCNT and pre-treated MWCNTs. Multi-walled nanotube (MWNT) are composed of a larger diameter nanotube surrounding smaller nested nanotubes. Each successive outer shell has a layer diameter but retains the characteristic rolled grapheme structure, (Sinnot et al., 2001).

3.2 Materials and Methods

The chemicals and, equipment, used for the experiment carried out are listed in Table 3.1.

Table 3.1: Materials and chemicals used

Chemical	Specification	Supplier
Multiwalled carbon nanotubes	95% 20-30 diameter	Cheap Tubes Inc.
Platinum on carbon black JM catalyst	Pt 50% on C black	Alfa Aesar
Platinum acetylacetonate	97%	Sigma Aldrich
Ruthenium acetylacetonate	97%	Sigma Aldrich
Vanadium acetylacetonate	97%	Sigma Aldrich
Iron acetylacetonate	97%	Sigma Aldrich
Nitric acid	55%	KIMIX
Titanium acetylacetonate	97%	Sigma Aldrich
Sulphuric acid	98%	KIMIX
Hydrochloric acid	99.9%	KIMIX
Ethylene glycol	99 +%	KIMIX
Chloroplatinic acid	99.9%	Sigma Aldrich
Sodium hydroxide		KIMIX
Formaldehyde		KIMIX

3.3 Experimental overview

A general schematic overview of each experimental procedure and characterisation techniques is presented in Figure 3.1.

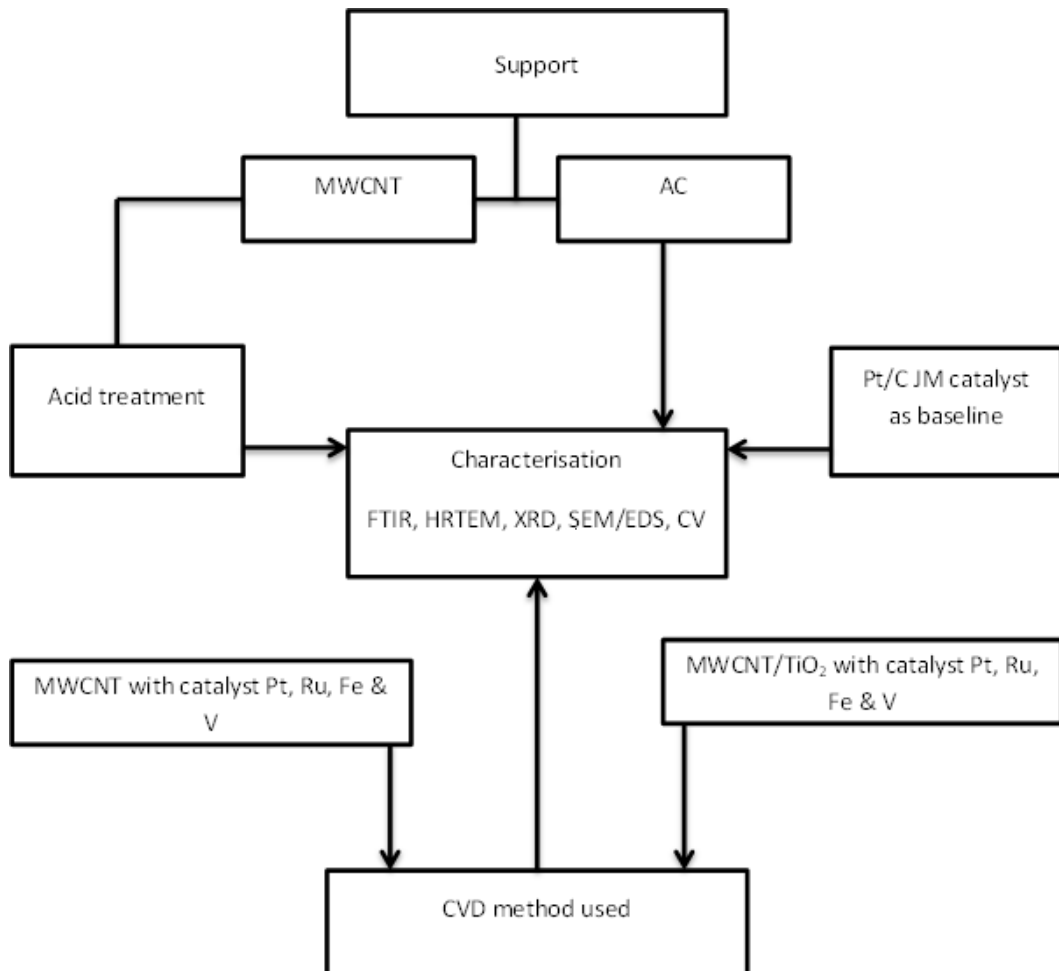


Figure 3.1: Research approach schematically outlines.

3.4 Pre-treatment of Multi-walled carbon nanotubes

Acid treatment or chemical etching methods were used to pre-treat the multi-walled carbon-nanotubes. This is also called the purification step; this step eats away the nanotube caps and creates defect sites on the CNT wall in addition to the

amorphous carbon and leads to short ended, opened nanotube structures, according to Sinnot et al., (2001).

0.1 g sample of MWCNTs (Cheap tubes) was weighed separately. A solution of concentrated H_2SO_4 (98%) mixed with HNO_3 (70%) at a volume ration of 3:1 v/v was used as an acid treatment. This treatment process was called the chemical etching method. The MWCNTs were stirred in this solution using a magnetic bar at approximately 150 rpm for 30 minutes. The sample was diluted, centrifuged and washed with deionised water to remove the residual acid solution. The resulting materials were dried in the oven at 100°C overnight (Park et al, 2008).

3.5 CVD method

A Labofurn tube furnace was used for the CVD process in which the acetyl acetate decomposition formed the supported PGM metal MWCNT/ TiO_2 nano-catalyst. The tube furnace (Figure 3.2) can heat up to 1000°C . A microprocessor programme controller was used to set the temperature, heating rate and holding time for the experiments that were carried out.

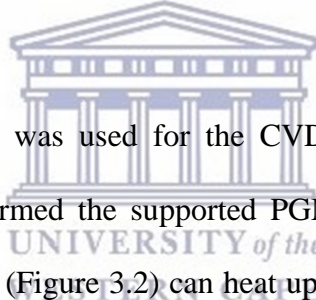




Figure 3.2: Furnace.

3.5.1 Chemical vapour deposition procedure

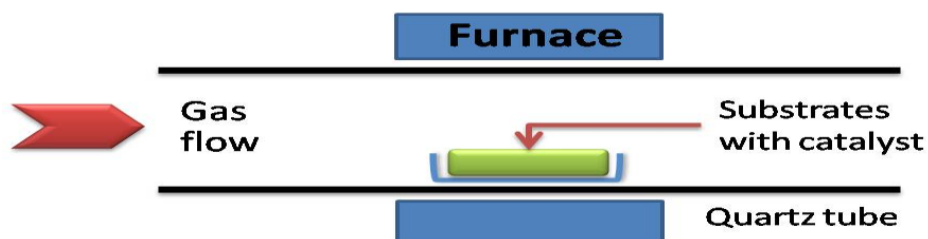


Figure 3.3: Schematic demonstration of horizontal furnace (Szabo et al., 2010).

The quartz tube in the furnace was pre purged with nitrogen gas for 45 min in order to suppress possible surface oxidation of Pt particles. After the desired temperature was reached, a ceramic (alumina) boat loaded with the precursors and MWCNT that had been ground together was inserted into the centre of the quartz

tube. After the heating time, the tube was cooled down while the nitrogen gas was still flowing. When the tube had cooled down the catalysts were removed and kept at room temperature.

3.5.2 Deposition of metal and nanoparticles

The method used was based on a modified dry mix method using chemical vapour deposition (CVD). A mortar and pestle was used to prepare the catalysts by crushing and grinding them into a fine powder. A pre-weighed amount of platinum acetylacetonate ($\text{Pt}(\text{acac})_2$) was thoroughly mixed with 500.0 mg of dry pre-treated multi-walled carbon nanotubes or multi-walled carbon nanotubes with or without titanyl acetylacetonate ($\text{acac})_2$, the deposition of TiO_2 onto MWCNT is explained in section 3.7.5. The TiO_2 supported upon MWCNTs with PGM is discussed from section 3.7.6. The sample was then transferred to the ceramic boat and placed into the quartz tube and introduced into the horizontally aligned tube furnace. The tube furnace was then ramped to 100 °C at a heating rate of 1 °C min^{-1} and held at this temperature for one (1) hour. The furnace was then ramped to 400 °C at a heating rate of 24 °C min^{-1} and held at the final temperature for thirty (30) minutes to decompose the platinum precursor. The tube was allowed to cool down to room temperature, and the sample was recovered. A similar procedure was used to deposit each of the different metals on the pre-treated multi-walled carbon nanotubes and upon the multi-walled carbon nanotubes with titanium dioxide.

3.6 Analytical methods

The following methods were used for the characterisation of the various components; Scanning Electron Microscopy/ Energy Dispersive Spectroscopy (SEM/EDS), Fourier Transform-Infrared (FTIR), X-ray Diffraction (XRD), and High Resolution Transmission Electron Microscopy (HRTEM).

3.6.1 Scanning electron microscopy/ Energy dispersive spectroscopy

The morphology of carbon nanotubes, and electro-catalysts as well as their dimensions, and orientation can be easily revealed using HRFEGSEM (high resolution field emission gun scanning electron microscopy) with high resolution.

This characterisation was carried out with the Auriga HRFEGSEM supplied by Carl Zeiss. The samples were transferred to the EDS for qualitative identification of the different elements contained by the sample.

Sample preparation and operational parameters

Specimens for SEM were prepared for the high-vacuum imaging environment. The procedure depends upon both the samples being examined and the aim of the study. The conductive powders of the catalytic samples were dispersed upon carbon stick tabs and mounted on an aluminium stub holder. After that, the holder was placed into the sample chamber.

Table 3.2: HRFEGSEM operational parameters

Parameter	Setting
Accelerating voltage	25 keV
Tilt Angle	0°
Aperture	0.4 mm
Resolution	3 nm
Working distance	15 mm
Magnification	Various

3.6.2 Fourier-Transform infrared

The samples were investigated using Fourier transform infrared (FTIR) so as to determine the structural configuration. Fourier-transform infrared spectroscopy (FTIR) was used to determine the molecular structure and chemical bonding of materials. This characterisation was done with a Perkin Elmer 100 FT-IR spectrometer. The powdered sample was placed on the attenuated total reflectance (ATR) cell. The sample was analysed in the range of 4000-380 cm^{-1} .

Sample preparation

A spatula tip of sample was subjected to FTIR analysis. The sample was placed directly onto the FTIR ATR. The probe was rotated into the sample which was situated on the sample holder. The experimental conditions are given in Table 3.3 below;

Table 3.3: Operational parameters for FTIR

Instrument Name	Perkin Elmer spectrum 100 series FT-IR Spectrometer
Scan Range	0 to 2000 cm ⁻¹
Scan number	4
Units	Absorbance

3.6.3 X-ray diffraction

XRD was used to confirm the PGM particle size and crystalline structure of the PGM and carbon nanotube electro-catalysts. Powder X ray diffraction is a technique that can be used to study the crystallinity and atomic structure of materials. The samples were analysed by X-ray diffraction using a D8 ADVANCE BRUKER AXS instrument equipped with a pw3830 X-ray generator operated at 40 kV and 40 mA. The specifications of the Siemens D8 Advance XRD unit and operation parameters are given in Table 3.4.

XRD can be used quantitatively for the determination of average particle size as mentioned above, using the Scherrer equation given below as:

$$D = 0.9 \lambda / (B \cos \theta) \quad (3.1)$$

Where D is the particle size, 0.9 the shape factor, λ the wavelength of the X-ray, β is the peak width at half peak height (radians), and θ being the angle of reflection [Cheng et al., 2011; Tseng et al., 2006].

Copper is generally the most used target material for single-crystal diffraction, with a CuK α radiation of 1.5418Å. These X-rays are collimated and directed onto the sample. As the sample and detector are rotated, the intensity of the reflected

X-rays is recorded. The interaction of the incident rays with the sample produces constructive interference and a peak in intensity occurs when the conditions satisfies Bragg's law (equation 3.2). A detector records and processes this X-ray signal and converts the signal to a count rate which is then output to a device such as computer or printer. The Braggs equation is given below:

$$n\lambda = 2d\sin\theta \quad (3.2)$$

$$d = \frac{n\lambda}{2\sin\theta}$$

By varying the angle θ , the Bragg's law conditions are satisfied by different d-spacing in polycrystalline materials. Now based on the principle of X-ray diffraction, a wealth of structural, physical and chemical information about the material being investigated can therefore be acquired [Tseng et al., 2006, Rodríguez-Reinosa, 1998].

Sample preparation and operational parameters

The sample material was ground to a fine powder. The catalyst powder was placed into a sample holder and levelled using a spatula. It was loaded into the X-ray diffractometer. Diffraction patterns were collected in the measured range of 2θ angles between 10 and 80 degrees. The mineral identification was done by comparing with available d-spacing data and major peaks from the International centre for diffraction Data and EVA software from Bruker.

Table 3.4: Operational parameters for (XRD)

Instrument	D8 Advance Bruker AXS
X ray- detector	Vantec-1
Generator voltage	40 kV
Generator current	40 mA
Scanning range (2θ)	0.4 to 7.99
Scan type	Locked coupled
Scan speed per step	0.50 sec
Scan time	40 min
Step size	2θ
Synchronous rotation	Cu K alpha at 1.540598

3.6.4 High Resolution Transmission Electron Microscopy

TEM is often used in the determination of average particle size, particle shape, and particle size distributions of supported nanophase electro-catalysts. The integrity of the catalyst after their exposures to the catalytic conditions was checked with high resolution transmission electron microscopy (HRTEM). The Auriga HRFEGSEM was used to perform the study of the morphology and the effect of the incorporation of various metals or metal alloy nanoparticles on the supports. This technique examines the internal structure of solids and provides information about the micro-structural detail.

Sample preparation and operational parameters

The TEM sample was prepared by suspending the supported catalyst powder in methanol solution and depositing a drop of the suspension on a standard copper grid covered with carbon. Samples were mounted in a sample holder, which was introduced directly into the shaft of the microscope. Samples were viewed and photographed using a Tecnai G2 electron microscope.

Table 3.5: Tecnai G2 transmission electron microscope operational parameters

Parameter	Setting
Accelerating voltage (kV)	200
Current (μA)	20
Condenser aperture	1
Objective aperture	3
Exposure time (sec)	3

3.6.5 Cyclic voltammetry

Cyclic voltammetry (CV) AUTOLAB was used to investigate electrode surface reactions, the behaviour of electrochemically-active species, and to examine the quality of electro-catalysts. CV provides information on the thermodynamics of redox processes and the kinetics of heterogeneous electron-transfer reactions.

The electro-catalytic activity for the methanol oxidation was characterised by cyclic voltammetry (CV) in a solution of 1M methanol (CH_3OH) and 0.5M sulphuric acid (H_2SO_4). The electrolyte was deaerated with nitrogen (N_2) gas for

10 minutes before the measurement and the experiment was conducted at room temperature.

Sample preparation

Working electrode preparation: Catalyst ink preparation

Electro-catalyst inks were prepared by suspending 9.8 mg of the catalyst powder in 5 mL ultra-pure deionised water with the addition of 75 mg (20 μ L) of 5% Nafion solution and 0.83 mL of isopropanol to make an ink stock solution. The mixture was then sonicated in an ice bath for 60 minutes to obtain a uniform suspension. After sonication the ink solution was pipetted the suspension (dropped) onto the glassy electrode tip (5 mm diameter) using a 10 μ L micropipette to form a film which was used to determine platinum loading. The electrode was covered with parafilm in order to avoid moisture ingress, and left to dry overnight, before characterised on the cyclic voltammetry as the working electrode. The electrode ink preparation method used in this study is similar to the one stated by Kimmel et al., (2014).

Electro-chemical activity

The electrochemical investigation was performed with an Autolab at room temperature. The 0.5M H₂SO₄ electrolyte solution was de-aerated with nitrogen for 1 hour prior to each analysis to eliminate the parasitic influence of oxygen and to establish a baseline.

Experimental parameters for the electro-chemical activity are shown in Table 3.6

Table 3.6: Standard Operating Parameters for CV

Parameter	Specification
Electrolyte	0.5 M sulphuric acid to the cell. Degassed with nitrogen by saturation
Methanol	Added 3.2 mL methanol to 100 mL sulphuric acid, Stirred for 15 min.
Working electrode	Catalyst Ink (see Working electrode preparation)
Counter electrode	Platinum wire
Reference electrode	Ag/AgCl
Scan rate	10, 20 & 50 mV Base run (0.5 M sulphuric acid).
Scan range	Scanning range: -0,2 to 1.0 V

Table 3.7: The % loadings of platinum group metals on MWCNT support and PGM/TiO₂/MWCNT electro-catalyst. The % metal loadings are presented at the appendices section.

Metal	Support	% metal loading for experiment	Synthesis Method	Catalyst name
Pt	MWCNT	10	WC	A1
Pt	MWCNT	10	CVD	A2
Pt	MWCNT	20	CVD	A3
Pt	MWCNT	30	CVD	A4
Pt/Ru	MWCNT	20:10	CVD	A5
Pt/Ru	MWCNT	10:10	CVD	A6
Pt/Ru	MWCNT	5:5	CVD	A7
Pt	MWCNT/TiO ₂	10	CVD	A8
Pt	MWCNT/TiO ₂	20	CVD	A9
Pt	MWCNT/TiO ₂	20:10	CVD	A10
Pt/Ru	MWCNT/TiO ₂	20:10	CVD	A11
Pt/Ru/V	MWCNT/TiO ₂	10:10	CVD	A13
Pt/Ru/V	MWCNT/TiO ₂	20:10	CVD	A12
Pt/Ru/Fe/V	MWCNT/TiO ₂	20	CVD	A14
Pt/Ru/Fe/V	MWCNT/TiO ₂	15:5:5:5	CVD	A15

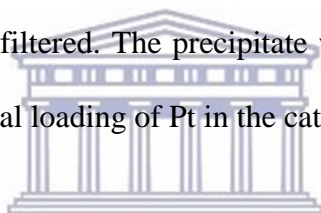
Refer to Appendix for theoretical Pt content calculations.

3.7 The synthesis method

Table 3.7 gives details of all catalysts prepared in this study.

3.7.1 Synthesis of 10% Pt supported on MWCNT with wet-chemical method (A1)

500 mg MWCNT support was mixed with 50 mL ethylene glycol (EG) and sonicated for 20 minutes to get a suspension. 16.45 mL of 7.4 mg/mL chloroplatinic acid, which used EG as solvent, was gradually added to the MWCNT suspension with a burette and stirred for 4 hours. The solution was then kept at 130°C in an oil bath for 3 hours. The solution was left to cool at room temperature before being filtered. The precipitate was dried under vacuum at 80 °C for 8 hours. The nominal loading of Pt in the catalyst was 10%.



UNIVERSITY of the
WESTERN CAPE

3.7.2 Synthesis of 10% Pt supported on MWCNT with CVD method (A2)

112 mg Platinum acetylacetonate [Pt (acac)₂] and 500 mg modified MWCNT support (Section 3.7.3) were physically mixed and ground with a mortar and pestle before the mixture was transferred to a ceramic boat and introduced into a quartz tube. The quartz tube was introduced into the furnace and purged with nitrogen. The tube furnace with the catalyst was then ramped to 100 °C at a heating rate of 1 °C min⁻¹ and held at this temperature for one (1) hour. The furnace was then ramped to 400 °C at a heating rate of 24 °C min⁻¹ and held at the final temperature for thirty (30) minutes to decompose the platinum precursor. The catalyst was then slowly ramped to 100 °C and kept at 100 °C for another 1

hour to remove traces of water. Thereafter the catalyst was ramped to 400 °C in the tube furnace and held for 30 min to decompose the platinum precursor properly. The quartz tube was cooled to room temperature, and the sample was removed. This catalyst was denoted A2.

3.7.3 Synthesis of 10%, 20%, and 30% Pt catalysts supported on multi-wall carbon nanotubes (A2-A4)

In order to synthesize Pt/CNT catalysts with different Pt wt. % loadings, 112 mg, 250 mg or 432 mg Platinum acetylacetonate [Pt (acac)₂] were separately weighed on an analytical balance and each mixed with 500 mg as received MWCNTs by grinding with a mortar and pestle, and the solid mixture was transferred to a ceramic boat and introduced into a quartz tube. The quartz tube was introduced into the furnace and purged with nitrogen. The catalyst was then slowly ramped to 100 °C and kept at 100 °C for another 1 hour to remove traces of water. The catalyst temperature was ramped to 400 °C and held for 30 min to decompose the platinum precursor properly. The quartz tube was cooled to room temperature, and the sample was removed. These series of catalysts were denoted A3-A5 (see Table 3.7).

3.7.4 Synthesis of 20:20 (w/w) PtRu supported on MCNTs (A5-A7)

In order to synthesize PtRu/MWCNT catalysts with different Pt wt. % loadings, 112 mg, 250 mg or 432 mg Platinum acetylacetonate [Pt (acac)₂] and 249 mg, 497 mg, 746 mg Ruthenium acetylacetonate [Ru(acac)₃] were separately weighed.

They were each well mixed with 0.500 g modified MWCNTs and ground with a mortar and pestle, and then heated following the synthesis procedure specified in Section 3.7.3 to produce catalyst A5-A7) (Table 3.7).

3.7.5 Synthesis of TiO₂- MWCNTs support

In this section TiO₂ was mixed with MWCNTs as supports and then the PGM electro-catalysts supported on TiO₂-MWCNTs are synthesised.

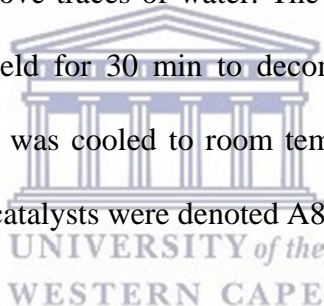
Platinum supported on TiO₂-MWCNTs was synthesised by using the following methodology. The theoretical molar ratio of TiO₂: Pt 1:1 was used in this study. The Pt/TiO₂ optimal molar ratio was found to be equal to 1:1 by James et al., (2009). The theoretical weight percentage of TiO₂ is 15% in this study.

167 mg TiO₂ (acac)₂ and 500 mg of MWCNTs were weighed separately on an analytical balance, there after mixed and ground with a mortar and pestle. There after the mixed powders were transferred into the ceramic boat which was then introduced into the quartz tube furnace. The quartz tube was introduced into the furnace. The supports were then slowly ramped to 100°C at heating rate of 20 °C/min and kept at 100 °C for 1 hour, then support was ramped to 400°C held for 30 minutes to form TiO₂/MWCNT composite substrate.

The following is the synthesis procedure as specified in section 3.7.2 and adding the TiO₂ upon the MCNTs as support for the catalyst to produce 10% Pt/MWCNT.

3.7.6 Synthesis of 10%, 20%, and 30% Pt catalysts supported on TiO₂/multi-wall carbon nanotubes (A8 - A10)

In order to synthesize PtTiO₂/CNT catalysts with different Pt wt. % loadings, 112 mg, 250 mg or 432 mg Platinum acetylacetonate [Pt (acac)₂] were separately weighed on an analytical balance and mixed with 500 mg mixture of TiO₂/MWCNTs (as the procedure specified in section 3.7.5) by grinding with a mortar and pestle, and the solid mixture was transferred to a ceramic boat and introduced into a quartz tube. The quartz tube was introduced into the furnace and purged with nitrogen. The catalyst was then slowly ramped to 100 °C and kept at 100 °C for another 1 hour to remove traces of water. The catalyst temperature was then ramped to 400 °C and held for 30 min to decompose the platinum precursor properly. The quartz tube was cooled to room temperature, and the sample was removed. These series of catalysts were denoted A8-A10 (see Table 3.7).



3.7.7 Synthesis of (w/w) 30%PtRu supported on TiO₂/MCNTs (A11)

250 mg Platinum acetylacetonate [Pt(acac)₂] and 249 mg Ruthenium acetylacetonate [Ru(acac)₃] were well mixed with 500 mg prepared TiO₂/MWCNTs mixture as specified in section 3.7.5 and ground with a mortar and pestle, and then heated following the CVD synthesis procedure specified in Section 3.5 to produce catalyst A11 (Table 3.7).

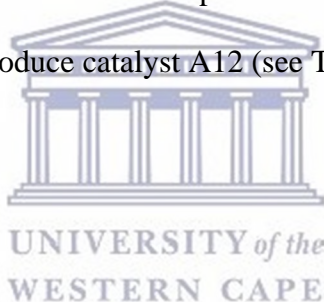
3.7.8 Synthesis of (w/w) 30%PtRuVFe supported on TiO₂/MCNTs (A15)

2513 mg Platinum acetylacetonate [Pt(acac)₂], 1638 mg Ruthenium acetylacetonate [Ru(acac)₃], 284 mg Vanadium acetylacetonate [V(acac)₃] and

262 mg Iron acetylacetonate [Fe(acac)₃] were physically well mixed with 500 mg TiO₂/MWCNTs as specified in Section 3.7.5 and ground with a mortar and pestle, and then heated following the synthesise procedure specified in Section 3.7.5 to produce catalyst A15 (see Table 3.7).

3.7.9 Synthesis of (w/w) 30% PtRuV supported on TiO₂/MCNTs (A12)

250 mg Platinum acetylacetonate [Pt(acac)₂], 1638 mg Ruthenium acetylacetonate [Ru(acac)₃] and 284 mg Vanadium acetylacetonate [V(acac)₃] were physically well mixed with 500 mg TiO₂/MWCNTs as specified in section 3.7.5 and ground with a mortar and pestle and then heated following the synthesise procedure to produce catalyst A12 (see Table 3.7).



CHAPTER FOUR

4 Results and discussion

4.1 Introduction

This chapter presents the results of the characterisation and interpretation of platinum catalysts with various noble metals loading supported on MWCNT, MWCNT/TiO₂ and compared to commercial Pt/C (JM). The characterisation of the different supports, MWCNT and activated carbon, was done initially, as well as the JM Pt/C catalyst. There after various Pt metal loadings on MWCNTs and Pt on TiO₂/ MWCNT as well as bi-metallic, tri-metallic and quaternary system were also investigated. The surface of the MWCNT was modified using acid treatment to improve dispersion of the metal particles on the support material as detailed in section 3.4. This section will be presenting the structure characterisation and interpretation of results for supports, commercial electro-catalyst and different electro-catalyst. The results will start off with examining structure crystallinity using XRD, there after FTIR, followed by surface morphology using HRSEM and HRTEM. The last section of this chapter will be the determination of catalytic activity using CV.

4.2 Results and discussion

4.1. XRD diffractogram of commercial Pt/C JM Catalyst as a reference catalyst

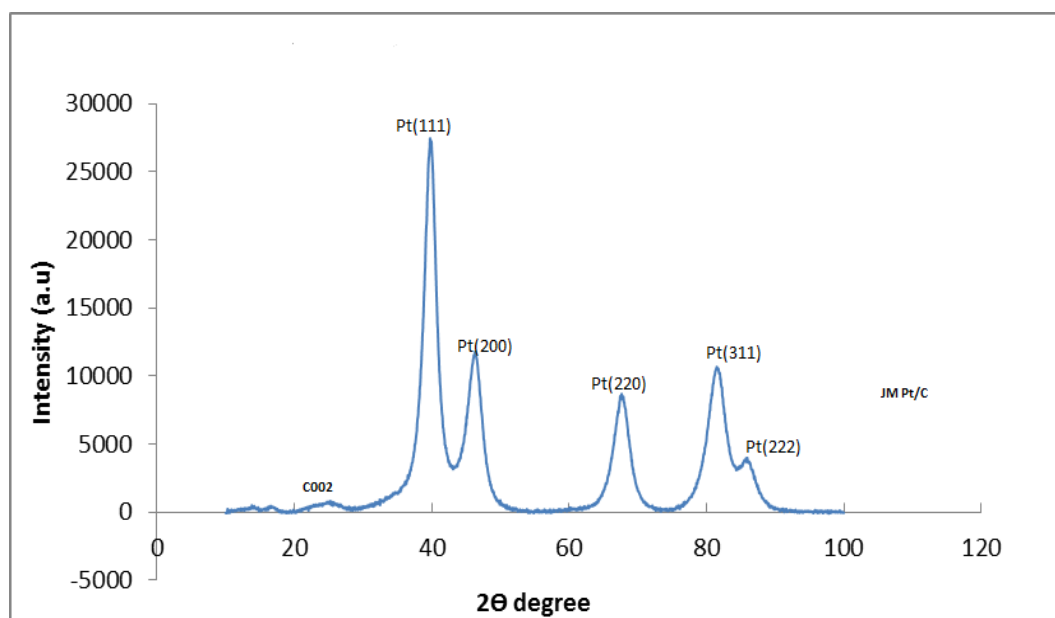


Figure 4.1: XRD pattern for Pt/C JM catalyst

The XRD pattern for a commercial Pt/C is given in Figure 4.1, which shows the characteristics of platinum diffraction peaks. The carbon peak C002 appears at 23.7° 2θ .

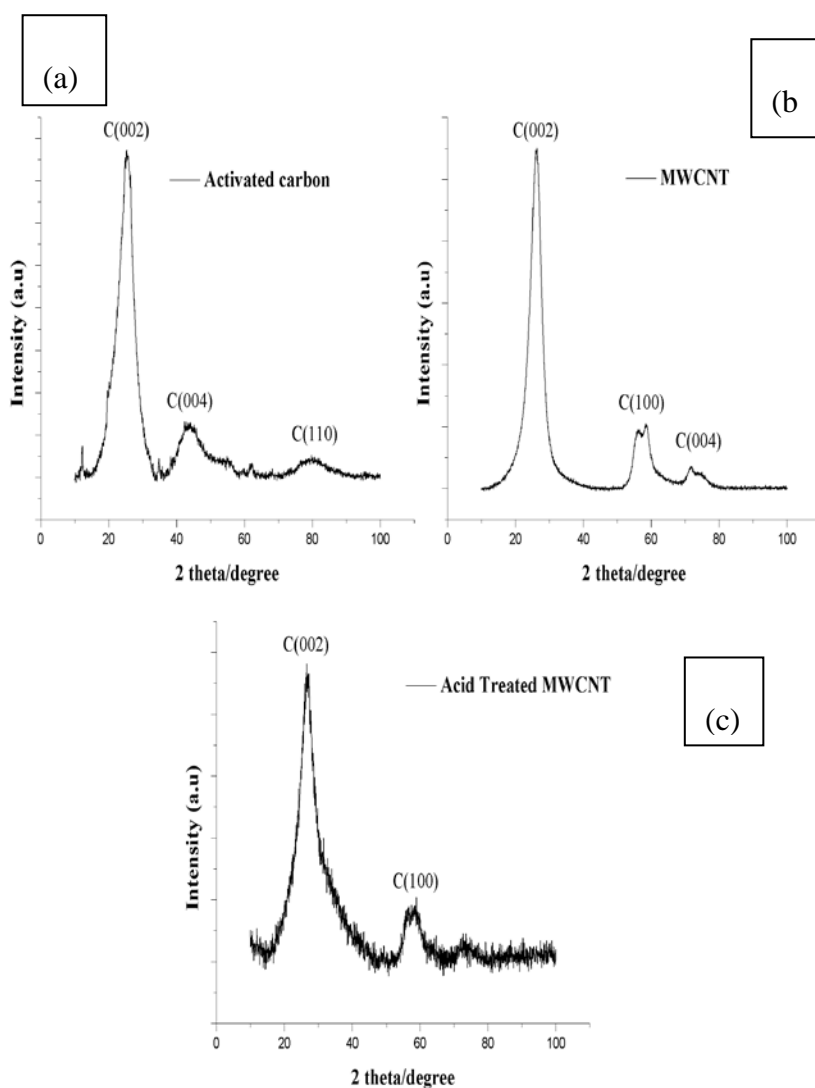
Table 4.1: Experimental comparison of the degree value (2θ)

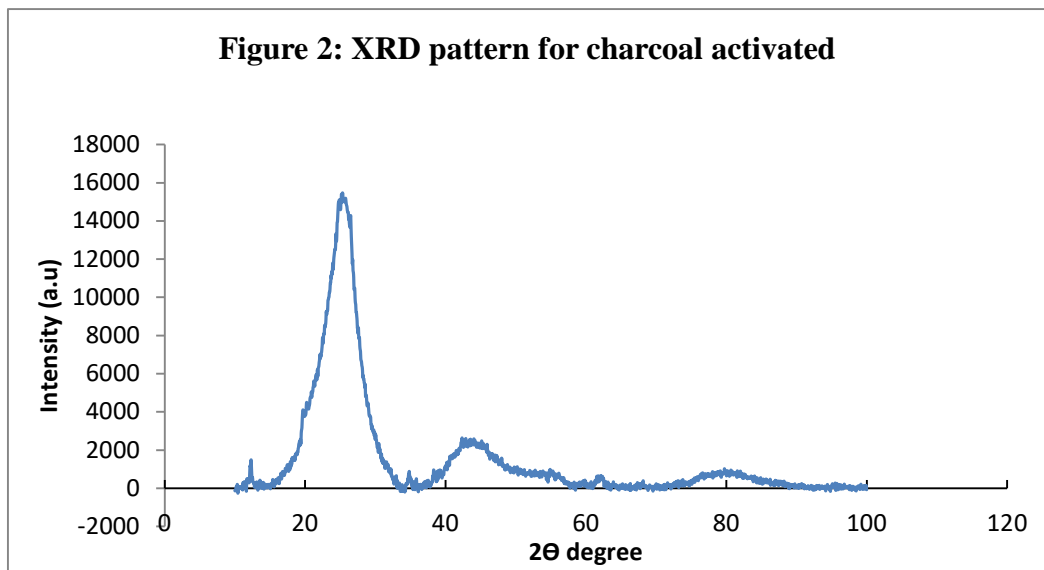
Peak	Degree value Experimentally	Degree value Literature	Plane (fcc) of Platinum
1 st	39.65	39.8	111
2 nd	45.92	46.2	200
3 rd	67.24	68.1	220
4 th	80.88	81.4	311
5 th	85,7	86.7	222

All Pt peaks are characterised as face centred cubic crystalline (fcc) Pt⁰, (Wang et al, 2012; Naidoo et al, 2012; Kim et al, 2009; Kuo et al, 2010).

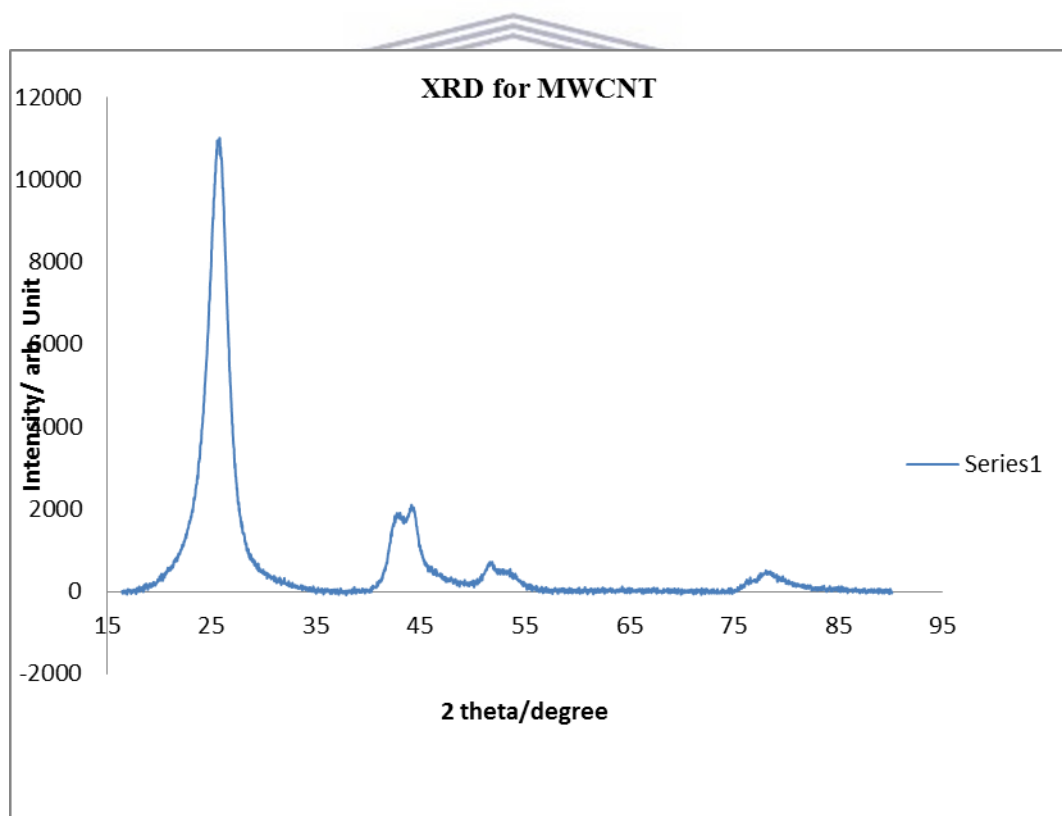


Figure 4.2a, Figure 4.2b and Figure 4.2c show XRD patterns for activated carbon, Multiwalled carbon nanotubes and acid treated carbon nanotubes. The detailed procedure for acid treatment is discussed in the experimental in chapter 3.

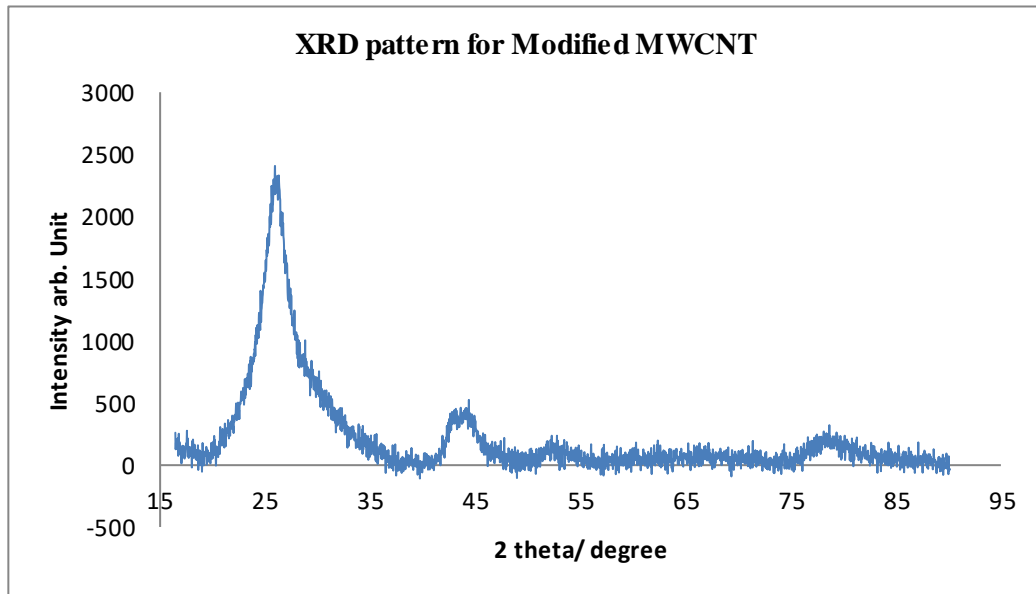




a



b



c

Figure 4.2: XRD pattern for (a) Activated carbon, (b) MWCNT and (c) Acid treated MWCNT.

XRD patterns of activated carbon and MWCNTs have a main diffraction peak around degrees 2θ of approximately 23.7° . These peaks are broad. According to Naidoo et al (2012), the peak for Pt/C JM (C002) which is at 23.7° , is due to the high ordered arrangement of graphene sheets and random structuring of the amorphous activated carbon.

When comparing Figure 4.2b & Figure 4.2c, it can be concluded that there was a strong signal near 23.7° which was corresponding to the 002 graphite planes in the case of MWCNT. The peaks are narrower than in the case of activated carbon thus showing greater ordering in the case of MWCNT prior to acid treatment. Both XRD patterns of MWCNTs are showing the characteristics of CNT, although the peak intensity of the acid treated MWCNT is lower than the untreated MWCNT.

The MWCNT and acid treated MWCNT XRD patterns that are shown in Figure 4.1b and Figure 4.1c showed the most intense peak at 2θ equal to 25.56° . The peaks of 2θ ca. 25° and 56° are characteristic of carbon-nanotubes whereas the peak at $44.03^\circ 2\theta$ that is seen in the case of activated carbon is absent.

In Figure 4.2 which also shows the acid modified carbon-nanotubes, the spectrum also showed a maximum peak at 25.62° . There was not much difference after acid washing; therefore, the MWCNT can be used as catalyst support even if not treated with acid. The acid treatment for MWCNT helps to get rid of metal impurities, (Naidoo et al., 2012). The following catalyst was the only prepared Pt/MWCNT (A1) catalyst in which the acid treated MCNTs was used.

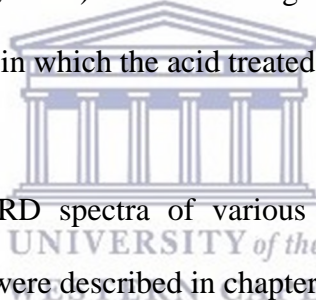


Figure 4.3 shows the XRD spectra of various loadings of the Pt/MWCNT. Experimental procedures were described in chapter 3. MWCNT was heated at 400 degrees Celsius using CVD to deposit the PGM metals as per method. 10% Pt/MWCNT catalyst was also treated with nitric acid as per the method in section 3.4.

Figure 4:3 XRD spectra comparing various loadings of Pt on a MWCNT support

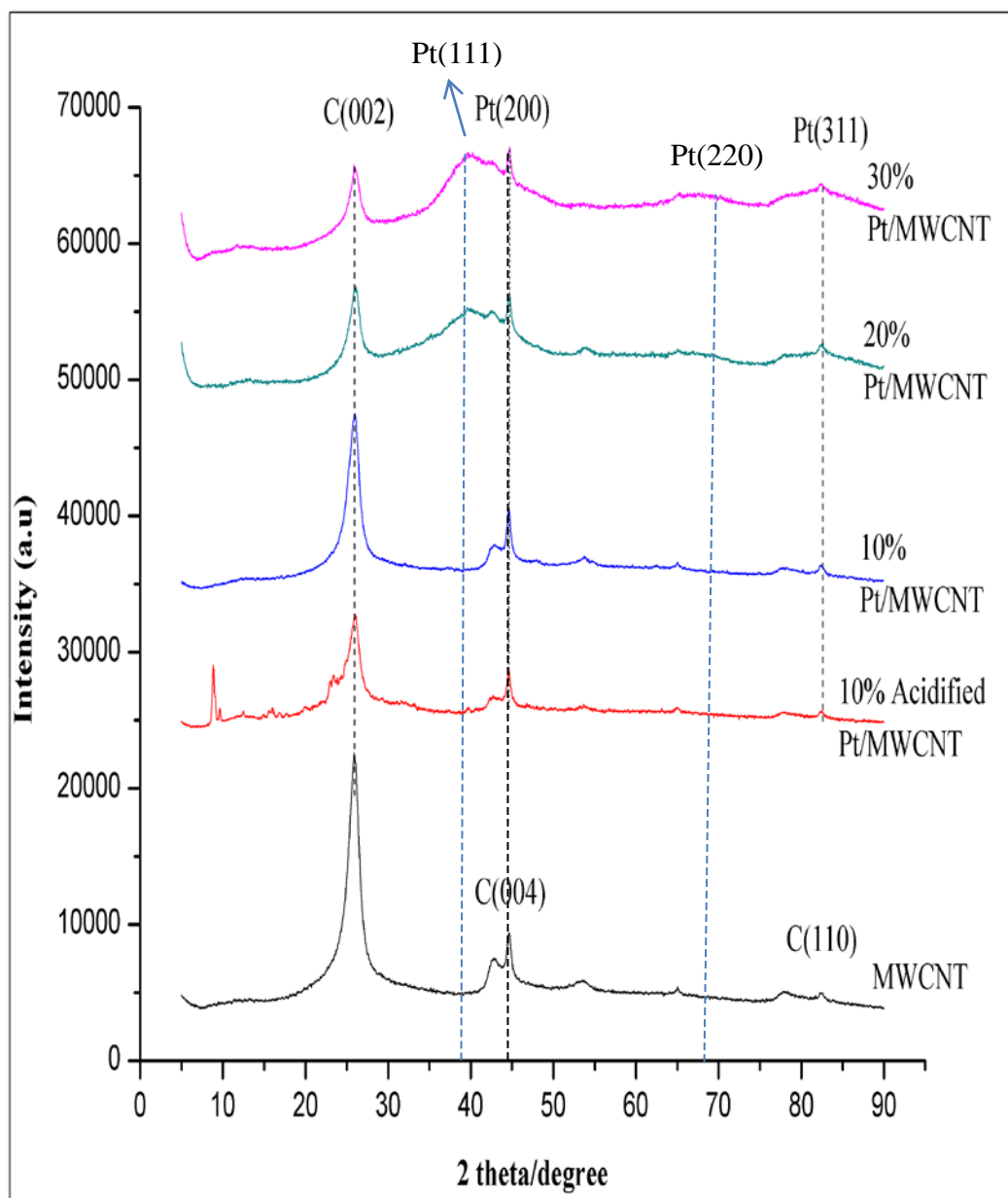


Figure 4.3: XRD spectra comparing various loadings of Pt on a MWCNT support.

(A1, A2, A3 and A4)

In Figure 4.3 it is shown that when the acid treated MWCNT was used as a support of the ten percent platinum precursor, and compared to the untreated MWCNT that was also used as a Pt support, there is a peak that became visible

around ten (10) degrees 2θ only in the case of Pt on acid modified MWCNT (A1) loading. There is a shoulder on the left of the maximum peak at $25^{\circ} 2\theta$, which is only observed on the acid modified sample (A1). There is a peak at 2θ that appears at around $45^{\circ} 2\theta$ on all the XRD patterns relating to C (004). The maximum peak at around $25.5^{\circ} 2\theta$ that is present in all patterns shows

Figure 4.3: XRD spectra comparing various loadings of Pt on a MWCNT support. (A1, A2, A3 and A4)

In Figure 4.3 it is shown that when the acid treated MWCNT was used as a support of the ten percent platinum precursor, and compared to the untreated MWCNT that was also used as a Pt support, there is a peak that became visible around $10^{\circ} 2\theta$ only in the case of Pt on acid modified MWCNT (A1) loading. There is a shoulder on the left of the maximum peak at $25^{\circ} 2\theta$, which is only observed on the acid modified sample (A1). There is a peak at around $25^{\circ} 2\theta$ that is present to all patterns shows the graphitic characteristics of the MWCNT C (002). At around $46^{\circ} 2\theta$ C (004) and Pt(200) are overlapping, and at approximately $68.1^{\circ} 2\theta$ the peak of Pt(220) is not visible. At around $39^{\circ} 2\theta$ Pt111 is observed at A3 and A4. The intensity of the Pt111 Pt peak is increasing as the Pt loadings increase when compared with that of MWCNT. There is a common peak on all the XRD patterns of Pt loaded MWCNTs at around $85^{\circ} 2\theta$ which is assigned to Pt (222). The Pt peaks are broad indicating that particle size of the Pt was in the nanoscale. Only Pt (3111) was visible on 10% Pt loaded samples probably due to inability of XRD to resolve at such low loading. Pt 111

Figure 4:4 shows Xray diffractograms of Pt/Ru supported on MWCNT, MWCNT heated using the CVD method and MWCNT that was not acid treated. The experimental procedure is described in detail in chapter 3 section 3.6.3. Ruthenium was added in order to reduce the amount of Pt used in catalyst, due to its cost. The ratios that are used for PtRu are as follow, 5:5 PtRu (10%) A7, 10:20 A6 and 20:10 A5, refer to Table 3.7.

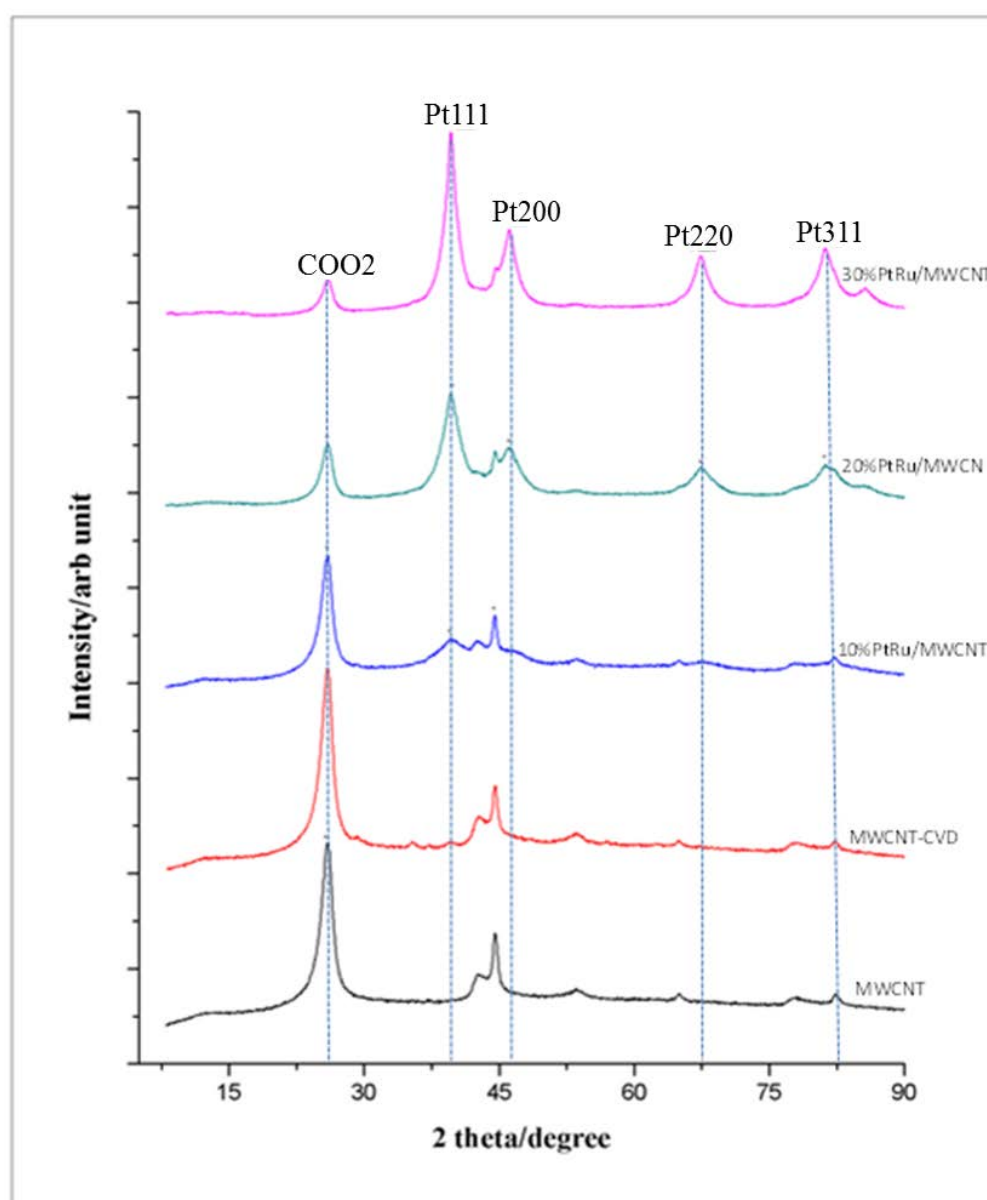


Figure 4.4: Various Pt/Ru compositions on the support of untreated MWCNTs support.

From the bottom up the Xray diffractograms of the MWCNTs and the catalysts are denoted as Black-MWCNT, Red-MWCNTs modified CVD, blue - A7, green – A6 and pink – A5 respectively.

MWCNT that was heat treatment with CVD and MWCNT that was not acid treated are also shown.

Figure 4.4 shows that there is a peak (C002) at 2θ around 25 degrees that is common to all spectra. In both treated and untreated MWCNT spectra there is a common peak around 45° , 52° , 65° and around 83° . As the literature shows Pt peaks are expected at 39.8; 46.2; 68.1; 81.4; and 86.7 degrees. In Figure 4.4 in the spectra of 10% (A7), 20% (A6) and 30% PtRu (A5), these peaks are observed. There is a peak observed at $45^{\circ} 2\theta$ for MWCNT, A7, A6 and A5, although it becomes a shoulder at A6 and A5. As the loading percentage of the composition of PtRu increases the intensity of the peaks increase and the peaks are becoming narrower.

According to Liu et al., (2011) Ru peaks at 2θ are observed at 38.3, 42.2, 44.0, 58.3, 69.4 and 78.4 which are assigned to the 100, 002, 101, 102, 110 and 103 respectively, which are diffraction planes of hexagonal close-packed (hcp) Ru metal. This is also confirmed by JCPDS card no. 06-0663. The shoulder peak approximately at 43,5 - 44 degree for A7, A6 and A5 in Figure 4.4 could be the indication of Ru's presence. This could confirm the overlapping of the 101 diffraction peak of C with the peak of 101 diffraction of hexagonal Ru metal, Liu et al., (2011) also observed the overlapping of peaks in their study. Peaks shift could be due to the evidence that accounts for formation of Pt Ru alloy in the catalyst.

Figure 4:5 shows the X-ray diffractograms of Pt loading on TiO₂/ MWCNT supports. Refer to section 3.7.6 for experimental loading for TiO₂ and to Table 3.7 for % metal loadings. The XRD of MWCNT/TiO₂ was not analysed as a blank.

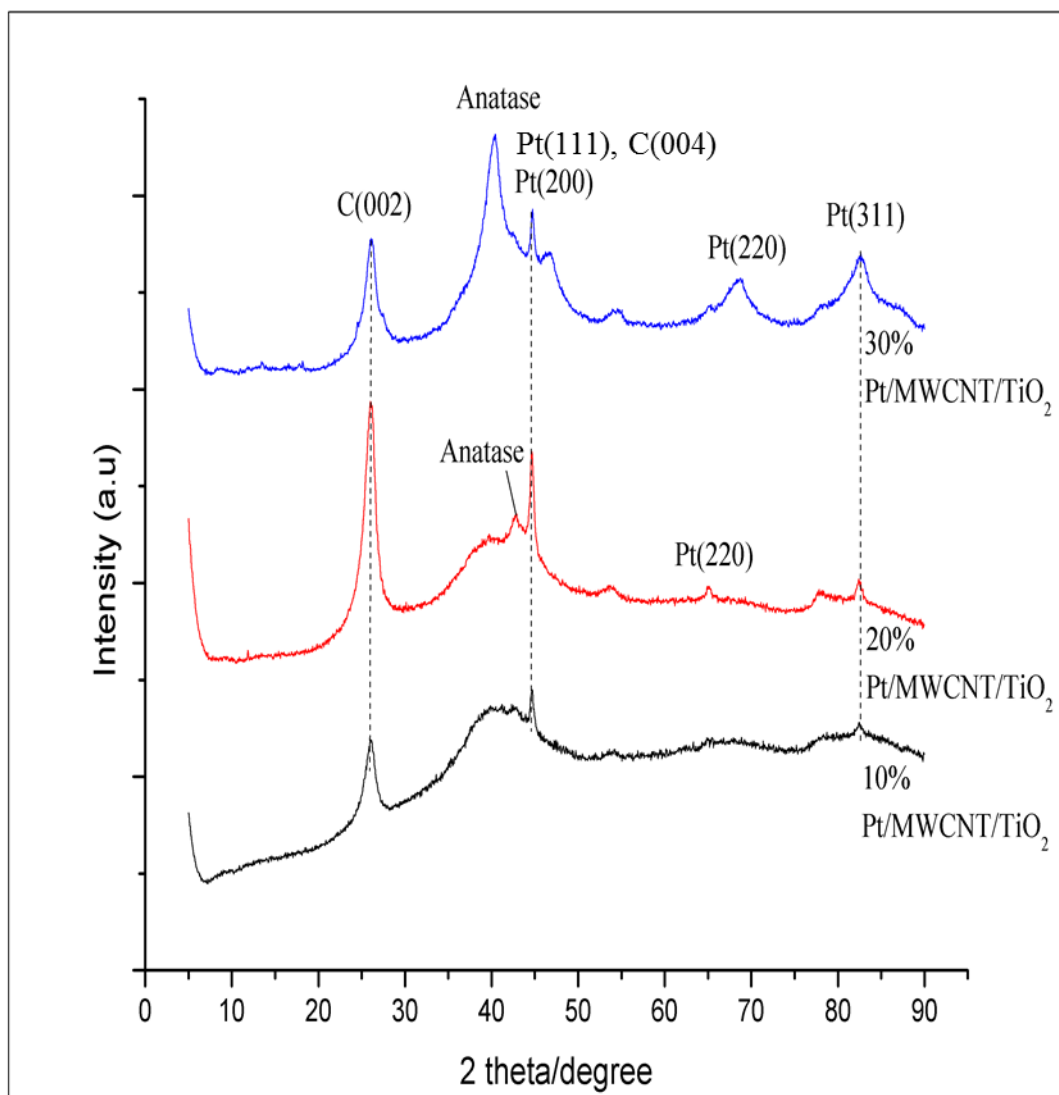


Figure 4.5: 10-30% Pt- MWCNT/TiO₂ (untreated) (A8-A10) catalyst prepared by the CVD method.

The XRD spectra were obtained to assess the effect of different platinum loadings on TiO₂/MWCNT support after CVD deposition as prepared in section 3.7.5.

Figure 4.5 demonstrates that the TiO₂ is crystalline and in the anatase form once deposited in TiO₂ using CVD on MWCNT samples which were not acid treated. As the platinum loading increased, the increasing peak intensities indicate that the anatase reflections as well as the Pt peaks became more defined with greater crystallinity. The Pt111 and anatase main peak overlap at 39.65 degree, and C (004) overlaps with Pt(200). Pt (311) was visible on 10% A8, 20%A9 and 30% A10 loaded samples, this could be probably due to inability of XRD to resolve at such low loading. This was also observed in XRD pattern of Figure 4.4. Around 68.1 degree Pt (220) is visible at A10, while there is shift that is observed at A9 and Pt(220) is not visible at A8 which 10% loaded. TiO₂ 2theta values are 24.8, 37.3, 47.6, 53.5, 55.1 and 62.2 respectively, Ba-Abbad et al., (2012). The JCPSDS card no. 21-1272 for anatase confirms values. The peaks at 25, 25.4 and 48 degree in the study by Ba-abbad et al., (2012) and Thamaphat et al.,(2008) confirmed anatase structure of TiO₂. Hence the peak around 37.4 degree confirms the anatase which is overlapping with Pt111 in Figure 4.5. Also around 55 degrees there are broader peaks that are observed in all three diffractograms which confirms anatase.

In Figure 4.6 the Xray diffractograms are shown of trimetallic catalysts on TiO₂ / MWCNT. The PtRuV/MWCNT/TiO₂, catalyst has been researched in this study. A portion of Pt was substituted with less expensive Vanadium to lower the overall cost of the catalyst. The experimental procedure is detailed in section 3.7.5. The metal ratios are as follow; 20:5:5 (A12) and 10:5:5 (A13).

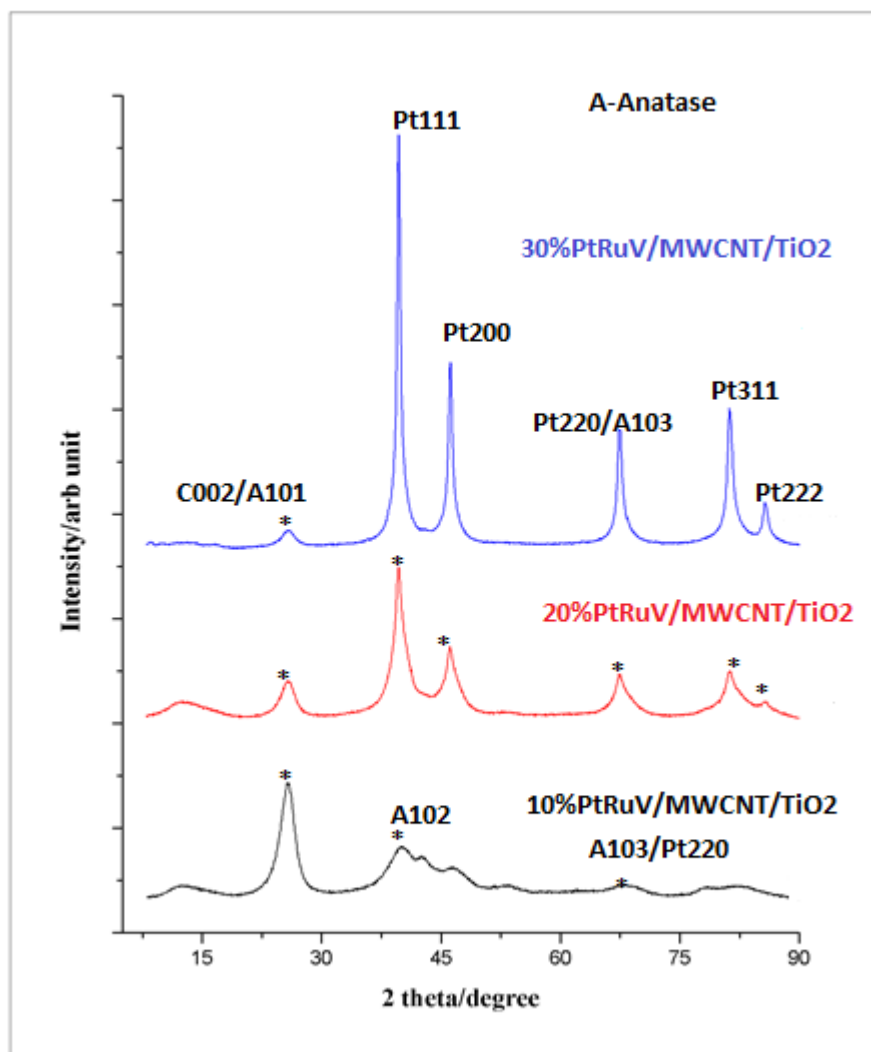


Figure 4.6: Xray diffractograms of different loadings of trimetallic catalysts on TiO_2 / MWCNT A12 and A13, trimetallic catalyst.

Figure 4.6 above shows the possibility of the overlapping of the graphene (C002) and anatase (A101) main peak at around $2\theta = 25.2$ degrees. This peak is assigned to both that of MWCNTs as well as the anatase form of TiO_2 respectively. The other peaks that overlapped are also observed at around $2\theta = 67/68$ degrees, which are assigned to Pt (220) and A (103), platinum and TiO_2 respectively. There were no metallic Ru, Fe and V diffraction peaks detected on the XRD patterns, which

indicated very small particles or alloyed PtRu or PtRuV or PtRuFeV. The study by Fu et al (2009) and Calderon et al (2012) also reported that no Ru peaks were observed.

The XRD spectra showed the presence of MWCNT carbon peaks on PtRu/MWCNT, PtRuVFe/MWCNT-TiO₂, PtRuV/MWCNT/TiO₂, Pt/MWCNT/TiO₂ and the peaks of the XRD confirm the formation of Pt as revealed by the peak at 2θ at 39° . On A13 there was shift observed on Pt (311) peak when comparing with A12 Pt (311) peak at 2θ . Around 37° 2θ there is an anatase overlapping with Pt111. There's another peak shift observed at 63° of Pt220/A103 on A13 compares with A12. The shift could be confirming that the alloying took place. According to Liu et al., (2011), the Vanadium peaks at 2θ are as follow; 21.6, 26.9, 32.3 and 45.3 degree, corresponding to 101, 110, 011 and 411 planes of V oxides. This is in agreement with JCPDS card no. 89-0612 that corresponds to orthorhombic structure.

In Figure 4.7 the Xray diffractograms are shown of multi-metallic catalysts on TiO₂ / MWCNT. The PtRuVFe/MWCNT/TiO₂, catalyst has been researched in this study.

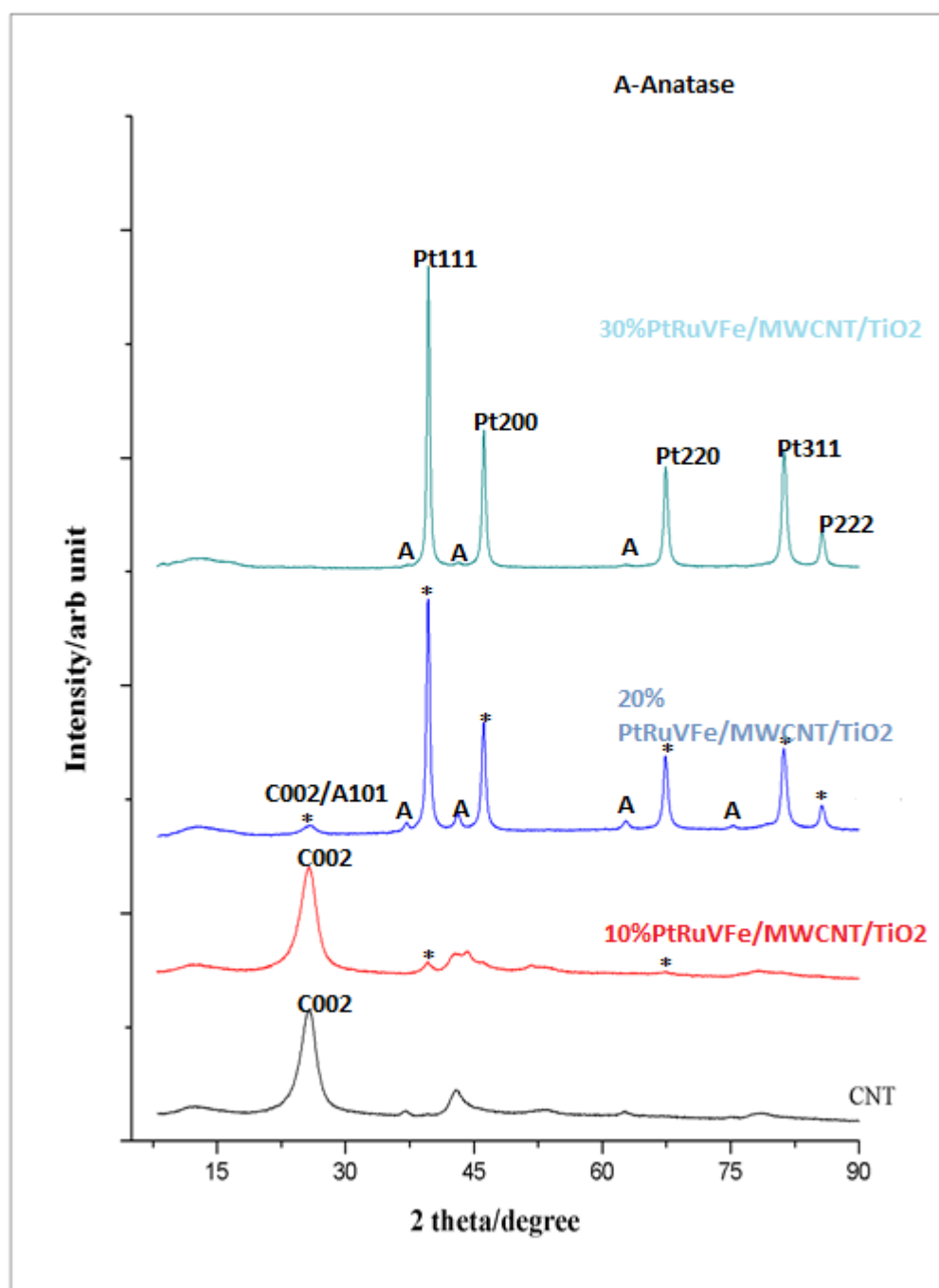


Figure 4.7: X-ray diffractograms of multi-metallic catalysts on TiO₂ / MWCNT [20%, 30% PtRuVFe/MWCNT/TiO₂, (A14, A15) multi-metallic catalyst.]

All the XRD patterns show the broadening diffraction peaks at around 2θ of C002 from MWCNT. This is assigned to hexagonal graphite

crystallographic planes (002) in carbon-nanotubes. This was also observed by Yang et al., (2012), Sebastian et al., (2012) and Negro et. al., (2015) in their study of electro-catalytic activity and durability of Pt-decorated non-covalently functionalised graphitic structures. These patterns exhibited the characteristic peaks corresponding to the Pt face centered cubic structure 111, 200, 220, and 311 reflection planes with characteristic of Miller indexes at $2\theta = 39.70^\circ$, 46.24° , 67.45° , 81.28° (Calderon et al 2012 and Fu et al 2009). There were no metallic Ru, Fe and V diffraction peaks detected on the XRD patterns, which was the indication of alloyed PtRu or PtRuV or PtRuFeV. The narrow peaks of A14 and A15 indicates that the samples were higher in crystallinity. Qin et al., (2011) observed the narrow peaks in their study, also mentioned that no other peaks were observed, which according to them, indicated high purity at prepared samples.

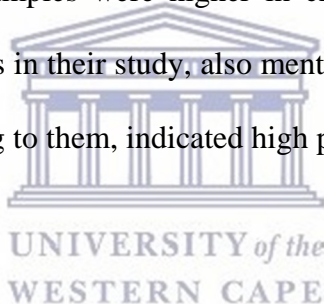
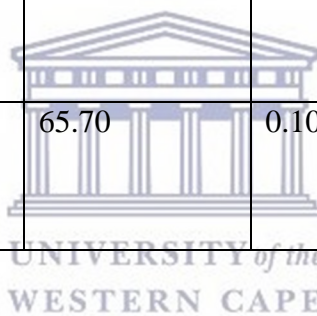


Table 4.2: Lattice parameter and crystalline size in nano-meter

Catalyst	Pt (220) position 2θ	Lattice parameter (nm)	Crystalline size (nm)
10% PtRu/MWCNT	67.58	0.1760	0.71
20% PtRu/MWCNT-	64.98	0.1220	1.06
30% PtRu/MWCNT	65.09	0.1031	1.25
10% PtRuV/MWCNT/TiO ₂	67.06	0.1620	0,78
20% PtRuV/MWCNT/TiO ₂	64.90	0.0811	1.60
30% PtRuV/MWCNT/TiO ₂	67.87	0.1488	0.84
20% PtRuFeV MWCNT/TiO ₂	65.46	0.0795	1.62
30% PtRuFeV MWCNT/TiO ₂	65.70	0.1078	1.19



4.2 FTIR results

FTIR spectra of supports and the commercial baseline catalyst JM are presented in this section.

Figure 4.8 shows FTIR spectra for Activated carbon and JM Pt/C

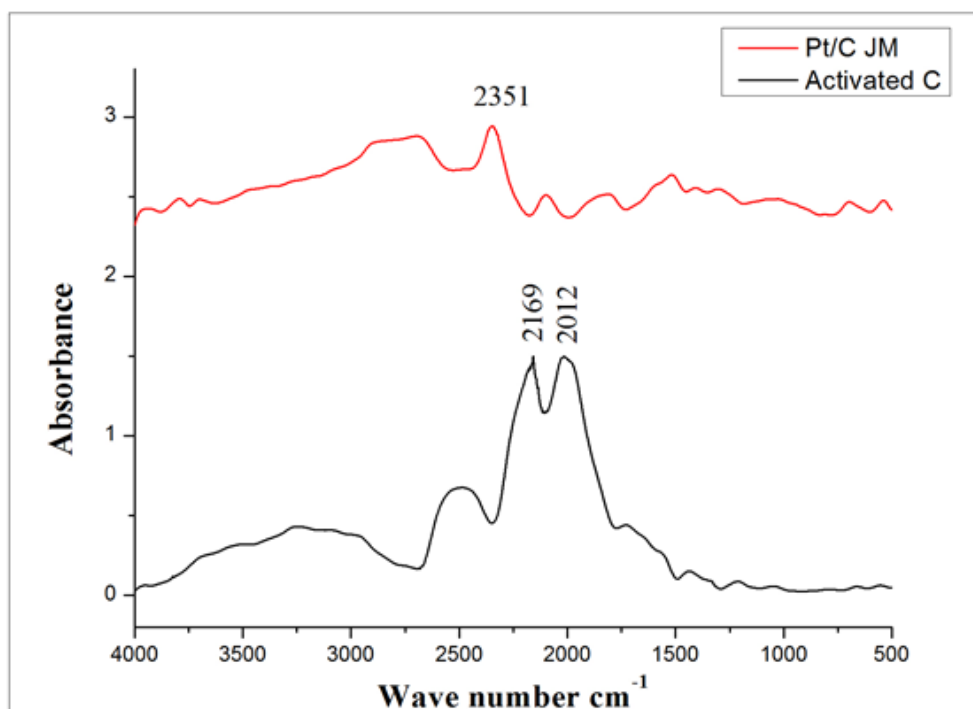


Figure 4.8: Comparison of a FTIR for activated carbon and JM Pt/C

The structures were investigated by FTIR. The two carbon supports were plotted on the same axis and compared. As observed in the Figure 4.8 above, both curves showed various types of functional groups. The bands at 2351 and 2169 cm⁻¹ are assigned to C-H stretching vibrations. The band at 2012 cm⁻¹ demonstrates the C=O group and -OH appears at 3260 cm⁻¹ and 3249 cm⁻¹. The JM Pt/C plotted on the same axis shows the shoulder that corresponds to the to the C-H stretching vibration around 2351 cm⁻¹.

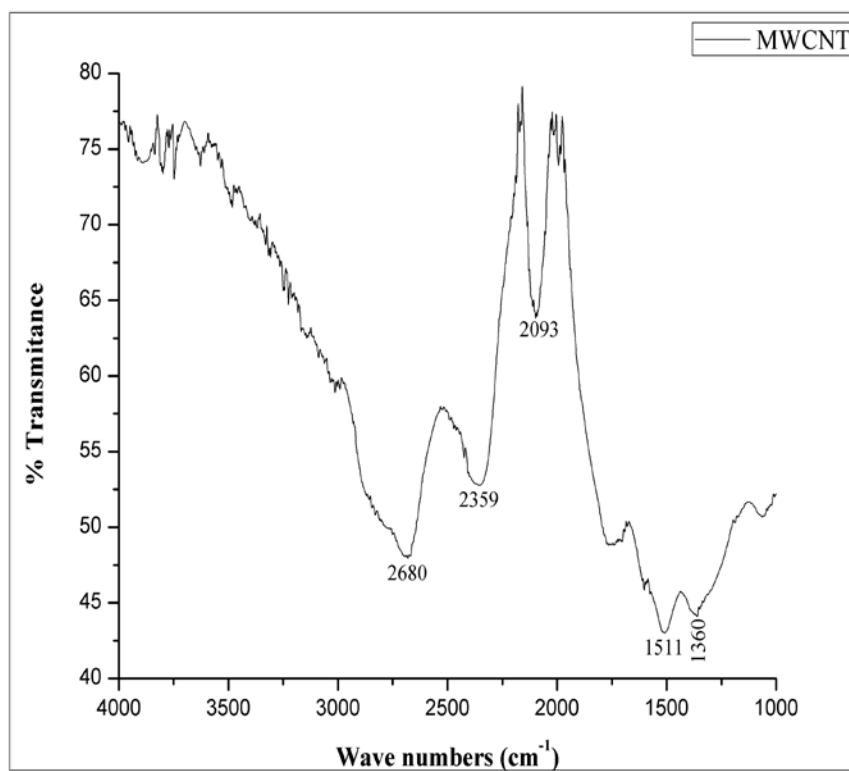


Figure 4.9: FTIR spectra of MWCNT.

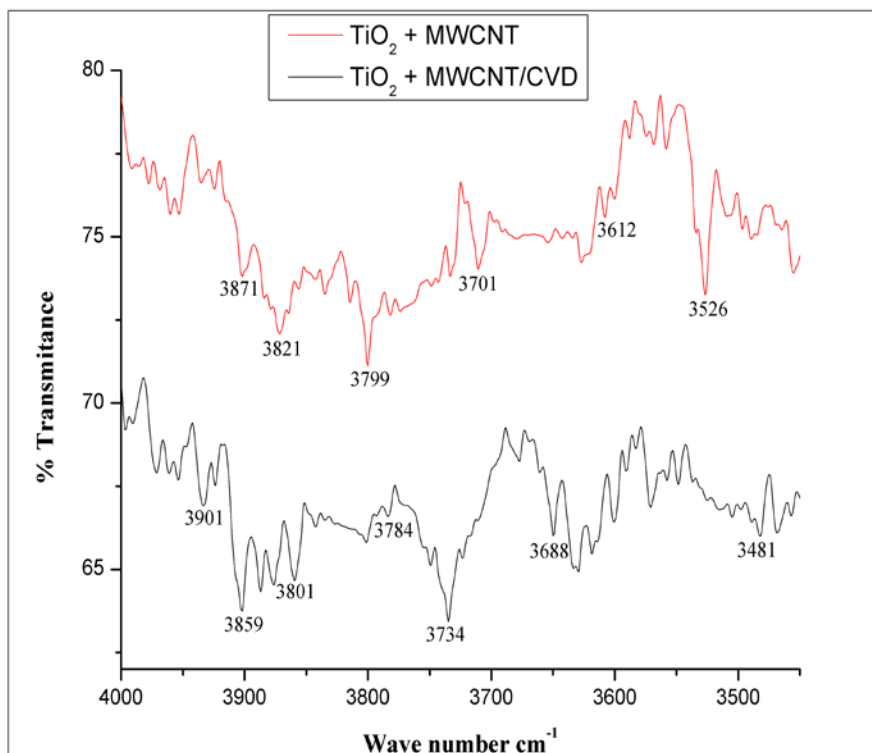


Figure 4.10: FTIR spectra of MWCNT/TiO₂ and MWCNT/TiO₂ (CVD).

In Figure 4.9 MWCNT, the broad band observed at 2680 cm⁻¹ was assigned to OH stretching. In Figure 4.9 the band at 1360 cm⁻¹ is assigned to CH in plane bending and that at 1511 cm⁻¹ could be associated with the stretching of the carbon nanotube backbone (Abuilaiwi et al., 2010). In Figure 4.10 the bands observed at 3734 cm⁻¹ and 3799 cm⁻¹ are assigned to the intermolecular hydrogen bonding of hydroxyl groups in MWCNT. There is a band shift after the heating (CVD) that is observed. The peaks at 3481 cm⁻¹ to 3612 cm⁻¹ are assigned to OH free stretching. There were no TiO₂ bands observed.

4.2.1 FT-IR of metal loaded MWCNT samples

The FT-IR spectra of PtRuV/MWCNT with and without TiO₂ and synthesised nano-materials in the range are shown in FTIR Figure 4.11 below.

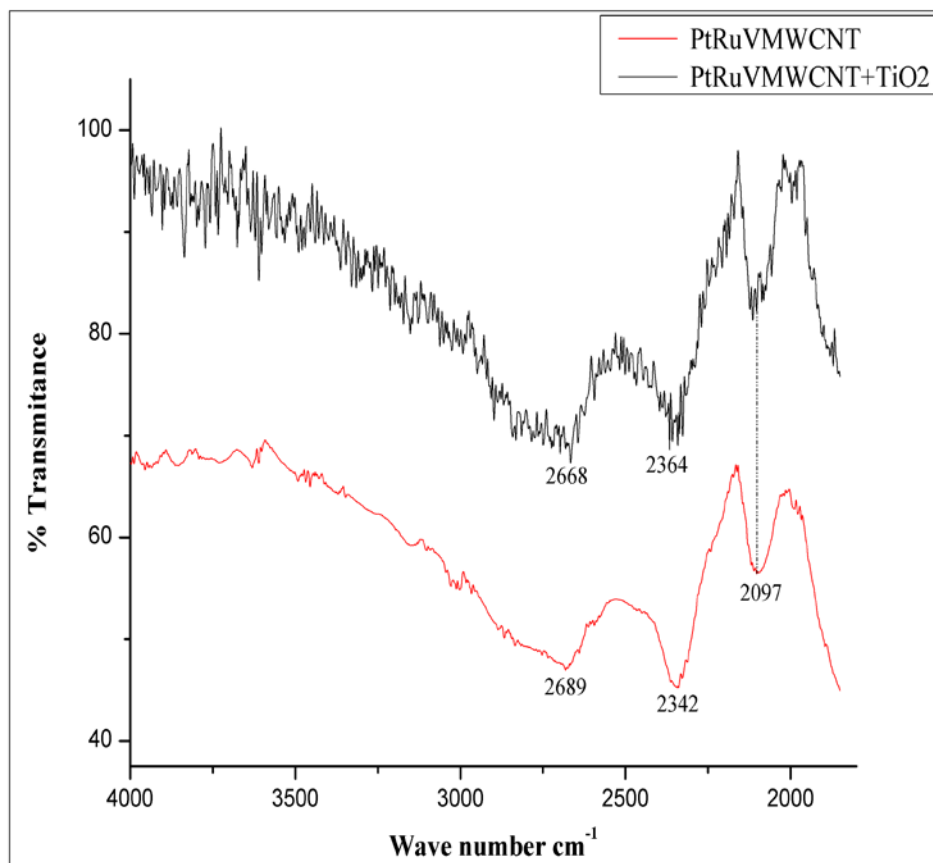


Figure 4.11: 10% PtRuV/MWCNT & 10% PtRuV/MWCNT/TiO₂ on the same axis .

In Figure 4.11, giving the spectrum of the 10% PtRuV/MWCNT and 10% PtRuV/MWCNT/TiO₂ both show spectra show a band which is assigned to CO adsorbed on platinum metal particles at 2097 cm⁻¹. There other catalysts were not tested by FTIR as the technique did not give relevant information.

4.3 Morphology of electrocatalyst, activated carbon and MWCNT

The HRSEM was utilised for structural identification and morphology study of MWCNT, activated carbon and the supported commercial JM Pt/C electrocatalyst. Morphological investigations were conducted by HRSEM and EDS following the procedure outlined in Section 3.6.1. The elemental content of MWCNT was conducted. The EDS revealed that the atomic % of carbon in the MWCNT was 99% and the other 0.44% was an atomic % of nickel, probably due to the Ni catalyst used to grow the MWCNT.

4.3.1 Support morphology compared to JM Pt/C catalyst

The HRSEM microgram for activated carbon is shown in Figure 4.12

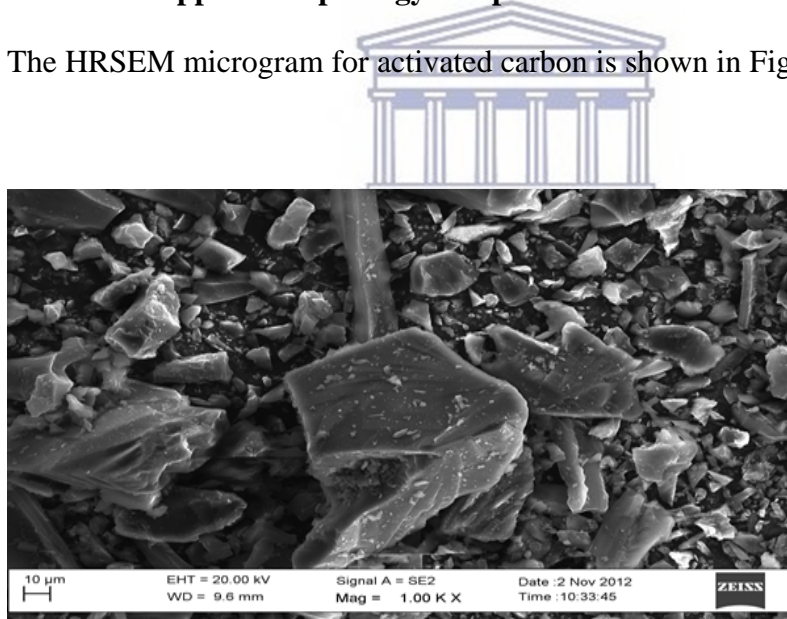


Figure 4.12: HRSEM for activated carbon.

4.3.2 Commercial electro-catalyst morphology

Figure 4.13 shows the morphology of the commercial JM electro-catalyst which was investigated using HRSEM following the procedure given in Section 3.6.1.

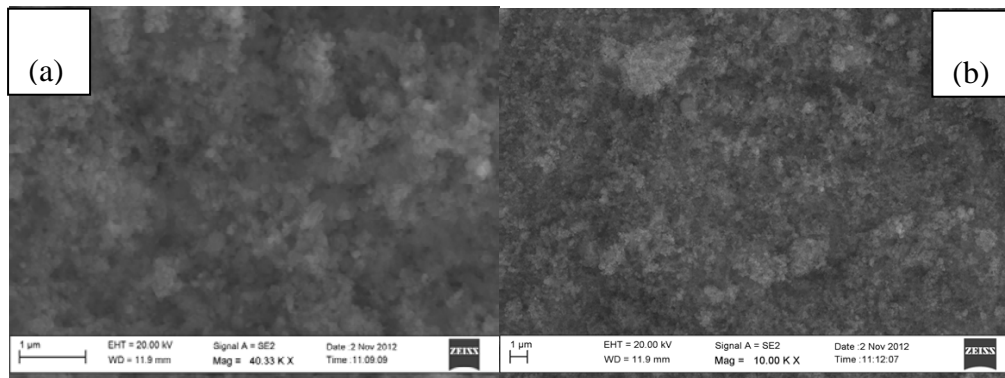


Figure 4.13: HRSEM images of JM Platinum/C electro-catalyst.

In Figures 4.13 (a & b), the image was obtained at different magnifications, in order to obtain a better image. As observed the coated images are still showing ill-defined images of the commercial electro-catalyst. The surface roughness is relevant for transport behaviour of carbons. Statistical parameters according to Artyushkova et al (2012) increase as the amount of pores (dark values) increases.

The following image are the morphology of MWCNTs which was conducted using HRSEM following the procedure given in Section 3.6.1. The following images were conducted at different magnifications. In Figure 4.14 the untreated MWCNT is shown.

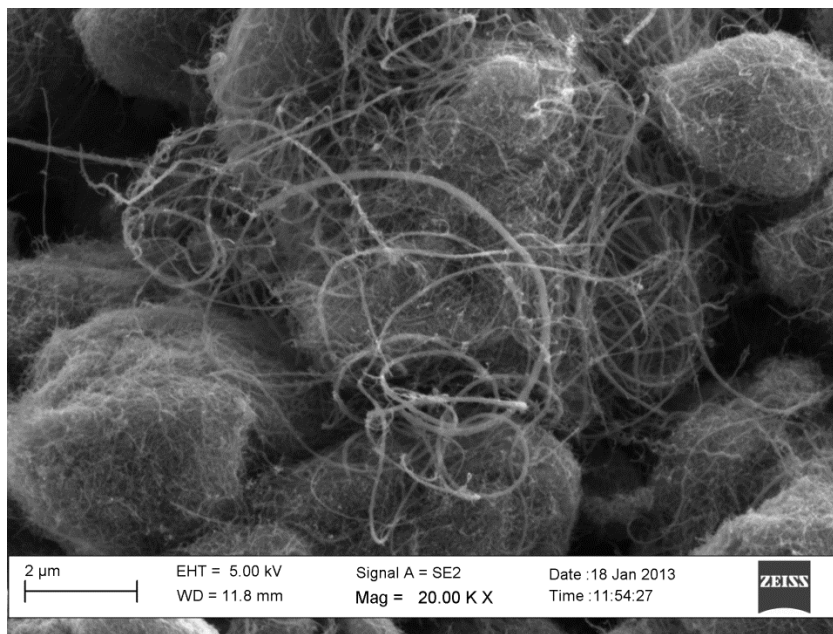


Figure 4.14: SEM image of Untreated MWCNTs.

The following images are the morphology of acid treated MWCNTs which were obtained using HRSEM following the procedure given in Section 3.6.1. The following images were obtained at different magnifications. The acid treatment of MWCNT was conducted following the pre-treatment procedure in section 3.4.

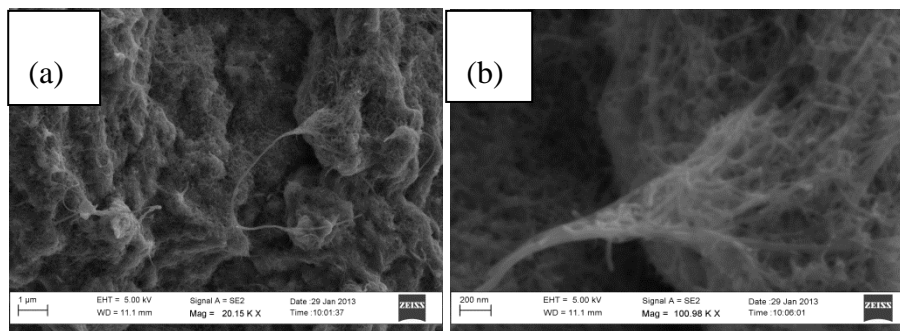


Figure 4.15: (a & b) HRSEM images of acid treated MWCNT.

Two types of MWCNTs were characterised by HRSEM, MWCNT and acid treated MWCNT samples Figure 4.15 (a & b). Acid treated MWCNT were observed to be similar to the untreated MWCNT. The morphology of acid treated MWCNT was smooth. During acid treatment, surface structure of MWCNTs was modified mainly at the end of the nanotubes.

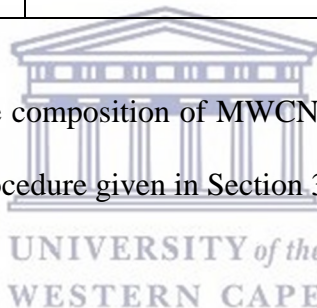
Energy dispersive spectroscopy (EDS) detector which is connected to the HRSEM was used to investigate the element composition of the MWCNT.

Table 4.3 represents the EDS results of the elemental composition of acid treated MWCNT.

Table 4.3: EDS composition for element in acid treated MWCNT

Element	Atomic %
Carbon	99.56
Nickel	0.44
Total	100

EDS in Table 4.3 give the composition of MWCNTs which was conducted using HRSEM following the procedure given in Section 3.6.1.



4.4 Structural characterisation using HRTEM

HRTEM was conducted to study the morphology of the carbon nanotubes and electro-catalysts. It was used to determine the particle size and the particle size distribution of the electro-catalysts in order to support the XRD studies. The morphology was determined using the HRTEM procedure given in section 3.6.4. This section will be presenting the structural characterisation and interpretation of results for MWCNTs acid treated and untreated, commercial electro-catalyst and home-made electro-catalyst with various loadings of metals.

4.4.1 Structural images of commercial JM Pt/C electro-catalyst

The following Figures 4.16(a-b) represent the HRTEM images of a commercial JM Pt/C. The electro-catalyst was imaged using HRTEM following the procedure in section 3.6.4.

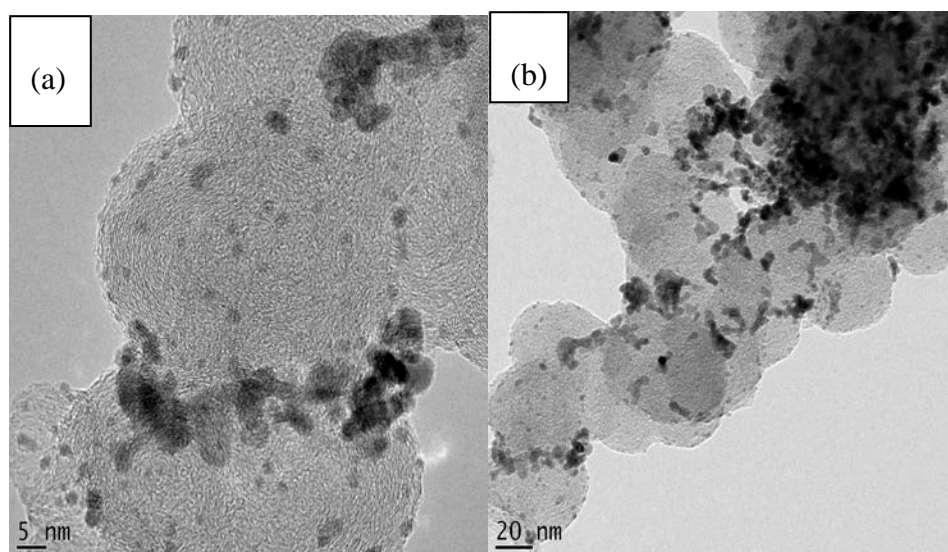


Figure 4.16:(a - b) HRTEM images of a commercial JM platinum/ carbon.

In Figure 4.16 (a – b) the platinum dispersion is observed on carbon; however, the presence of some particle agglomeration can be seen. The presence of agglomeration may be due to the amount of Pt added. HRTEM showed that the platinum is not evenly dispersed on carbon, but particles are cluster.

Figure 4.17 represents the SAED of the commercial JM Pt/C.

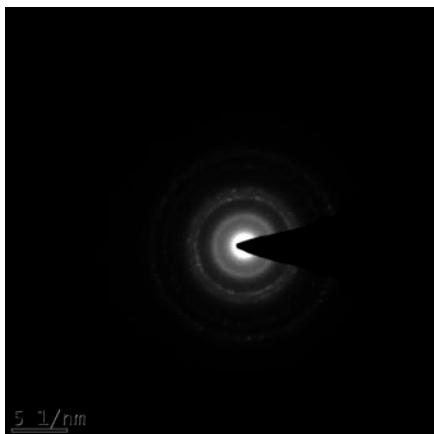


Figure 4.17: Selected Area Electron Diffraction (SAED) for commercial Pt/C.

The carbon support is visible in the HRTEM micrographs, as large grey particles with the small black Pt particles distributed upon them. It was easy to identify the Pt nanoparticles, due to their higher density than the carbon, enhancing the contrast between them. SAED in Figure 4.17 showed the diffuse rings related to polycrystalline materials (Chan et al., (2011).

4.4.2 Structural images of MWCNT as received

The following images show the HRTEM images for MWCNT (Multi-walled carbon-nanotubes) which are commercial.

Figures 4.18 and Figure 4.19 are HRTEM images of MWCNT that were not acid treated.

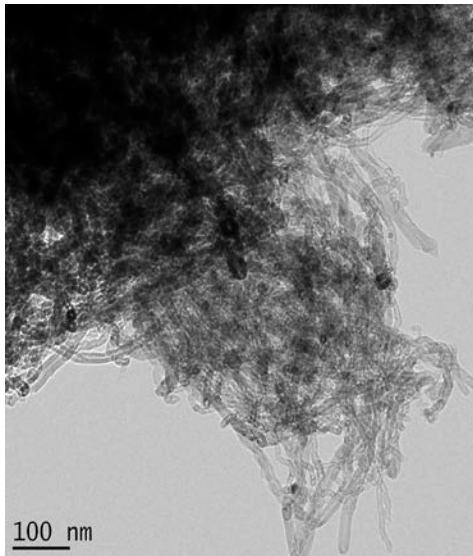


Figure 4.18: HRTEM image for MWCNT.

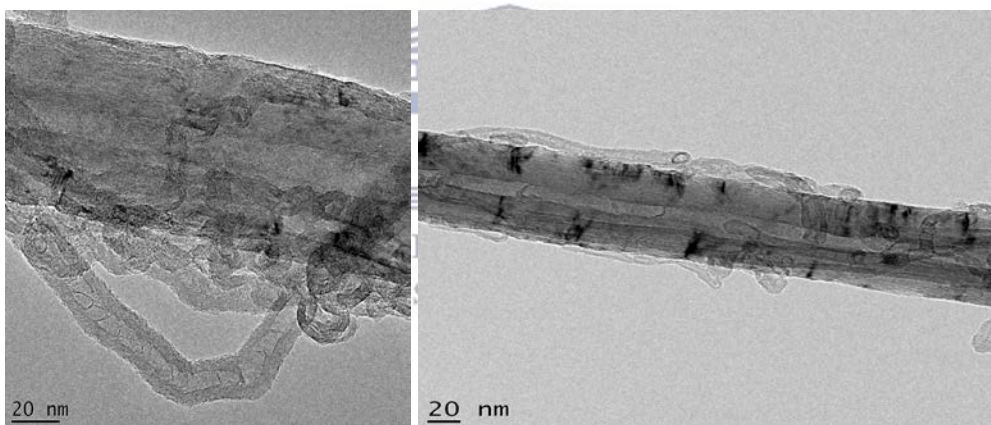


Figure 4.19: HRTEM bright-field micrographs without purification, for a commercial MWCNT (Multi-walled carbon nanotube).

In Figure 4.19 the bright field micrograph shows that the MWCNT are agglomerated together. Li et al., (2003) observed in their research that MWCNT are packed together because they are accompanied by many carbon nanoparticles and carbonaceous impurities. Figure 4.20 dark spots were observed which may be due to Ni impurities as mentioned in Table 4.2 for EDS.

4.4.3 Structural images of acid treated MWCNT

The following HRTEM images are for acid treated MWCNT. The following acids (sulphuric acid and nitric acid) were used to treat multi-walled carbon nanotubes.

Figures 4.21 (a-c) shows the images of acid treated MWCNT, with sulphuric acid and nitric acid following the pre-treatment procedure in section 3.4. In the pre-treatment process both sulphuric acid and nitric acid were mixed together at a volume ratio of 3:1 v/v. This treatment process was called the chemical etching method.

MWCNTs were treated using sulphuric and nitric acid mixture. The un-purified MWCNT were immersed in an ethanol solution and sonicated prior to the HRTEM analysis.

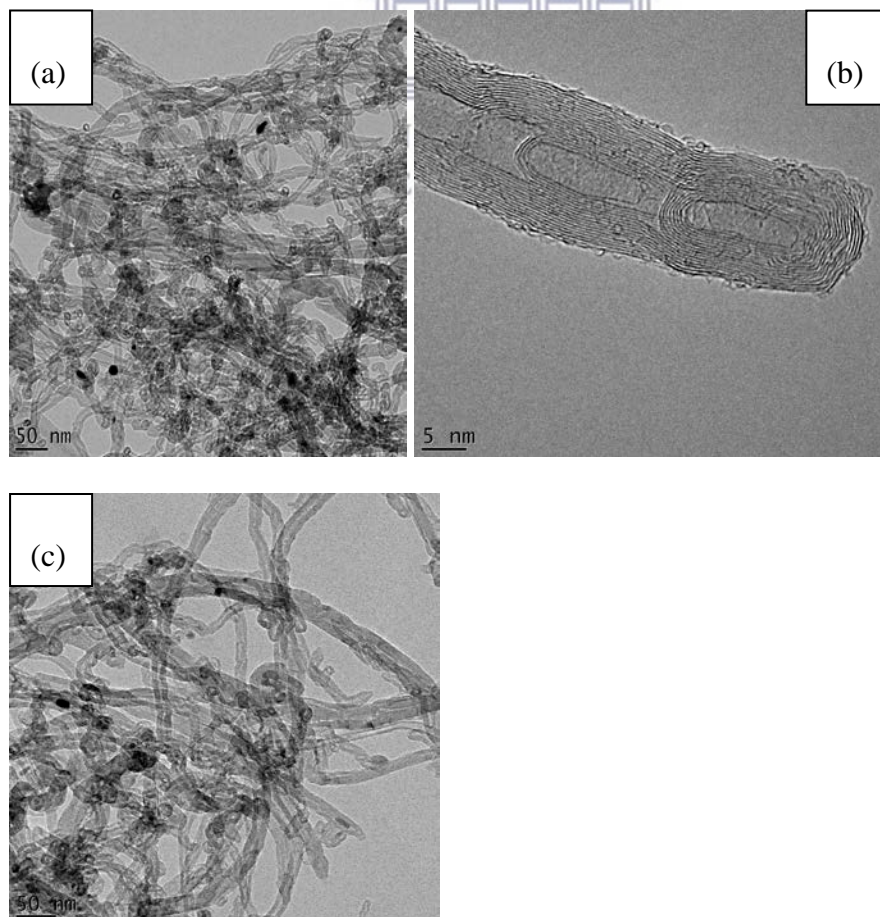


Figure 4.20: (a – c) HRTEM are bright-field micrographs for acid treated MWCNT that were purified with $\text{H}_2\text{SO}_4\text{-HNO}_3$.

It can be seen that most MWCNTs were isolated and slight agglomeration was observed. The purification or modification with acid could result in an increase in the density of functional groups on the acid modified MWCNTs, FTIR have given some insight among the functional groups could be carboxyl, hydroxyl and carbonyl groups. In Figure 4.2 of treated MWCNT the tubular structure of the carbon nanotubes was observed, and low nickel impurities were present as shown in EDS presented in Table 4.3. Li et al., (2003) also mentioned that the MWCNTs were treated by acid and slow oxidation in a mixture of nitric-sulphuric acid.

4.6 Electro-catalysts morphology

This section will be presenting the HRTEM micrographs and EDS used for structural characterisation and interpretation of results for various electro-catalysts. The procedure that was followed is presented in section 3.6.4. The electro-catalysts were supported upon MWCNT and TiO_2 as metal oxide. MWCNTs were coated or decorated using CVD, following the procedure as detailed in section 3.5. CVD is a dry mix method which is faster, with no wet preparation required. The following high resolution HRTEM images illustrate electro-catalyst samples' morphology which provides insight into the structure of the catalysts. The HRTEM images showed the successful attachment of metallic nanoparticles upon the MWCNT/ TiO_2 support. Figure 4.22 presents the images of 30% PtRu-MWCNT

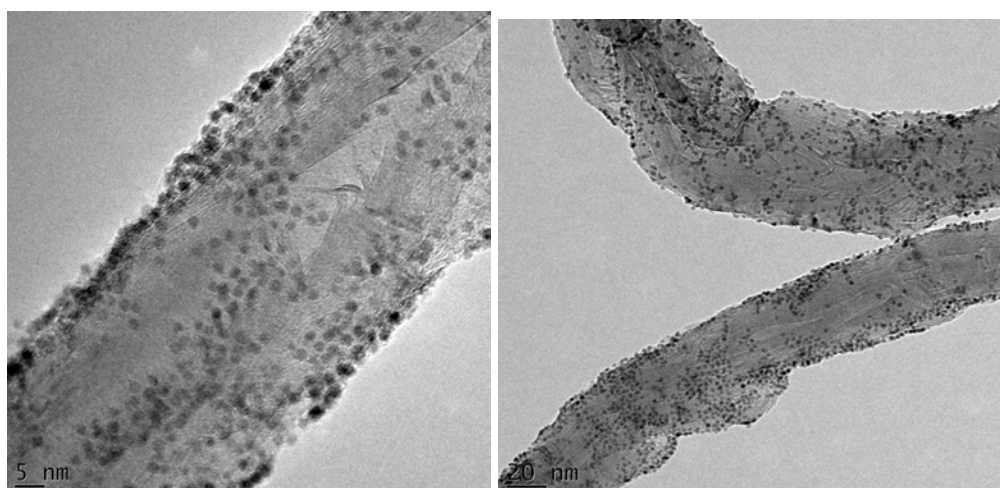


Figure 4.21: 30% PtRu-MWCNT

Figures 4.22 presenting the images of 30% PtRuV-MWCNT/TiO₂

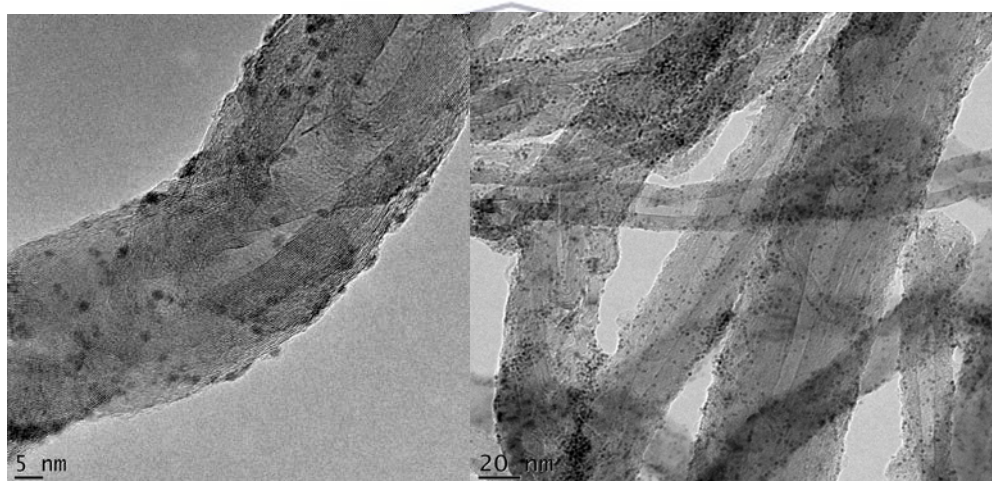


Figure 4.22: 30%PtRuV-MWCNT/TiO₂

Figures 4.23 presenting the images of 30% PtRuVFe-MWCNT/TiO₂

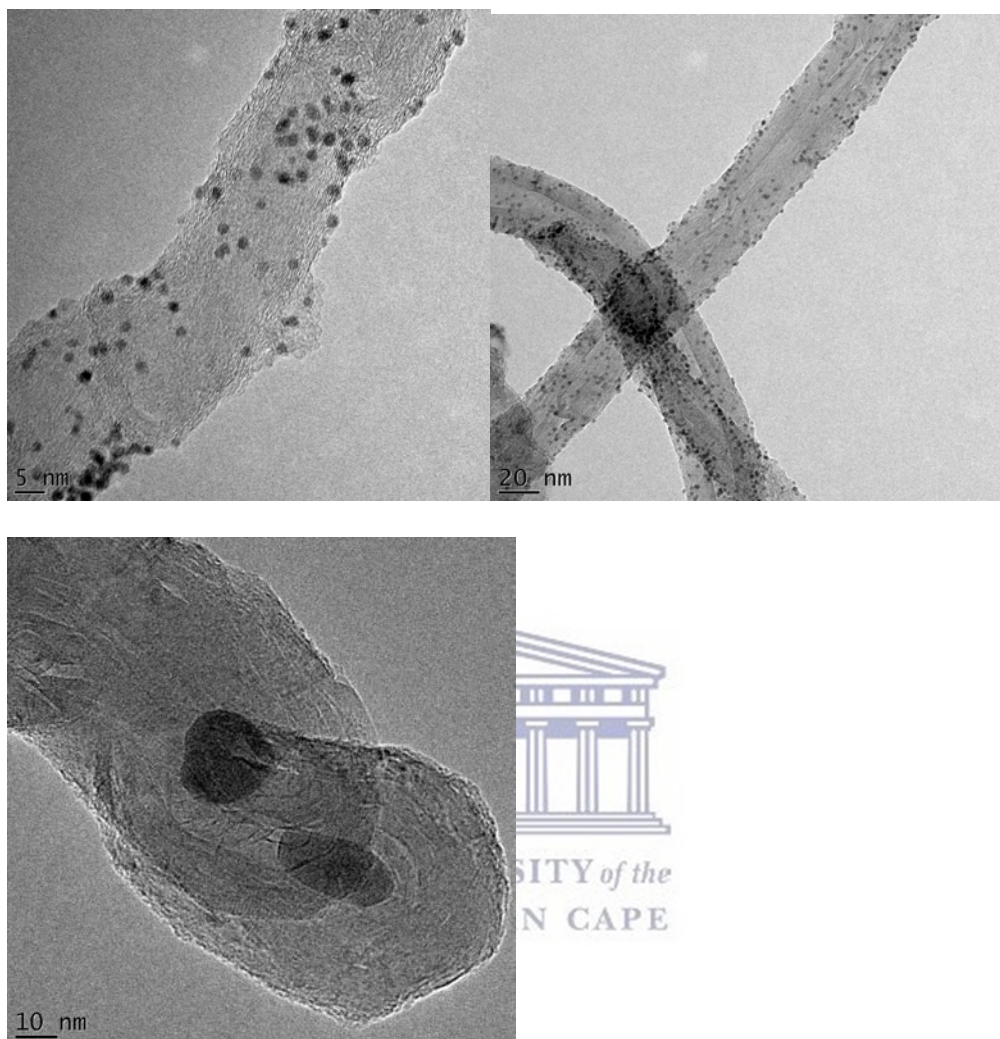


Figure 4.23: 30%PtRuVFe-MWCNT/TiO₂.

The MWCNT support is visible in all the micrographs, with the small black particles on them.

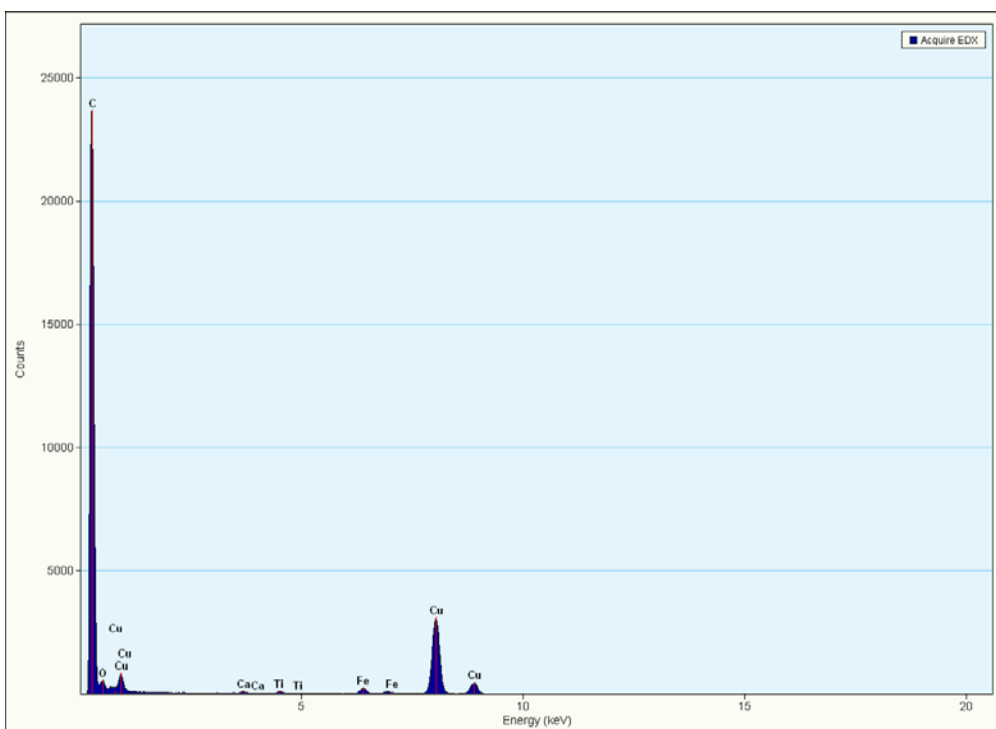
HRTEM has shown that the support was well coated with the metals that were dispersed uniformly with some agglomeration. The loading of MWCNT/TiO₂ as supports showed a similar morphology compared to the MWCNT on its own. The study also shown that platinum group metal (PGM) could be loaded upon the MWCNT with various mixed metals deposited evenly on the MWCNT support.

HRTEM images show slight agglomeration, however metal nanoparticles are generally well dispersed on the carbon support without formation of clusters.

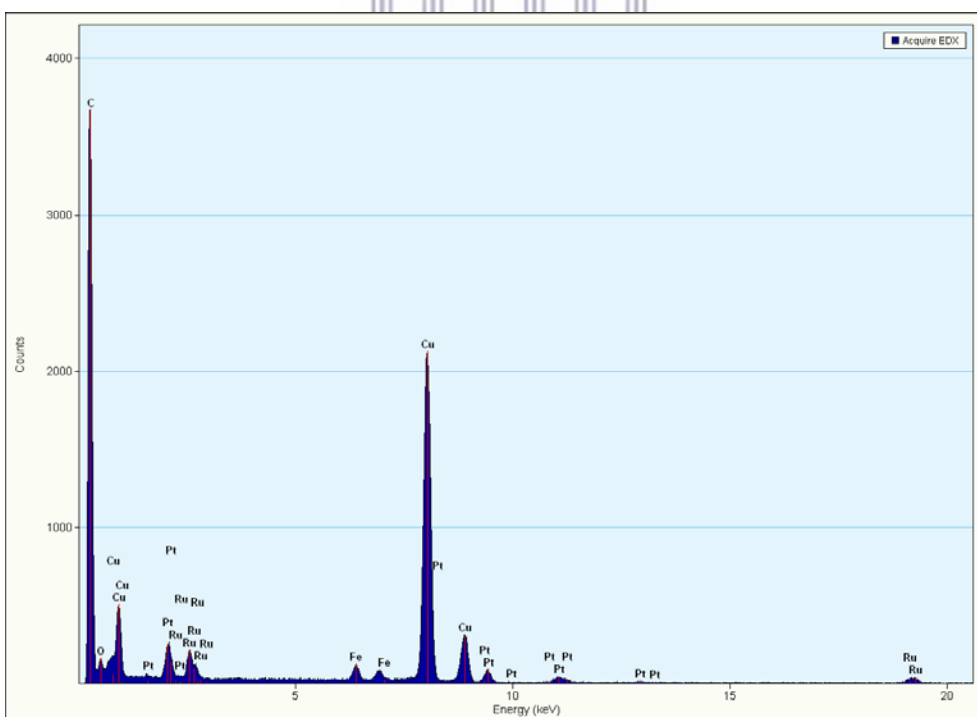
Generally, the micrographs show that the metals' clusters were at the range of the nanometer scale as they are not visible on the images as clusters, unlike the JM catalyst which showed a lot of agglomeration. As observed from Figures 4.21, 4.22, and 4.23, the catalysts were dispersed uniformly and without agglomeration upon TiO₂/MWCNT support. The catalyst showed a well-separated nanoparticle by the combination of the additional metals with Pt. In addition, 30%PtRuVFe-MWCNT/TiO₂ showed a better dispersion than catalyst 30%PtRu-MWCNT, while in the case of 30%PtRuV-MWCNT/TiO₂ bigger particles were observed. 30%PtRuV-MWCNT/TiO₂ catalyst showed a smaller crystalline size in 0.84 nm in XRD analysis as presented in Table 4.2. The smaller crystalline size leads to a bigger surface area and may produce better electro-catalytic activity of the catalyst. This will be further confirmed by electrochemical-activity analysis in section 4.7.

EDS for the various catalysts

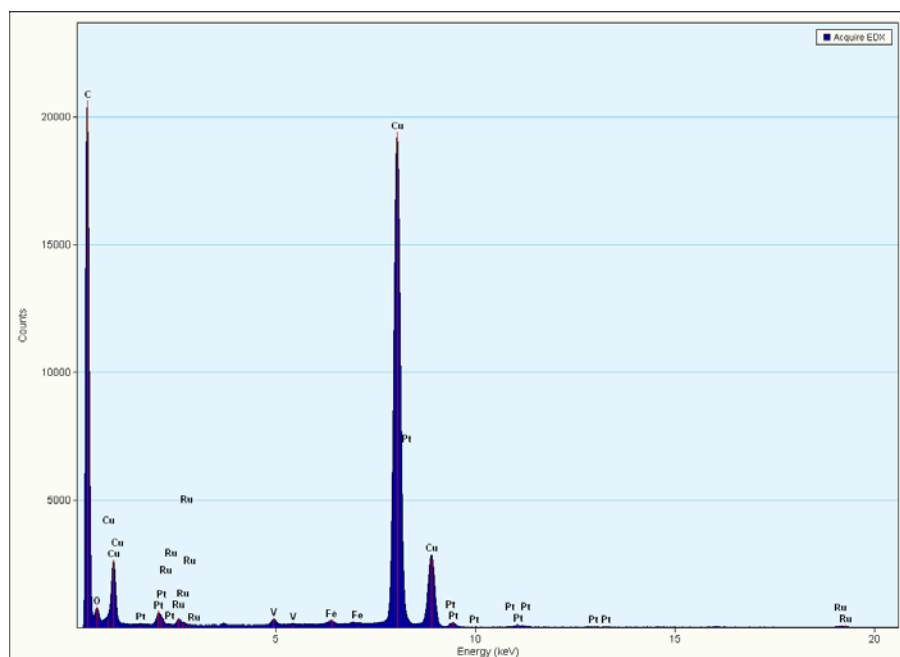
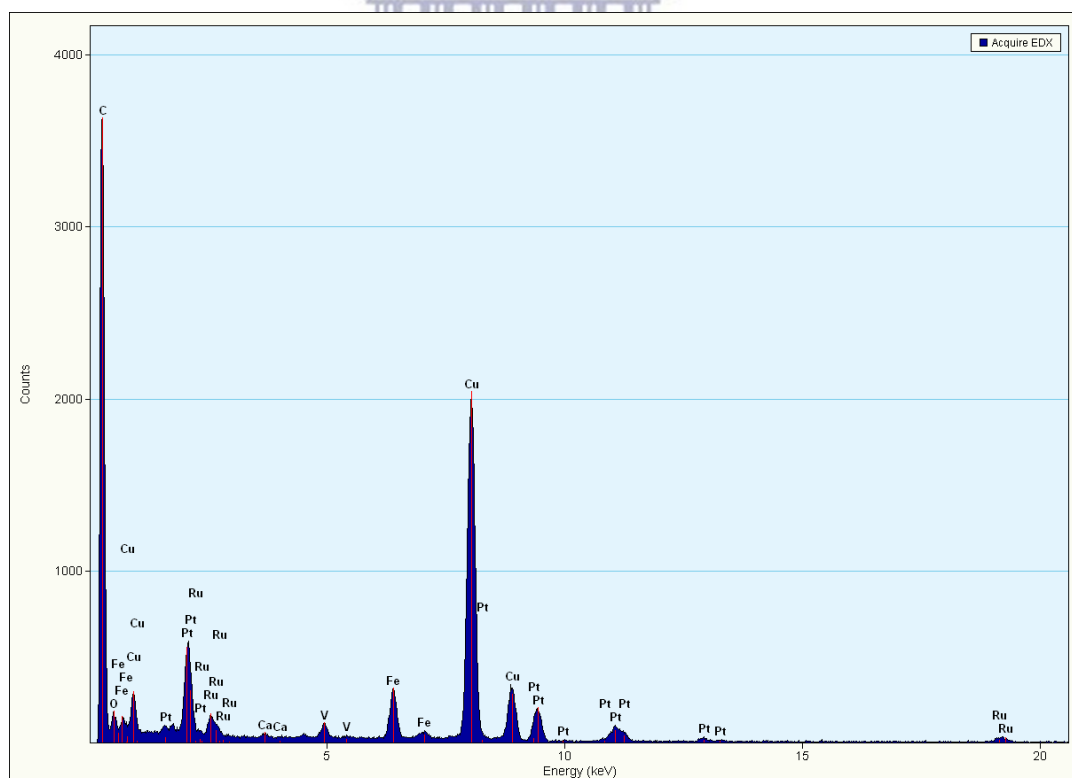
The elemental composition was investigated using Energy dispersive spectroscopic (EDS) emission analysis with HRTEM. EDS is telling what is present on the surface of the sample. The EDS for A-MWCNT/TiO₂, B-30%PtRu-MWCNT, C-30%PtRuV-MWCNT/TiO₂ and D-30%PtRuVFe-MWCNT/TiO₂ can be seen below.



A- MWCNT/TiO₂ EDS



B-30% PtRu/MWCNTs

C-30% PtRuV/MWCNT-TiO₂D-30% PtRuVFe/MWCNT-TiO₂

In EDS of A-MWCNT/TiO₂ some trace amount of Fe metal is observed, this might be due to the Fe nanoparticles used as a catalyst. This shows that the

supplier used Fe as a catalyst during the synthesis of MWCNTs. In all EDSs there is copper metal observed this is due on a standard copper grid that is used when depositing a drop of suspension. In EDS A the MWCNTs is in abundance and some Ti metal is observed; only 15% of TiO₂ was used in this study. In EDS-B Pt and Ru metals are observed in MWCNT support. In EDS-C Pt, Ru and V are observed, although it seems that there is some overlapping of metals Pt and Ru. The peaks are not distinct because of the overlapping although they are showing. Pt, Ru, V, and Fe metals are observed in EDS-D, and also the Pt and Ru showed some overlapping. In C-30%PtRuV and D- PtRuVFe/MWCNT-TiO₂ overlapping of Pt Ru is observed.

4.7 Cyclic voltammetry results and discussion

This section presents the results of the characterisation using cyclic voltammetry as a technique of platinum catalysts with PGM/noble metals loading supported on MWCNT or MWCNT/TiO₂. For the electro-catalysis analysis, the following catalysts were chosen in this study 30%PtRu/MWCNT, 30%PtRuV/MWCNT-TiO₂ and 30%PtRuVFe/MWCNT-TiO₂. In each catalyst there is a metal added, this was done to investigate if the additional metal will lower the amount of Pt as it is costly. Also to observe, if a portion of Pt was substituted, will this lower the overall cost of the catalyst.

The following figures show the various cyclic voltammograms of selected catalysts. The methanol oxidation reaction was measured in 0.5 M aqueous sulphuric acid (H₂SO₄) and 0.5 M aqueous methanol (CH₃OH) at a scan rate of 10, 20, or 50 mVs⁻¹. The glassy-carbon was used as a working electrode, Ag/AgCl

as a reference electrode and a platinum wire as a counter electrode. The sulphuric acid and methanol solution were saturated with nitrogen (N_2). The CVs in 0.5 H_2SO_4 only or with both H_2SO_4 and 0.5 M methanol solutions, respectively, were scanned between the potential windows of -0.2 to 1.0 V.

Cyclic voltammograms of in-house prepared different catalysts are presented below. The CVs of 30% PtRuMWCNT, 30% PtRuVFeMWCNT/ TiO_2 and 30% PtRuV MWCNT/ TiO_2 are shown below in Figures (4.24, 4.25 and 4.26) and Figures 0.1, 0.2, 0.3, 0.4, 0.5, 0.6, 0.7, 0.8, and 0.9 are shown on the Appendices at different scan rates. The baseline with MWCNT & TiO_2 /MWCNT was not characterised on their own.

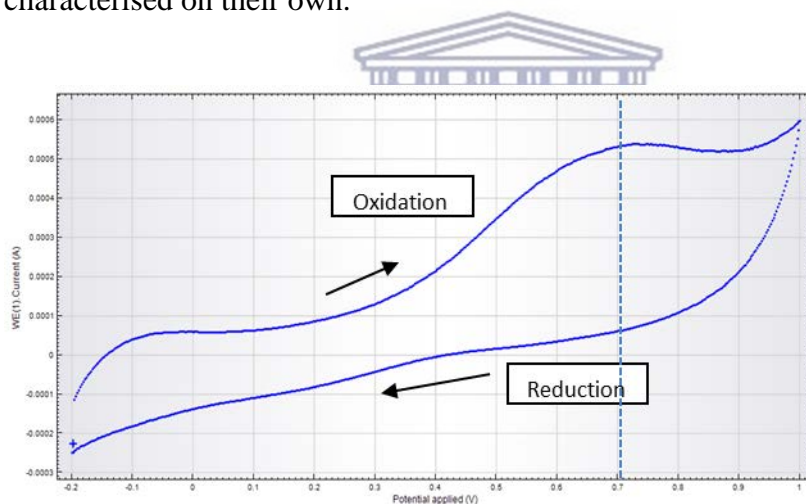


Figure 4.24: Cyclic voltammogram of 30%PtRuMWCNT ($20mVs^{-1}$) electro-catalyst with $H_2SO_4 + CH_3OH$.

The typical shape of the cyclic voltammograms is observed at all sweep rates in acid solutions only. The shape changes once the methanol has been added at all the different scan rates, and the methanol oxidation peak is evident at between +0.7 – 0.8V at all scan rates and all the rest of the scans were done at $20mV/s^{-1}$.

The rectangular shape in this voltammogram shows a sharp cathodic peak like the but the oxygen reduction peak on the reverse scan is evident at a potential of 0.44V, at Figure 4.31.

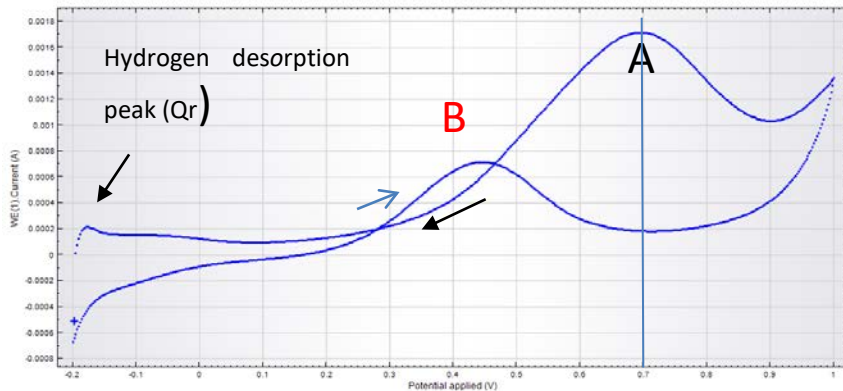


Figure 4.25: Cyclic voltammogram 30% PtRuVFeMWCNT/TiO₂ (20mVs⁻¹) electro-catalyst with H₂SO₄ + CH₃OH.

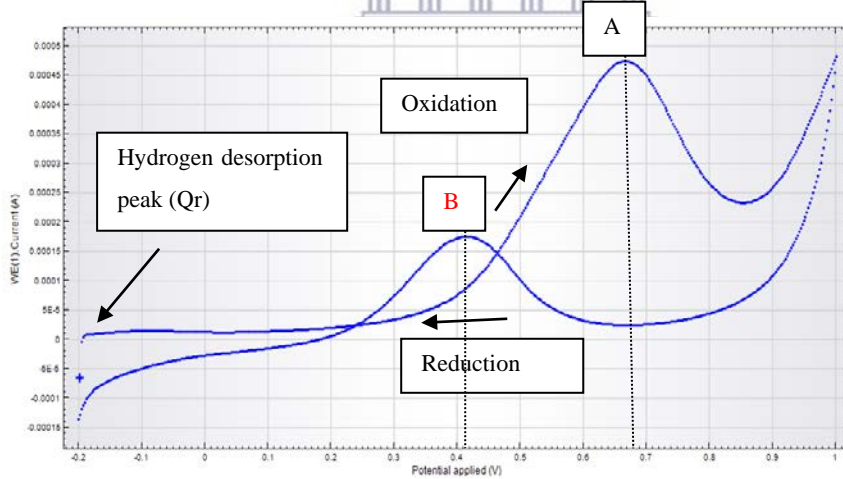


Figure 4.26: Cyclic voltammogram 30% PtRuV MWCNT/TiO₂ (20mVs⁻¹) electro-catalyst with H₂SO₄ + CH₃OH.

In Figure 0.6 & Figure 4.25 the catalyst with PtRuVFe showed the hydrogen desorption peak around -0.22 to -0.25 V and an oxygen reduction peak from potential 0.3 to 0.6 V. These results indicate that all catalysts are active for

hydrogen desorption and oxygen reduction which were enhanced according to the areas of the reaction with methanol. In Figure 4.26 it is observed that the amplitude increases with the addition of methanol.

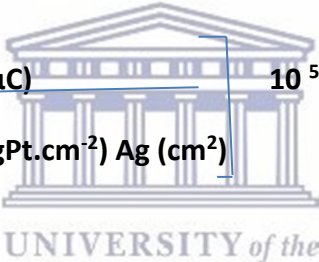
There is a shift to lower potential (0.68V) that is observed in Figure 4.26 compares to Figure 4.25 and Figure 4.24 which are showing potentials of 0.7V. According to Andrienko 2008, this indicates that the species is getting hard to reduce on reference electrode due to the roughness of the surface. In Figure 4.26, peak A has shifted slightly to a lower overpotential and the amplitude is greater, therefore less energy is required to do MOR which is equal to greater activity.

Non-noble metal oxide (TiO_2) that was used on this study as a support has also improved the catalytic activity of platinum based catalysts for MOR. This was due to its suitable surface properties as a promoter of methanol electro-oxidation reaction when combined with Pt/MWCNT.

In Figures (4.24 – 4.26) and Figures (0.1- 0.9) the voltammogram of the electro-catalysts in methanol and sulphuric acid are illustrated. There are methanol oxidation peaks which are observed at approximately 0.70V, in the forward sweep. In Figures 0.6 and Figure 4.2 in the reverse scan there are an anodic peak observed at approximately 0.45V and 0.4V respectively. This increase in current is also observed when the sweep rate was increased to 50mV/s. This was reported by Liao et al (2006), as the improvement to the catalytic activity for methanol which was due to electrochemical active surface area of the catalyst. There are adsorption/desorption hydrogen peaks observed on the region of -0.2V- 0.1V in the voltammograms that have methanol addition, this could be attributed to the atomic hydrogen adsorption on the platinum surface.

Effective surface area

The effective surface area of the catalyst was calculated from the area of the hydrogen desorption peak after subtracting the contribution from the double layer charging. This area was then converted into the effective surface area by using the factor $210 \mu\text{C}\cdot\text{cm}^2$ for the monolayer of hydrogen adsorbed on polycrystalline platinum. The hydrogen desorption peak (Q_r) was well defined by autolab software. The results were collected and presented in Table 4.3 below. All ECSA calculations were done following the equation below and ECSA is measured in ($\text{m}^2\cdot\text{g}^{-1}\text{Pt}$).

$$\text{ECSA} = \frac{Q_r(\mu\text{C})}{210\mu\text{C cm}^{-2} \text{LPt (mgPt}\cdot\text{cm}^{-2}) \text{Ag (cm}^2)} \cdot 10^5 \quad (4.7)$$


$\text{Ag} = 0.196 \text{ cm}^2$ is the geometric surface area of the glassy carbon electrode. The values for ECSA are reported in $\text{m}^2\text{g}^{-1}\text{Pt}$.

Where Q_r (mC/cm^2) was measured from the area of the hydrogen desorption peak on the corresponding CV in the initial $0.5 \text{ M H}_2\text{SO}_4$ electrolyte and C ($0.21 \text{ mC}/\text{cm}^2$) is the charge of a monolayer of hydrogen desorbed on a smooth platinum surface.

Table 4.4 represents the Electro-chemical active surface area parameters of the selected electro-catalysts.

Table 4.4: ECSA values of electro-catalysts supported in MWCNT/TiO₂

CATALYST	HRTEM Pt (weight %)	Qr (μC)	ECSA($\text{m}^2\text{g}^{-1}\text{Pt}$)	Scan rate (mV^2)
30%PtRu/MWCNT (A5)	5.62	1.8782	81	20
30%PtRuV/MWCNT-TiO ₂ (A11)	3.02	3.6211	291	20
30%PtRuVFe/MWCNT-TiO ₂ (A15)	11.06	1.547	34	20

The platinum loading that was used to calculate electro-chemical active surface area is from element composition weight % analyse by HRTEM. The ECSA equation (4.7) was used for the calculations.

4.8 Electrocatalytic activity discussion of results

In all voltammograms that undergoes methanol oxidation there is a direct oxidation peak (A) observed and a methanol re-oxidation peak (B) as well. It can be seen that all the onset of methanol oxidation reaction of the catalysts occurred in various potential windows between (0.27 V – 0.4 V), which is after desorption of adsorbed hydrogen. The hydrogen desorption peak occurred between -0.2V to 0.1V in all the voltammograms of methanol oxidation. The oxidation currents increase with increasing potential until the current peaks are observed. Even though the methanol oxidation peaks are seen in potential window approximately between (0.6 V – 0.8 V) the catalysts differed slightly in their activities of methanol oxidation with 30% PtRuV/MWCNT-TiO₂ having the lower potential which correlate with the higher ECSA value. The Pt surface at +0.80 V should be

oxidised as mentioned by Yin et al., 2009. In this study with the Pt loaded with MWCNTs and TiO₂ the similar behaviour was observed. ECSA for 30% PtRuV is higher than the 30% PtRuVFe and 30%PtRu. PtRuV-MWCNT/TiO₂ presented the best active surface area of 291m²g-Pt compared to the other catalyst. This may attribute to the small crystalline size of 0.84 nm showed in Table 4.2. 30%PtRuVFe/MWCNT-TiO₂ displayed the smallest ECSA of 34 m²g⁻¹Pt when compared to the other catalysts, which is followed by 30%PtRu-MWCNT at 81 m²g⁻¹Pt.

4.9 Summary

Catalysts on MWCNT/TiO₂ were characterised using techniques such as HRTEM, HRSEM, XRD and electro-chemical characterisation was done using cyclic voltammetry. MWCNTs were treated using acid mixture of nitric and sulphuric acid to remove metal particles. MWCNTs were also coated with the catalyst using the CVD method, thereafter characterised using the techniques which are mention above. On binary, tri-metallic and quartenary catalysts, MWCNT/TiO₂ were used as supports. In this section 30 wt. % Pt loading samples which were produced by CVD was discussed. XRD analysis confirmed that Pt catalysts have fcc structures. Electrochemical activities of the catalysts were measured by CV. The results showed that the electro-catalysts are active methanol oxidation reaction.

Platinum was alloyed with Ruthenium as indicated from the literature to be able to prevent CO poisoning of the platinum catalyst. The focus of the study was the addition of the extra metal to be alloyed with Pt. Therefore, there was an addition of iron and vanadium on the PtRu catalyst. These pluri metallic catalyst still

performed well in the MOR whilst the Pt content was lower, which was the purpose of the study. The lower platinum content can be observed in Table 4.4, which were analysed using HRTEM (weight %) on EDS.



Chapter five

5 Conclusions

The importance of this study of electro-catalysis is to reduce or replace Pt with the other platinum group metals or non-noble metals. There were two approaches in order to obtain cheaper yet active catalysts. The first one was to develop multi-component catalysts with an activity similar or higher than that of Pt. The metals that are non-platinum group metal and active metals which are considerably cheaper exist.

As presented in chapter 4, it can be concluded that the CVD process could be applied in order to achieve changes in catalysts properties such as dispersion of metal support, morphology, electro-catalytic activity, and CVD could also improve agglomeration. The CVD method demonstrated that it is a fast and environmental accommodating method to produce mono-metallic, binary metallic and pluri-metallic catalysts without using chemicals or reducing agents, as well as avoiding traditional stages such as impregnation, washing, drying and calcination. The study has shown that although the acid treatment of the MWCNT support can be effective for removal of impurities, it is not necessary to perform acid washing prior to the loading of metals since it did not materially alter the support.

Pluri-metallic catalysts have been successfully synthesised on different supports that is MWCNT and MWCNT/TiO₂. According to the ECSA and the electrochemical analysis, the trimetallic catalyst (30% PtRuV/MWCNT-TiO₂) and quarternary (30% PtRuVFe/MWCNT-TiO₂) catalyst displayed better results compared to PtRu/MWCNT which was a binary catalyst. XRD and HRTEM of the catalysts that were analysed for their properties after the chemical vapour

deposition method showed small metal particle size. These results indicated that the additional metals integrated with Pt can reduce the particle size, and maintain a high activity.

CV showed that the methanol oxidation reaction was enhanced depending upon the percentage metal combination, when methanol is added in a sulphuric acid solution. This has been observed for different percentage loadings of metals. When TiO_2 was added as a support (30%PtRuV/MWCNT- TiO_2 , 30% PtRuVFe/MWCNT- TiO_2) the methanol oxidation of the catalyst activity increased. The over-potential decreased and current density increased, which implied that the 30% PtRuV/MWCNT- TiO_2 catalysts were active for methanol oxidation. The interaction of the second or the third or the fourth metal could thus have a positive effect upon the activity of the catalysts. The catalytic activity of the Pt based catalysts have been studied and found to be dependent on the composition, structure, particle size and support material. It is very important to synthesise these metal particles as electro-catalytic materials with uniform size and good dispersion on the support. Hence adding the non-noble metal and catalytic support strategies will be able to increase performance and reducing the cost of platinum catalyst. In this study it is concluded that MWCNTs/ TiO_2 proved to be the best support material, since catalysts supported on them showed good MOR activity in acid electrolytes. All supported electro-catalysts showed activities in the presence of methanol. As a result, the presence of the third and fourth metal could enhance the reaction of methanol oxidation in direct methanol fuel cells. Therefore, in order to reduce the metal loading of the expensive

platinum, TiO₂ with MWCNTs will work as support, as well as iron and vanadium when added with ruthenium and platinum.

Recommendation

This study recommended that, for the better ECSA results ICP results should be employed instead of the calculated platinum loading. The use of the plurimetallic catalysts should be considered for CO tolerance. Catalyst supported on both titanium oxide and MWCNTs has shown that they are more stable.



REFERENCES

References

Abuilaiwi, F.A., Laoui, T., Al-Harhi, M. and Atieh, M.A., 2010. Modification and functionalization of multiwalled carbon nanotube (MWCNT) via fischer esterification. *The Arabian Journal for Science and Engineering*, 35(1c), pp.37-48.

Ahmad A., Kholoud M.M., Abou E.N, Reda A.A., Warthan A. A. 2012. Carbon Nanotubes, Science and Technology Part (I) structure, synthesis and characterisation. *Arabian Journal of Chemistry* 5, 1–23.

Anderson, J.A., Castaldi, M.J. and Centi, G., 2009. *Catalysis* (Vol. 21). Royal Society of Chemistry.

Angelucci, C.A., Silva, M.D.V. and Nart, F.C., 2007. Preparation of platinum–ruthenium alloys supported on carbon by a sonochemical method. *Electrochimica acta*, 52(25), pp.7293-7299.

Arico, A.S., Antonucci, P.L., Modica, E., Baglio, V., Kim, H. and Antonucci, V., 2002. Effect of Pt□Ru alloy composition on high-temperature methanol electro-oxidation. *Electrochimica Acta*, 47(22), pp.3723-3732.

Artyushkova, K., Pylypenko, S., Dowlapalli, M. and Atanassov, P., 2012. Structure-to-property relationships in fuel cell catalyst supports: Correlation of surface chemistry and morphology with oxidation resistance of carbon blacks. *Journal of Power Sources*, 214, pp.303-313.

Academia Romana: 2004. Romanian Journal of Physics. Editura Academiei Romane, Volume 49 (770) ebook.

Andrienko, D., 2008. Cyclic voltammetry. *Cyclic Voltammetry*.

Ba-Abbad, M.M., Kadhum, A.A.H., Mohamad, A.B., Takriff, M.S. and Sopian, K., 2012. Synthesis and catalytic activity of TiO₂ nanoparticles for photochemical

REFERENCES

oxidation of concentrated chlorophenols under direct solar radiation. *International Journal of Electrochemical Science*, 7, pp.4871-4888.

Bai, Y., Wu, J., X., Xi, J., Wang, J., Li, J., Zhu, W. and Chen, L., 2007. Electrochemical characterization of Pt-CeO₂/C and Pt-Ce_xZr_{1-x}O₂/C catalysts for ethanol electro-oxidation. *Applied Catalysis B: Environmental*, 73 (1), pp.144-149.

Berkowitz, A.E., Mitchell, J.R., Carey, M.J., Young, A.P., Zhang, S., Spada, F.E., Parker, F.T., Hutten, A. and Thomas, G., 1992. Giant magnetoresistance in heterogeneous Cu-Co alloys. *Physical Review Letters*, 68(25), p.3745.

Bailon-Garcia E., Maldonado-Hodar F.J., Perez-Cadenas A.F., and Carrasco-Marín F. 2013. Catalyst supported on carbon materials for the selective hydrogenation of Citral. *Catalysts* 3, 853-877.

Balcerzak, M., 2002. Sample digestion methods for the determination of traces of precious metals by spectrometric techniques. *Analytical sciences*, 18(7), pp.737-750.

Bandaru Prabhakar R. 2007. Electrical Properties and Applications of Carbon Nanotube Structures, *Journal of Nanoscience and Nanotechnology* (7) 1–29.

Barczuk P.J., Lewera A., Miecznikowski K., Zurowski A., Kulesza P.J. 2011. Enhancement of catalytic activity of platinum based nanoparticles towards electro-oxidation of ethanol through interfacial modification with heteropolymolybdates. *Journal of Power Sources* (195) 2507.

Brar K.S., Verma M., Tyagi R.D., Surampalli R.Y. 2010. Engineered nanoparticles in wastewater sludge-evidence and impacts. *Waste Management* (30), 504-520.

Britton T.B., Jiang J., Guo Y., Vitalta-Clemente A., Wallis D., Hansen L.N., Winkelmann A., Wilkinson A.J. 2016. Tutorial: Crystal orientations and EBDS-Or which way is up. *Material characterization*. (117) 113-126.

REFERENCES

Cai J., Huang B., Zheng S., Guo Y. 2014. Enhanced activity of platinum nanoparticle catalysts supported on manganese oxide- carbon nanotubes for ethanol oxidation. *International Journal of Hydrogen Energy* (39) 798-807.

Calderon J.C., Mahata N., Pereira M.F., Figueiredo J.L., Fernandes V.R., Rangel C.M., Calvillo L., Larazo M.J., Pastor E. 2012. Pt-Ru catalysts supported on carbon xerogels for PEM fuel Cells. *International Journal of Hydrogen Energy* (37) 7200-7211.

Chellaram C., Murugaboophathi G., John A.A., Sivakumar R., Ganesam S, Kritika S, and Priya G. 2014. Significance of nanotechnology in food Industry. Asia-Pacific Chemical, Biological and Environmental Engineering (APCBEE) *Procedia* (8) 109-113, *Science Direct*.

Chan, C. K., Peng, H., Liu, G., McIlwrath, K., Zhang, X. F., Huggins, R. A., & Cui, Y. (2011). High-performance lithium battery anodes using silicon nanowires. In *Materials for Sustainable Energy: A Collection of Peer-Reviewed Research and Review Articles from Nature Publishing Group* (pp. 187-191).

Chen J., Wang M, Lieu B, Zhen F, Cui K, and Kuang Y. 2006. Platinum catalyst prepared with functional carbon nanotube defects and its improved catalytic performance for methanol oxidation. *Journal of Physical Chemical B* (110) 11775-11779.

Chen J., Lim B., Lee, E.P., Xia Y. 2008. Shape-controlled synthesis of platinum nanocrystals for catalytic and electrocatalytic applications. *Nano Today* (4) 81-95.

Chandrasekar R., Zhang L., Howe J., Hedin M., Zhang Y., Fong H. 2009. Fabrication and characterization of electrospun titania nanofibers. *Journal of Material Science* (44) 1198-1205.

Colmati, F., Antolini, E. and Gonzalez, E.R., 2006. Effect of temperature on the mechanism of ethanol oxidation on carbon supported Pt, PtRu and Pt 3 Sn electrocatalysts. *Journal of Power Sources*, 157(1), pp.98-103.

REFERENCES

- Cuenya, B.R., 2010. Synthesis and catalytic properties of metal nanoparticles: Size, shape, support, composition, and oxidation state effects. *Thin Solid Films*, 518(12), pp.3127-3150.
- Dai A., Javey A., Pop E., Mann D., and Lu Y. 2006. Electrical transport properties and field-effect transistors of carbon nanotubes, *Nano Reports and Reviews*, (1) no. 1, pp. 1–4.
- Dumbrava, A., Ciupina, V. and Prodan, G., 2005. Dependence on grain size and morphology of zinc sulfide particles by the synthesis route. *Romanian Journal of Physics*, 50(7/8), p.831.
- Dybkaer, R., 2002. The tortuous road to the adoption of katal for the expression of catalytic activity by the General Conference on Weights and Measures. *Clinical chemistry*, 48(3), pp.586-590.
- Esteves M. D., De Amorim M.T., Lomel C.: Application of cyclic voltammetry on dye concentrated control in aqueous solution.
- Eltom A.E., Lessa M.P.F., da Silva M. J., da Rocha J.C. 2012. Production and characterization of activated carbon membranes. *Journal of materials research and technology*. Vol (1) 80 – 83).
- Elzubair, A., Fournier, M.P., Da Silva, M.J. and Da Rocha, J.C., 2011. Production and characterization of activated carbon membranes. *Tecnologia em Metalurgia, Materiais e Mineracao*, 20110718, pp.1644-1651.
- Fragkou, V., Ge, Y., Steiner, G., Freeman, D., Bartetzko, N. and Turner, A.P., 2012. Determination of the real surface area of a screen-printed electrode by chronocoulometry. *Int. J. Electrochem. Sci*, 7, pp.6214-6220.
- Fu X.Z., Liang Y., Chen S.P., Lin J.D., Liao D.W. 2009. Pt rich shell coated Ni nanoparticles as catalysts for methanol electro-oxidation in alkaline media. *Catalysis. Commum.* (10) 1893-1897.

REFERENCES

- Ganesh, E.N., 2013. Single walled and multi walled carbon nanotube structure, synthesis and applications. *International Journal of Innovative Technology and Exploring Engineering*, 2(4), pp.311-320.
- Gázquez, M.J., Bolívar, J.P., Garcia-Tenorio, R. and Vaca, F., 2014. A review of the production cycle of titanium dioxide pigment. *Materials Sciences and Applications*, 5(07), p.441.
- Hamnett, A., 1997. Mechanism and electrocatalysis in the direct methanol fuel cell. *Catalysis Today*, 38(4), pp.445-457.
- Harris, P.J., 1999. Carbon nanotubes and related structures: new materials for the twenty-first century. Cambridge, Cambridge University press
- Halder, A., Sharma, S., Hegde, M.S. and Ravishankar, N., 2009. Controlled attachment of ultrafine platinum nanoparticles on functionalized carbon nanotubes with high electrocatalytic activity for methanol oxidation. *The Journal of Physical Chemistry C*, 113(4), pp.1466-1473.
- He, H., Pham-Huy, L.A., Dramou, P., Xiao, D., Zuo, P. and Pham-Huy, C., 2013. Carbon nanotubes: applications in pharmacy and medicine. *BioMed research international*, 2013.
- Hintsho, N., Petrik, L., Nechaev, A., Titinchi, S. and Ndungu, P., 2014. Photocatalytic activity of titanium dioxide carbon nanotube nano-composites modified with silver and palladium nanoparticles. *Applied Catalysis B: Environmental*, 156, pp.273-283.
- Hogarth M.P., Ralph T.R. 2002. Platinum metals Revised (46). Sun, X., Li, R., Villers, D., Dodelet, J.P. and Desilets, S., 2003. Composite electrodes made of Pt nanoparticles deposited on carbon nanotubes grown on fuel cell backings. *Chemical Physics Letters*, 379(1), pp.99-104.

REFERENCES

Hongbing, Z., Chan, Z., Wenzhe, C. and Minquan, W., 2005. Characterization and nonlinear optical property of a multi-walled carbon nanotube/silica xerogel composite. *Chemical physics letters*, 411(4), pp.373-377.

Humphreys, F.J. and Hatherly, M., 2012. *Recrystallization and related annealing phenomena*. Elsevier.

Iijima, S., 1993. Growth of carbon nanotubes. *Materials Science and Engineering: B*, 19(1-2), pp.172-180.

Iwasita, T., 2002. Electrocatalysis of methanol oxidation. *Electrochimica Acta*, 47(22), pp.3663-3674.

Jang J and Ma J. Carbon Nanotubes as Catalyst Support. Hyperion *Catalysis International*, Inc.

James J., Spivey K.K., Dooley. M. 2009. The Royal Society of Chemistry. *Catalysis Jour* Kim J., Rabbani M.M., Kim D., Ree M., Yean J.H., Ko C.H., Kim Y., Bae J., Oh N. 2010. Structural and electrochemical properties of gold – deposited carbon nanotube composites. *Current Applied Physics* (10) 5201-5205.

Kniess C.T., Cardoso de Lima J., and Prates, P.B., 2005. The quantification of crystalline phases in materials: *applications of Rietveld method*, Sintering – methods and products/the-quantification of crystalline phase in materials application of rietveld method (Verified 15 August 2014).

Kulesza, P.J., Pieta, I.S., Rutkowska, I.A., Wadas, A., Marks, D., Klak, K., Stobinski, L. and Cox, J.A., 2013. Electrocatalytic oxidation of small organic molecules in acid medium: Enhancement of activity of noble metal nanoparticles and their alloys by supporting or modifying them with metal oxides. *Electrochimica acta*, 110, pp.474-483.

Kim, J., Rabbani, M.M., Kim, D., Ree, M., Yeum, J.H., Ko, C.H., Kim, Y., Bae, J.S. and Oh, W., 2010. Structural and electrochemical properties of gold-

REFERENCES

deposited carbon nanotube composites. *Current Applied Physics*, 10(2), pp. S201-S205.

Kimmel, Y.C., Yang, L., Kelly, T.G., Rykov, S.A and Chen, J.G.,2014. Theoretical prediction and experimental verification of low loading of platinum on Titanium carbide as low cost and stable electrocatalysts. *Journal of Catalysis*, 312, pp 216-220

Kniess, C.T., Cardoso de Lima, J. and Prates, P.B., 2012. The quantification of crystalline phases in materials: applications of Rietveld method, Sintering–methods and products. Available at <http://www.intechopen.com/books/sintering-methods-and-products/the-quantification-of-crystalline-phases-in-materials-applications-of-rietveld-method.pdf>. [Verified 15 August 2014.

Kuo, P.L., Hsu, C.H., Li, W.T., Jhan, J.Y. and Chen, W.F., 2010. Sea urchin-like mesoporous carbon material grown with carbon nanotubes as a cathode catalyst support for fuel cells. *Journal of Power Sources*, 195(24), pp.7983-7990.

Lamy, C., Lima, A., LeRhun, V., Delime, F., Coutanceau, C. and Léger, J.M., 2002. Recent advances in the development of direct alcohol fuel cells (DAFC). *Journal of Power Sources*, 105(2), pp.283-296.

Léger, J.M., Coutanceau, C. and Lamy, C., 2009. *Electrocatalysis for the direct alcohol fuel cell* (pp. 337-367). Wiley-VCH: Weinheim.

Léger, J.M., Coutanceau, C. and Lamy, C., 2009. *Electrocatalysis for the direct alcohol fuel cell* (pp. 337-367). Wiley-VCH: Weinheim.

Li, W., Liang, C., Qiu, J., Zhou, W., Han, H., Wei, Z., Sun, G. and Xin, Q., 2002. Carbon nanotubes as support for cathode catalyst of a direct methanol fuel cell. *Carbon*, 40(5), pp.791-794.

REFERENCES

- Li, W., Liang, C., Zhou, W., Qiu, J., Zhou, Z., Sun, G. and Xin, Q., 2003. Preparation and characterization of multiwalled carbon nanotube-supported platinum for cathode catalysts of direct methanol fuel cells. *The Journal of Physical Chemistry B*, 107(26), pp.6292-6299.
- Li N., Liang C., Qiu I., Zhou W., Han H., Wei Z., Sun G., Xin, Q. 2002. Carbon nanotubes as support for cathode catalyst of a direct methanol fuel cell. *Carbon* (40) 787-803.
- Li, L., Liu, E., Li, J., Yang, Y., Shen, H., Huang, Z., Xiang, X. and Li, W., 2010. A doped activated carbon prepared from polyaniline for high performance supercapacitors. *Journal of Power Sources*, 195(5), pp.1516-1521.
- Li, X., Ge, S., Hui, C.L. and Hsing, I.M., 2004. Well-dispersed multiwalled carbon nanotubes supported platinum nanocatalysts for oxygen reduction. *Electrochemical and solid-state letters*, 7(9), pp. A286-A289.
- Liu, Z., Ling, X.Y., Su, X. and Lee, J.Y., 2004. Carbon-supported Pt and PtRu nanoparticles as catalysts for a direct methanol fuel cell. *The Journal of Physical Chemistry B*, 108(24), pp.8234-8240.
- Liu, H., Song, C., Zhang, L., Zhang, J., Wang, H. and Wilkinson, D.P., 2006. A review of anode catalysis in the direct methanol fuel cell. *Journal of Power Sources*, 155(2), pp.95-110.
- Liu, J., Bai, P. and Zhao, X.S., 2011. Ruthenium nanoparticles embedded in mesoporous carbon microfibers: preparation, characterization and catalytic properties in the hydrogenation of D-glucose. *Physical Chemistry Chemical Physics*, 13(9), pp.3758-3763.
- Lordi, V. and Yao, N., 2000. Molecular mechanics of binding in carbon-nanotube-polymer composites. *Journal of Materials Research*, 15(12), pp.2770-2779.

REFERENCES

- Liao, S., Holmes, K.A., Tsapraillis, H. and Birss, V.I., 2006. High performance PtRuIr catalysts supported on carbon nanotubes for the anodic oxidation of methanol. *Journal of the American Chemical Society*, 128(11), pp.3504-3505.
- Macwan, D.P., Dave, P.N. and Chaturvedi, S., 2011. A review on nano-TiO₂ sol-gel type syntheses and its applications. *Journal of Materials Science*, 46(11), pp.3669-3686.
- Malik, M.A., Wani, M.Y. and Hashim, M.A., 2012. Microemulsion method: A novel route to synthesize organic and inorganic nanomaterials: 1st Nano Update. *Arabian journal of Chemistry*, 5(4), pp.397-417.
- Matsumoto, T., Komatsu, T., Nakano, H., Arai, K., Nagashima, Y., Yoo, E., Yamazaki, T., Kijima, M., Shimizu, H., Takasawa, Y. and Nakamura, J., 2004. Efficient usage of highly dispersed Pt on carbon nanotubes for electrode catalysts of polymer electrolyte fuel cells. *Catalysis Today*, 90(3), pp.277-281.
- McDonald, D. and Hunt, L.B., 1982. *A history of platinum and its allied metals*. Johnson Matthey Plc.
- Meher, S.K. and Rao, G.R., 2013. Morphology-controlled promoting activity of nanostructured MnO₂ for methanol and ethanol electrooxidation on Pt/C. *The Journal of Physical Chemistry C*, 117(10), pp.4888-4900.
- Mani P., Srivastava R., Strasser P. 2011. Dealloyed binary PtM₃ (M=Cu, Co, Ni) and ternary PtNi₃M (M=Cu, Co, Fe, Cr) electrocatalysts for the oxygen reduction reaction: Performance in Polymer electrolyte membrane fuel cells. *Journal of Power Sources* (37) 196, 666-673.
- Naidoo, Q.L., Naidoo, S., Petrik, L., Nechaev, A. and Ndungu, P., 2012. The influence of carbon based supports and the role of synthesis procedures on the formation of platinum and platinum-ruthenium clusters and nanoparticles for the development of highly active fuel cell catalysts. *International Journal of Hydrogen Energy*, 37(12), pp.9459-9469.

REFERENCES

Nakashima, T., Nohara, S., Inoue, H. and Iwakura, C., 2006. A new simple preparation of platinum-nickel alloy nanoparticles and their characterization as an electrocatalyst for methanol oxidation. *Research on chemical intermediates*, 32(5), pp.561-573.

Nashner, M.S., Frenkel, A.I., Adler, D.L., Shapley, J.R. and Nuzzo, R.G., 1997. Structural characterization of carbon-supported platinum– ruthenium nanoparticles from the molecular cluster precursor PtRu₅C (CO)₁₆. *Journal of the American Chemical Society*, 119(33), pp.7760-7771.

Neto, A.O., Giz, M.J., Perez, J., Ticianelli, E.A. and Gonzalez, E.R., 2002. The electro-oxidation of ethanol on Pt-Ru and Pt-Mo particles supported on high-surface-area carbon. *Journal of the Electrochemical Society*, 149(3), pp. A272-A279.

Negro E., Stassi A., Baglio V., Arico A. S., Koper J.M. 2015. Electrocatalytic activity and durability of Pt-decorated non-covalently functionalized graphitic structures. *Catalysts* (5) 1622-1635.

Nogxina S., Moloi N., Mngomezulu M.A. and Harding A.J. 2003. Platinum-Group Metals Mines in South Africa. *Department of Mineral and Energy*

Oguri, K., Shimoda, G. and Tatsumi, Y., 1999. Quantitative determination of gold and the platinum-group elements in geological samples using improved NiS fire-assay and tellurium coprecipitation with inductively coupled plasma-mass spectrometry (ICP-MS). *Chemical Geology*, 157(3), pp.189-197.

Park, J.Y., Hwang, K.J., Lee, J.W. and Lee, I.H., 2011. Fabrication and characterization of electrospun Ag doped TiO₂ nanofibers for photocatalytic reaction. *Journal of materials science*, 46(22), pp.7240-7246.

Park, H.J., Park, M., Chang, J.Y. and Lee, H., 2008. The effect of pre-treatment methods on morphology and size distribution of multi-walled carbon nanotubes. *Nanotechnology*, 19(33), p.335702.

REFERENCES

Petrik, L., Ndungu, P. and Iwuoha, E., 2010. Hall measurements on carbon nanotube paper modified with electroless deposited platinum. *Nanoscale research letters*, 5(1), p.38.

Pingali, K.C., Deng, S. and Rockstraw, D.A., 2005, October. Synthesis of binary metal nanoparticles of Ru-Ni with core and shell structure. In *05AICHE: 2005 AIChE Annual Meeting and Fall Showcase*. American Institute of Chemical Engineers.

Pop, E., Mann, D., Wang, Q., Goodson, K. and Dai, H., 2006. Thermal conductance of an individual single-wall carbon nanotube above room temperature. *Nano letters*, 6(1), pp.96-100.

Peng Z., and Yang H. 2008. Designer platinum nanoparticles: Control of shape, composition in alloy, nanostructure and electro-catalytic property. *Nano Today* (4) 143-164.

Petrik, L., Ndungu, P. and Iwuoha, E., 2010. Hall measurements on carbon nanotube paper modified with electroless deposited platinum. *Nanoscale research letters*, 5(1), p.38.

Sample, J.L. and Charles Jr, H.K., 2012. Systems Engineering at the Nanoscale. *Johns Hopkins APL Technical Digest*, 31(1), pp.50-57.

Sebatian D., Lazaro M.J., Suelves I., Moliner R., Baglio R., Stassi V., Arico A. S. 2012. The influence of carbon nanofiber support properties on the oxygen reduction behaviour in proton conducting electrolyte-based direct methanol fuel cells. *International Journal of Hydrogen energy* (37) 6253-6260.

Sharma, S., Ganguly, A., Papakonstantinou, P., Miao, X., Li, M., Hutchison, J.L., Delichatsios, M. and Ukleja, S., 2010. Rapid microwave synthesis of CO tolerant reduced graphene oxide-supported platinum electrocatalysts for oxidation of methanol. *The Journal of Physical Chemistry C*, 114(45), pp.19459-19466.

REFERENCES

Singh, R.N., Awasthi, R. and Sharma, C.S., 2014. An overview of recent development of platinum-based cathode materials for direct methanol fuel cells. *International Journal Electrochemical Science* 9, pp.5607-5639.

Sinnot B.S. and Andrew R. 2010. Synthesis, properties and applications. Critical reviews of Solid states and Materials Science. (2633) 145-249.

Sun, X., Li, R., Villers, D., Dodelet, J.P. and Desilets, S., 2003. Composite electrodes made of Pt nanoparticles deposited on carbon nanotubes grown on fuel cell backings. *Chemical Physics Letters*, 379(1), pp.99-104.

Schulz, M.J., Kelkar, A.D. and Sundaresan, M.J. eds., 2005. *Nanoengineering of structural, functional and smart materials*. CRC Press.

Su, M., Zheng, B. and Liu, J., 2000. A scalable CVD method for the synthesis of single-walled carbon nanotubes with high catalyst productivity. *Chemical Physics Letters*, 322(5), pp.321-326.

Szabó, A., Perri, C., Csató, A., Giordano, G., Vuono, D. and Nagy, J.B., 2010. Synthesis methods of carbon nanotubes and related materials. *Materials*, 3(5), pp.3092-3140.

Spinacé, E.V., Neto, A.O. and Linardi, M., 2004. Electro-oxidation of methanol and ethanol using PtRu/C electrocatalysts prepared by spontaneous deposition of platinum on carbon-supported ruthenium nanoparticles. *Journal of Power Sources*, 129(2), pp.121-126.

Stahl H., Appenzeller J., Martel R., Avouris P., Lengeler B. 2000. Intertube coupling in ropes of single-wall carbon nanotubes. *Physical Review Letters* 85(24): 5186-5189.

Su, M., Zheng, B. and Liu, J., 2000. A scalable CVD method for the synthesis of single-walled carbon nanotubes with high catalyst productivity. *Chemical Physics Letters*, 322(5), pp.321-326.

REFERENCES

Smalley R.E., Dai H.J., Rinzler A.G., Nikolaev P., Thess A., Colbert D.T. 1996. Single-wall nanotubes produced by metalcatalyzed disproportionation of carbon monoxide. *Chemical Physics. Letter* (260) 471–475.

Sundarrajan S., Allakhverdiev S., Ramakrishmas S. 2012. Progress and perspectives in micro direct methanol fuel. *International Journal of Hydrogen Energy* (37) 8765-8786.

Szabó, A., Perri, C., Csató, A., Giordano, G., Vuono, D. and Nagy, J.B., 2010. Synthesis methods of carbon nanotubes and related materials. *Materials*, 3(5), pp.3092-3140.

Thamaphat, K., Limsuwan, P. and Ngotawornchai, B., 2008. Phase characterization of TiO₂ powder by XRD and TEM. *Kasetsart Journal of Natural. Science*, 42(5), pp.357-361.

Thackray, A. and Myers, M., 2000. *Arnold O. Beckman: One hundred years of excellence* (Vol. 1). Chemical Heritage Foundation,

Tseng, Y.H., Kuo, C.S., Huang, C.H., Li, Y.Y., Chou, P.W., Cheng, C.L. and Wong, M.S., 2006. Visible-light-responsive nano-TiO₂ with mixed crystal lattice and its photocatalytic activity. *Nanotechnology*, 17(10), p.2490.

Tojo, C., Dios, M.D. and Barroso, F., 2010. Surfactant effects on microemulsion-based nanoparticle synthesis. *Materials*, 4(1), pp.55-72.

Qin, W., Yang, C., Yi, R. and Gao, G., 2011. Hydrothermal synthesis and characterization of single-crystalline α -Fe₂O₃ nanocubes. *Journal of Nanomaterials*, 2011, p.3.

Radmilovic, V., Gasteiger, H.A. and Ross, P.N., 1995. Structure and chemical composition of a supported Pt-Ru electrocatalyst for methanol oxidation. *Journal of Catalysis*, 154(1), pp.98-106.

REFERENCES

Rodríguez-Reinoso, F., 1998. The role of carbon materials in heterogeneous catalysis. *Carbon*, 36(3), pp.159-175.

Varshney, K., 2014. Carbon nanotubes: a review on synthesis, properties and applications. *International Journal of Engineering Research*, 2(4), pp.660-677.

Yaldagard M., Jahanshahi M., Seghatoleslami N. 2013. Carbonaceous Nanostructured Support Materials for Low Temperature Fuel Cell Electrocatalysts. *World Journal of Nano Science and Engineering*, (3), 121-153

Wang H., Shan Ji, Wmang W, Linkov V, Pasupathi S. 2012. Platinum decorated PdFe/C: Extreme high electrocatalytic activity for methanol oxidation. *International Journal Electrochemical Science* 7390-3398

Wang, L.L. and Johnson, D.D., 2009. Predicted trends of core– shell preferences for 132 late transition-metal binary-alloy nanoparticles. *Journal of the American Chemical Society*, 131(39), pp.14023-14029.

Wright, S.I., Nowell, M.M. and Field, D.P., 2011. A review of strain analysis using electron backscatter diffraction. *Microscopy and microanalysis*, 17(3), pp.316-329.

Wu, J., Gross, A. and Yang, H., 2011. Shape and composition-controlled platinum alloy nanocrystals using carbon monoxide as reducing agent. *Nano letters*, 11(2), pp.798-802.

Wu, M., Han, M., Li, M., Li, Y., Zeng, J. and Liao, S., 2014. Preparation and characterizations of platinum electro-catalysts supported on thermally treated CeO₂-C composite support for polymer electrolyte membrane fuel cells. *Electrochimica Acta*, 139, pp.308-314.

Wright, S.I., Nowell, M.M. and Field, D.P., 2011. A review of strain analysis using electron backscatter diffraction. *Microscopy and microanalysis*, 17(3), pp.316-329.

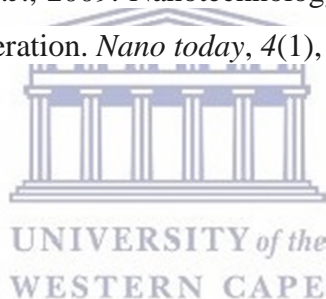
REFERENCES

Xie, J., Wu, C., Hu, S., Dai, J., Zhang, N., Feng, J., Yang, J. and Xie, Y., 2012. Ambient rutile VO₂ (R) hollow architectures with rich grain boundaries from new-state nsutite-type VO₂, displaying enhanced hydrogen adsorption behavior. *Physical Chemistry Chemical Physics*, 14(14), pp.4810-4816.

Xu H., Wang J., Zhang H., Huang Y. 2010. The effect of synthesis procedures on the structure and morphology of multiwalled carbon nanotubes/ titania nanocomposites prepared by hydrothermal method. *Journal of Material Science* (45): 6200-620

Zhang, F., 2015. *Photon upconversion nanomaterials* (Vol. 416). Heidelberg, Germany: Springer.

Zhang, L. and Webster, T.J., 2009. Nanotechnology and nanomaterials: promises for improved tissue regeneration. *Nano today*, 4(1), pp.66-80.



Appendices



Figure 1&2 represents the preparation of the catalysts,



Figure 3 pestle and mortar with MWCNT.



Figure 5: preparation for HRTEM

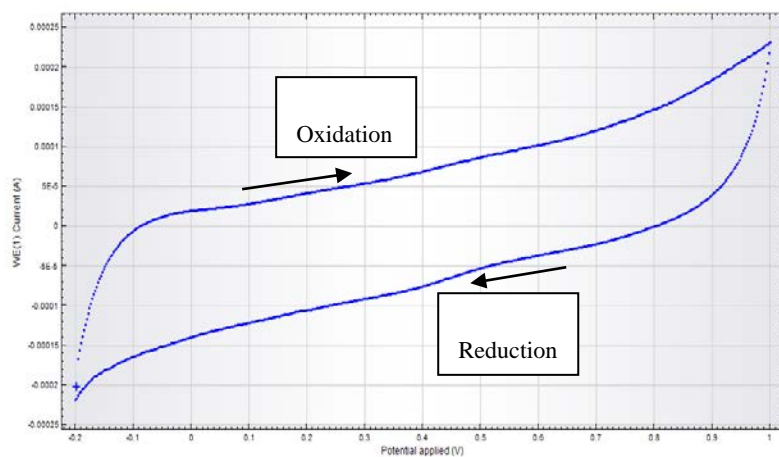


Figure 0.1: 30% PtRuMWCNT (10mVs^{-1}) catalyst with H_2SO_4

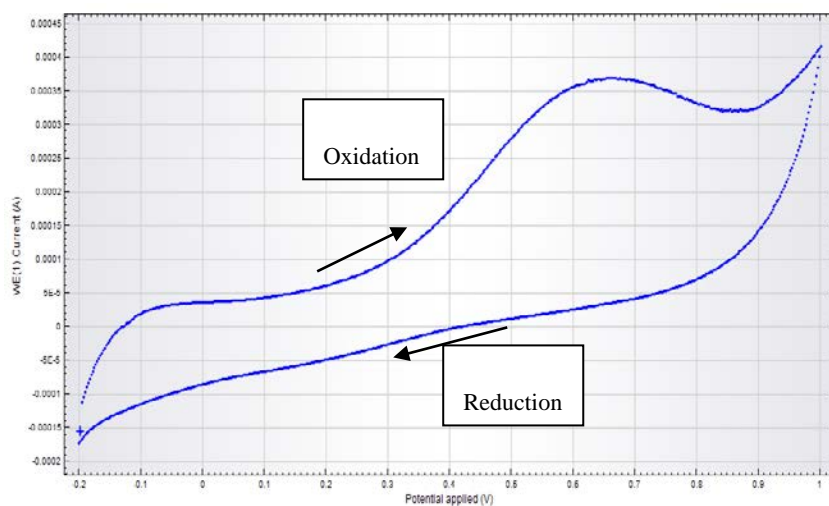


Figure 0.2: 30% PtRuMWCNT (10mVs^{-1}) catalyst with H_2SO_4 and CH_3OH

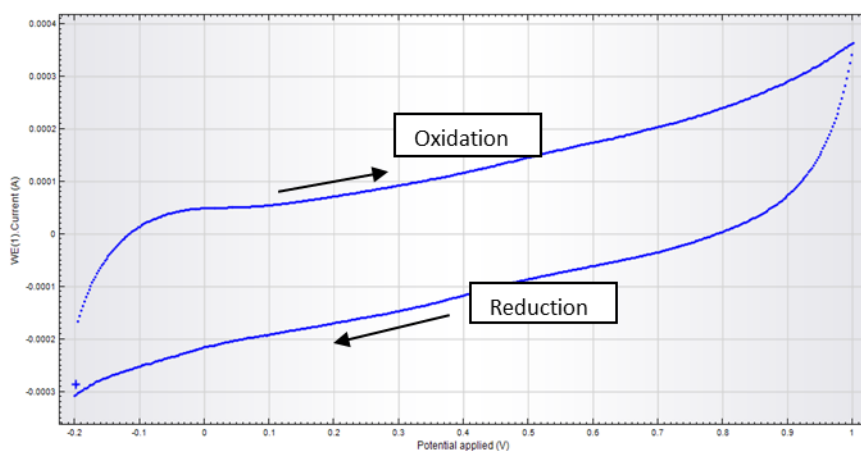


Figure 0.3: 30% PtRuMWCNT (20mVs^{-1}) catalyst with H_2SO_4 .

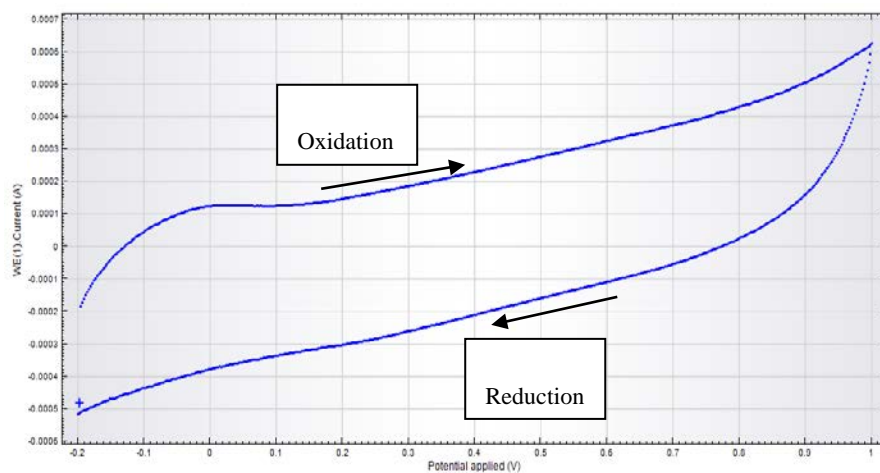


Figure 0.4: 30% PtRuMWCNT (50mVs^{-1}) catalyst with H_2SO_4

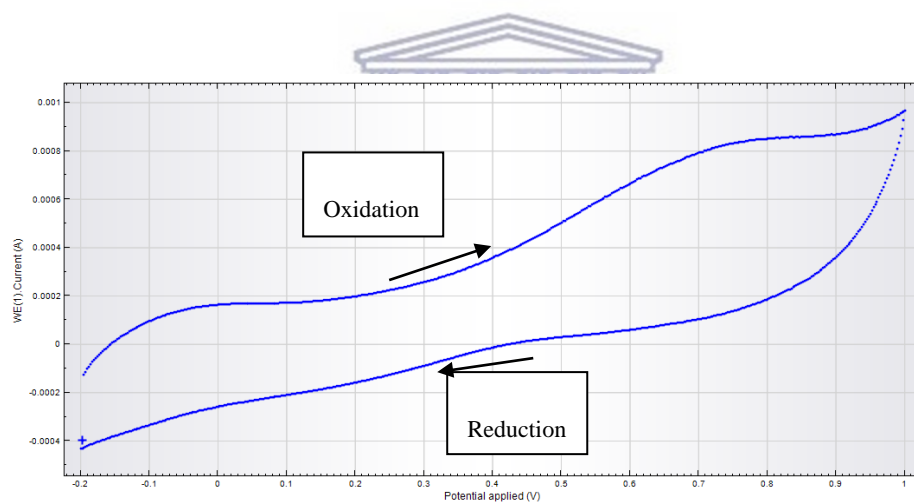


Figure 0.5: 30% PtRuMWCNT (50mVs^{-1}) catalyst with $\text{H}_2\text{SO}_4 + \text{CH}_3\text{OH}$.

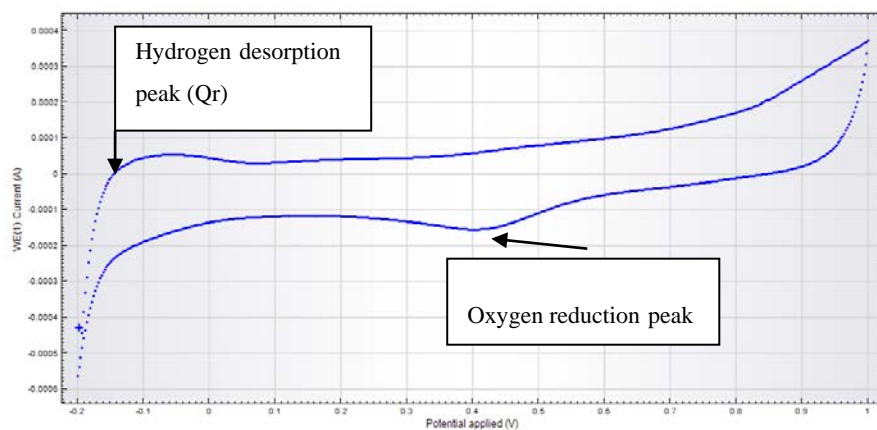


Figure 0.6: 30% PtRuVFeMWCNT/TiO₂ (10mVs⁻¹) Catalyst with H₂SO₄.

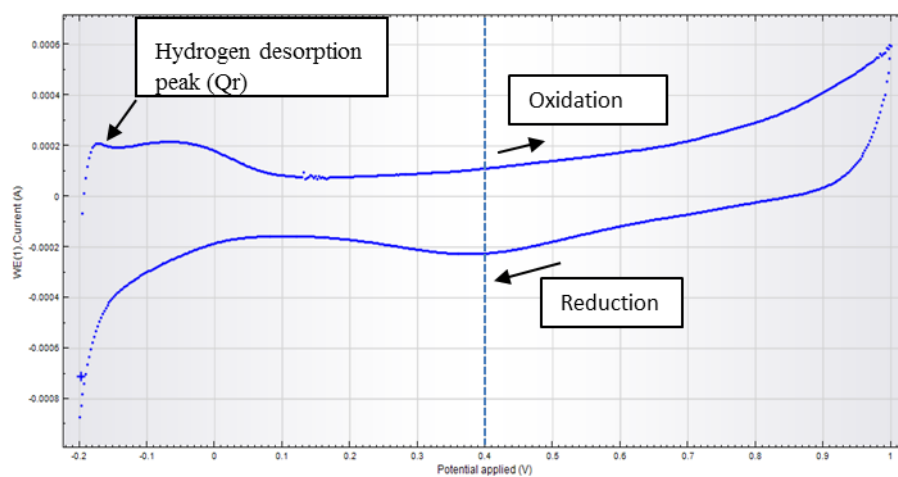


Figure 0.7: 30% PtRuVFeMWCNT/TiO₂ (20mVs⁻¹) Catalyst with H₂SO₄.

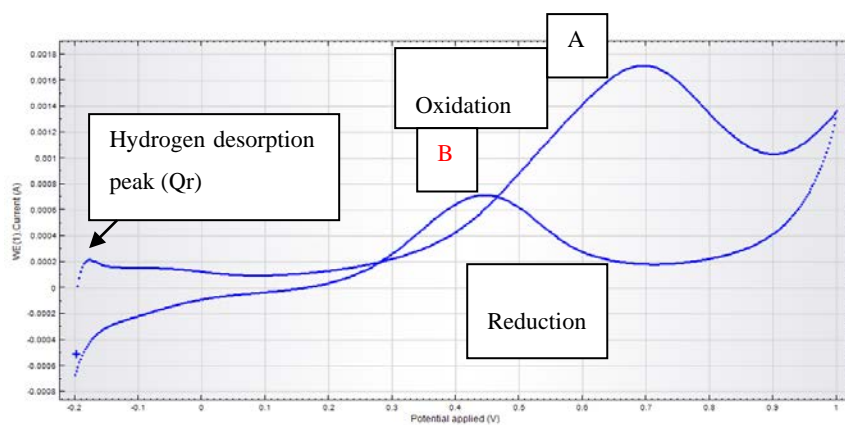


Figure 0.8: 30% PtRuVFeMWCNT/TiO₂ (50mVs⁻¹) catalyst with H₂SO₄ + CH₃OH.

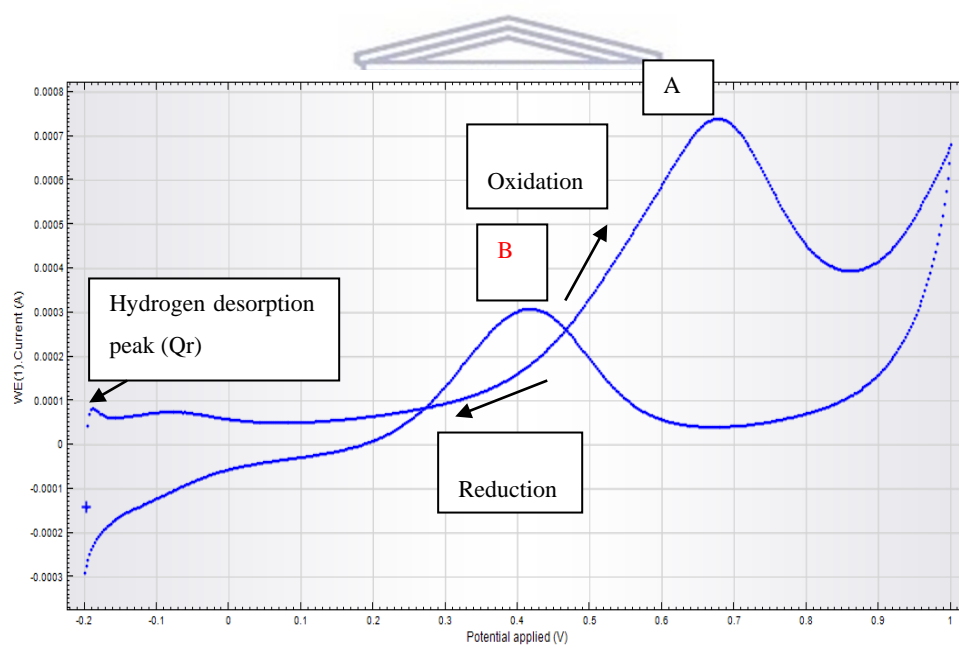
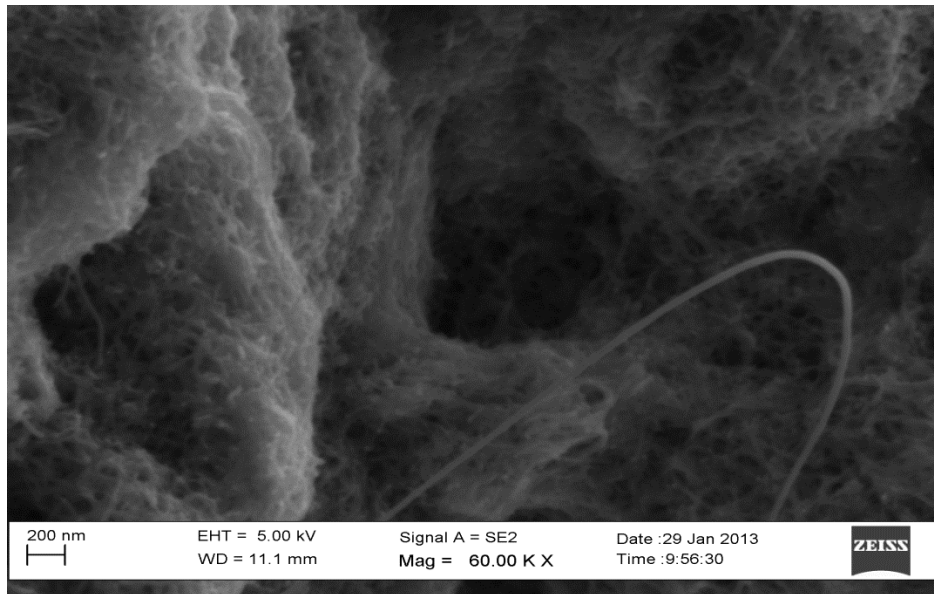
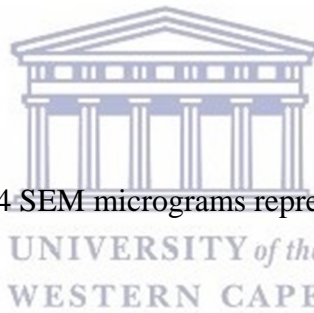


Figure 0.9: 30%PtRuV MWCNT/TiO₂ (50mVs⁻¹) Catalyst with H₂SO₄ + CH₃OH.



4: 3 (1): HRSEM image of a treated MWCNT



The following Figures 4.14 SEM micrograms represent untreated MWCNTs

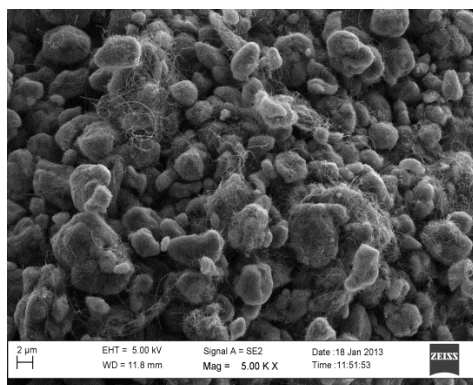


Figure 0.10: SEM images of Untreated MWCNTs.

Calculations

APPENDICES

- Calculations for theoretical platinum and other metal contents which were synthesised using CVD method, wt % is shown below;

10% Pt/MWCNT catalyst

Mole of Pt = mole of Pt (acac)₂

$$\begin{aligned} &= (\text{mass of (acac)}_2) / (\text{molecular weight of Pt (acac)}_2) \\ &= 0.11205 / 393 = 2.85 \times 10^{-4} \text{ mol} \end{aligned}$$

mass of Pt = (MW of Pt x mole Pt)

$$= 195 \times 2.85 \times 10^{-4} = 55.57 \text{ mg}$$

Wt% loading of Pt = $\text{massPt} / (\text{mass Pt} + (\text{mass MWCNTs}) \times 100\%$

$$= 55.57 / (55.57 + 500) \times 100\% = 10\%$$

20% Pt 20% Ru/MWCNT catalyst

Mole of Pt = mole of Pt (acac)₂

$$\begin{aligned} &= (\text{mass of (acac)}_2) / (\text{molecular weight of Pt (acac)}_2) \\ &= 0.335 / 393.29 = 8.52 \times 10^{-4} \text{ mol} \end{aligned}$$

mass of Pt = (MW of Pt x mole Pt)

$$= 195 \times 8.52 \times 10^{-4} = 166.14 \text{ mg}$$

Wt% loading of Pt = $\text{massPt} / (\text{mass Pt} + (\text{mass MWCNTs}) \times 100\%$

$$= 55.57 / (55.57 + 500) \times 100\% = 10\%$$

Mole of Ru = mole of Ru (acac)₂

$$\begin{aligned} &= (\text{mass of (acac)}_2) / (\text{molecular weight of Ru (acac)}_2) \\ &= 0.6548 / 381.43 = 1.722 \times 10^{-3} \text{ mol} \end{aligned}$$

mass of Ru = (MW of Pt x mole Pt)

APPENDICES

$$= 101.07 \times 1.72 \times 10^{-3} = 173.84 \text{ mg}$$

$$\text{Wt\% loading of Pt} = \frac{\text{massPt}}{(\text{mass Pt} + (\text{mass Ru} + \text{mass MWCNTs}))} \times 100\%$$

$$= \frac{166.14}{(166.14+173.84+500)} \times 100\% = 19.8\%$$

$$\text{Wt\% loading of Ru} = \frac{\text{massRu}}{(\text{mass Pt} + (\text{mass Ru} + \text{mass MWCNTs}))} \times 100\%$$

$$= \frac{173.84}{(166.14+173.84+500)} \times 100\% = 20\%$$

- Hydrogen desorption area on Auto lab software

Import the plot , peak search, choose the area of hydrogen desorption and obtain the peak area.



UNIVERSITY *of the*
WESTERN CAPE